EFFECT OF STRESS AND SUCTION HISTORIES ON DYNAMIC PROPERTIES OFSTATICALLY COMPACTED SILTY SAND

by

WILLIAM ALLAN DOUGLAS

Presented to the Faculty of the Graduate School of
The University of Texas at Arlington in Partial Fulfillment
of the Requirements
for the Degree of

MASTER OF SCIENCE IN CIVIL ENGINEERING

THE UNIVERSITY OF TEXAS AT ARLINGTON

May 2012

ACKNOWLEDGEMENTS

I would like to extend my genuine appreciation to Dr. Laureano Hoyos for his direction and aid throughout my experimental research study. It was a privilege to have worked with such an astute and highly esteemed professor. My only hope is to meet his expectations in both the experimental procedures and consequent research paper. I have developed my understanding of many essential theoretical concepts, and hope to be able to transfer these ideas in a practical sense in my future endeavors.

I would also like take an opportunity to thank the entire faculty and staff at The University of Texas, and particularly the people in the Department of Civil Engineering. My sincerest appreciation is also extended to other members of my thesis committee: Dr. Md Sahadat Hossain and Dr. Anand Puppala for reviewing this document and for their invaluable advice.

I would like to thank Andrės, Jairo, Claudia, Priya, and all other friends who supported me throughout my journey at UTA.

Finally, and most of all, I express my deepest gratitude to the Lord above for the necessary tools and people which have been crucial in my development and have helped me along my path.

February 17, 2012

ABSTRACT

THE EFFECT OF STRESS AND SUCTION HISTORIES ON
DYNAMIC PROPERTIES OF STATICALLY
COMPACTED SILTY SAND

William Allan Douglas, M.S.

The University of Texas at Arlington, 2012

Supervising Professor: Laureano R. Hoyos

This paper is devoted to the analysis of an experimental study whose intent is to find the effect of the stress/suction history on the dynamic properties of silty sand subjected to small- to mid-strains. The practical application of this study includes determining the effect on soil stiffness properties of an increased soil suction (transpiration of water) followed by loading induced by shallow foundations, and vice versa. Small-strain stiffness properties such as shear modulus, material damping, and shear wave velocity, are important subsoil parameters for proper analysis and design of unsaturated earth structures subject to static and dynamic loading. Traditional soil testing methods are unable to accurately assess this small strain behavior, thereby significantly underestimating the soil stiffness. Currently, a great deal of research efforts are being made to conduct field and laboratory based measurements of soil suction, assessments of soil-water retention properties, and analyses of swell-collapse behavior; however, very few efforts have been focused on small strain response of unsaturated soils and their dynamic characterization at small- to mid-strains.

The overall purpose of this research is to study the dynamic properties of unsaturated soils at very small shear strain amplitudes upon being subjected to various hydro-mechanicalstates via resonant column testing. This research work uses a suction-controlled, proximitor-based resonant column device featuring a PCP-15U pressure control panel that allows for the implementation of the axis-translation technique via the independent and simultaneous control of pore-air and pore-water pressures in the specimen.

A total of three comprehensive experimental series were conducted with varying loading paths. Each series of testing measured the small- to mid-strain stiffness properties of the soil at sixteen different suction and net mean stress states. The three series of suction-controlled resonant column tests were conducted on statically compacted samples of silty sand for a range of suction states between 50 kPa and 200 kPa, and net confining pressures also ranging from 50kPa to 200kPa. Results show the critical role of matric suction and stress/suction histories in the small-strain response of the tested soil.

TABLE OF CONTENTS

LIST OF ILLUSTRATIONS

Figure Page

LIST OF TABLES

Table Page

CHAPTER 1

INTRODUCTION

Civil engineers continue to be challenged by problems associated with Geotechnical infrastructure that remain under partially saturated conditions throughout any given year. The lack of understanding of the behavior of unsaturated soils has resulted in unreasonably conservative designs, construction delays, and deficient long-term performance of road and railway embankments, shorelines, earth dams, and shallow foundations. Traditional soil mechanics idealizes soils as being either in a dry or saturated state; however, a region immediately above the water table is in an unsaturated state. Currently, unsaturated soil mechanics is receiving increasing attention from researchers and practitioners worldwide, thus providing better explanations for soil behavioral patterns than conventional saturated soil mechanics.

Unsaturated soil behavior cannot be predicted using either Terzaghi's effective stress principle or any single stress variable combining pore-air pressure (u_a), pore-water pressure (u_w), and total stress tensor (Aitchison 1961; Bishop 1959; Jennings 1961). Adopting matric suction, ($u_a - u_w$), and the excess of total stress over air pressure, ($\sigma - u_a$), as relevant stress state variables, various features of unsaturated soil behavior have been modeled via suction-controlled oedometer, triaxial, and direct shear tests using the axis-translation technique (Fredlund and Morgenstern 1977, Alonso et al. 1987, Toll 1990, Alonso et al. 1990, Wheeler and Sivakumar 1992, Fredlund and Rahardjo 1993). Since the static/dynamic response of unsaturated soils is known to heavily depend on suction states, the lack of consideration of these suction effects in the small-strain dynamic characterization of unsaturated soils may lead

to erroneous property measurements and, ultimately, faulty and/or excessively conservative designs of earth structures.

Traditional geotechnical testing methods cannot detect this small-strain behavior and, hence, seriously underestimate the true soil stiffness, largely due to inaccuracies in small strain measurements. One of the most dependable and well known testing methods used for assessing dynamic properties of soils at very small strains is the resonant column (RC). This test method requires a special device where a cylindrical specimen is excited torsionally and then sweep at varying frequencies until resonance is found. The shear modulus is ascertained as a function of the resonant frequency of the soil-driver system. The issue of small strain behavior of unsaturated soils under unsaturated conditions is important for engineering applications as it offers the possibility of taking into account the influence of these conditions on key soil parameters, such as stiffness and damping, which effect the performance of geo-structures with regards to soil deformations (Vassallo 2006). The compacted soil, which is a key component of these geo-systems, is normally in an unsaturated state and subjected to small strains; therefore, there is a need for a clearer understanding of the dynamic response of the soil under these conditions. A great deal of research effort has been devoted to field and laboratory based measurements of soil suction, assessments of soil-water retention properties, and analyses of swell-collapse behavior; however, few efforts have been focused on small-strain response of unsaturated soils and the effect of stress/suction history on this response. This research work, which uses the RC device is partly motivated by these needs.

The intent of the current research work is to gain a clearer understanding of the effect of the stress/suction history on the small-strain dynamic properties of unsaturated soils, such as small strain shear modulus (G), shear wave velocity (v_s), and small strain material damping (D). These key sub-soil parameters are vital for an appropriate design and/or analysis of unsaturated soils subjected to static and dynamic loading, as depicted in Figure 1-1. In order to

solve practical geotechnical engineering problems, rational procedures must be based on a complete understanding of the effects of season-dependent suction states (i.e., seasonal variations that include wet-dry or freeze-thaw cycles), coupled with the stresses induced by foundation loads, on small-strain stiffness properties of unsaturated foundation soils. The present work is an attempt to contribute towards this goal.

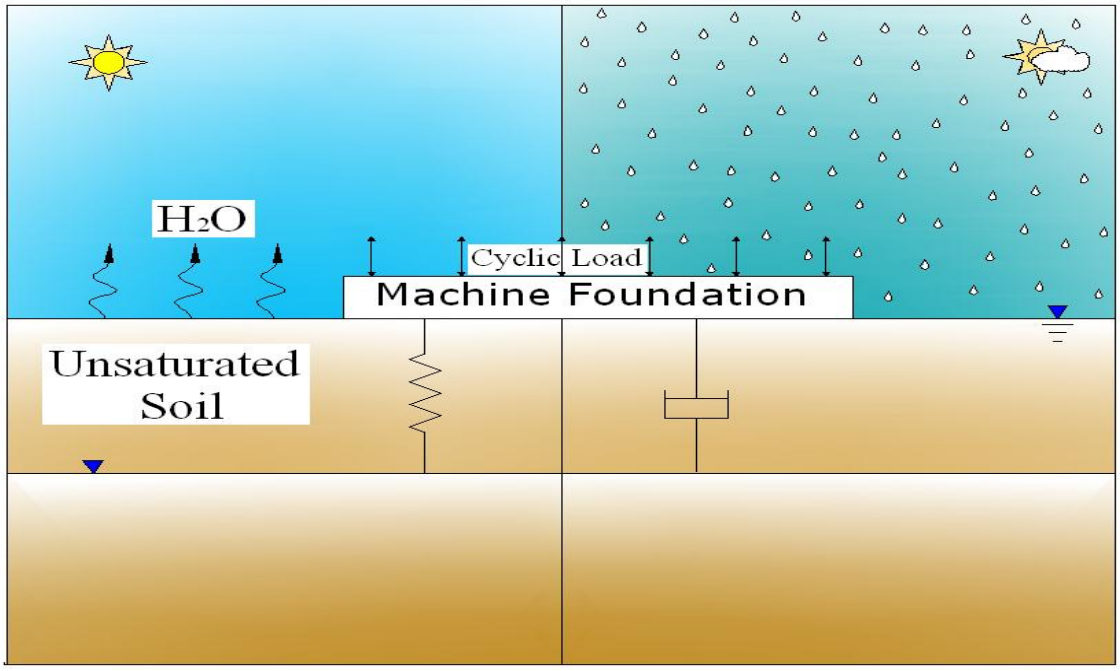

Figure 1.1 Idealization of common unsaturated Geotechnical infrastructure subjected to dynamic loading and seasonal changes in soil suction.

1.2 Research Objectives

The main objective of this research work is to study the effect of stress/suction history on the dynamic properties of unsaturated soils. Specific tasks within the scope of this research work are described in the following:

- To review the literature available on dynamic properties measured via resonant column in partially saturated soils.
- To conduct resonant column tests under suction controlled states to evaluate the influence of stress/suction history over the shear modulus and damping response of compacted silty sand at very small strains.
- To analyze the linear and non-linear behavior of compacted silty sand from very small to small shear-strain amplitude levels, for different suction and net mean stress states.
- To assess the normalized shear modulus, normalized damping and threshold strain as functions of strain and loading path.

1.3 Thesis Organization

A brief summary of the chapters included in this thesis is presented in the following:

Chapter 2 outlines the implications of dynamic properties of soils for engineering purposes. Existing means for measuring shear modulus and material damping of soils in the laboratory are also defined. The essentials of the resonant column, as well as the fundamental concepts of unsaturated soil mechanics and its role in dynamic geotechnical engineering are also incorporated. A brief literature review of current works related to similar goals and findings is also included.

Chapter 3 is dedicated to describing the functioning of the proximitor-based resonant column device. The inherent properties of the soil used in this research program are also defined in this section. Pressure control and monitoring systems for both confining pressure and pore-air pressure are also described as main components of the proximitor-based resonant column device.

Chapter 4 describes Experimental Program I and the testing procedures followed in this first research work. The sample preparation process and the basic properties of the test soil are

also described. A list of all experimental variables is included, as well as a description of the suction/loading paths induced on the specimens prior to resonant column testing.

Chapter 5 describes Experimental Program II and the testing procedures followed in this second research work. A list of all experimental variables is included, as well as a description of the suction/loading paths induced on the specimens prior to resonant column testing.

Chapter 6 describes Experimental Program III and the testing procedures followed in this third and last research work. A list of all experimental variables is included, as well as a description of the suction/loading paths induced on the specimens prior to resonant column testing.

Chapter 7 is devoted to a comparative analysis of all test results from Experimental Programs I, II, and III to assess the effect of stress/suction history on small strain stiffness properties of unsaturated soils.

Chapter 8 includes the summary and conclusions from this research study, and also provides some recommendations for future research work.

CHAPTER 2

LITERATURE REVIEW

2.1 Introduction

This section includes a review of the fundamentals of small-strain stiffness characteristics of soils including their reactions under the influence of partially saturated conditions. A review of methods for calculating these properties in the laboratory is also discussed.

The beginning of this chapter describes the importance of shear modulus, G, and the material damping ratio, D, as dynamic properties. Different ways to calculate their value in the laboratory is also discussed. This chapter also defines the basics of the Resonant Column (RC) test as a part of this research. Elementary definitions and instrument principles are offered in this work. This chapter also covers essential information about unsaturated soil mechanics, including the basic behavior of unsaturated soils and the current procedures intended to measure total suction and matric suction.

The Resonant Column test is the most reliable and most widely used laboratory test for assessing the dynamic properties of soil at low to medium strains. The test is performed by sweeping the frequency spectrum by vibrating a soil or hollow soil column at increasing frequency rates in order to determine its nature mode. The natural mode is defined as the frequency at which the specimen experiences the most shear strain amplitude as a result of torsional excitation. The shear wave velocity is then determined as a function of the resonant frequency.

Lastly, this chapter reviews the recent research works that have assessed the influence of suction levels on dynamic properties of soils. A brief description of the findings from these

previous works is included in this section, and the experimental models to foretell the small-strain shear modulus and damping ratio.

2.2 Importance of shear modulus and material damping ratio

The dynamic response of a soil is characterized by two vital material properties, the shear modulus, represented by G, and damping, represented by D. The shear modulus is the slope of the graph depicting shear stress as a function of shear strain. Figure 2-1 presents the correlation concerning shear stresses and shear strains. At low strain levels, G is high and the curve is naturally linear.

This dynamic soil is termed the low-strain shear modulus (G_{max}). With progressive increases in strain, the curve losing this linear variation and the shear modulus linked to this relationship is termed the secant shear modulus (G_{sec}).

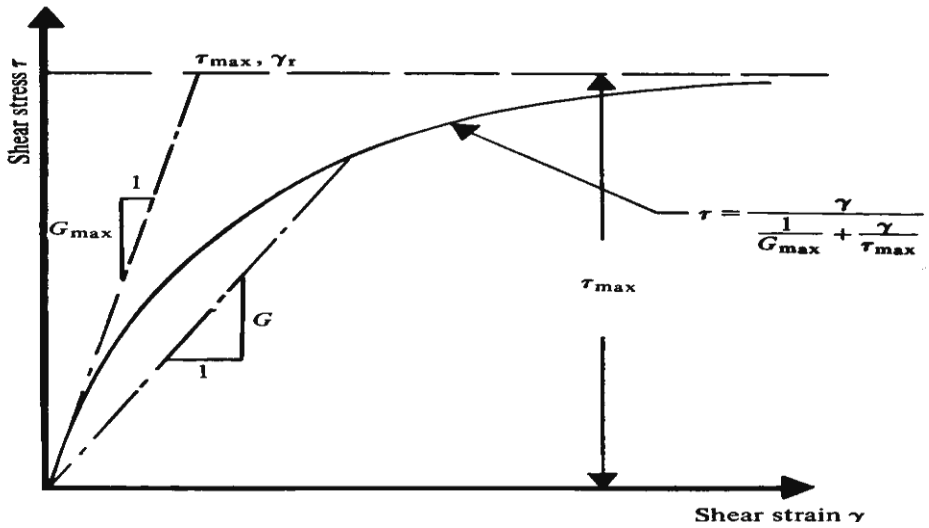

Figure 2.1 Deviation of shear stress versus shear strain (Hardin and Drnevich, 1972)

Shear modulus is essential in the evaluation of many types of geotechnical engineering problems including stability of foundations for superstructures and deep foundation systems, deformations in embankments, dynamic soil structure interaction, protection of structures against earthquakes, and machine foundation design (Gazetas, 1982; Dyvik and Madshus, 1985).

Much attention is being given among engineers both in the application of state-of-the-art technology to practical problems and in research studies of the effects of the seismic excitation on dynamic properties of soil. These ground vibrations are treated as elastic wave propagation since the strain developed is less than 1×10^{-5}.

Seismic wave diminution in soils is a multifaceted phenomenon that is a result of the interface of numerous mechanisms that contribute to the energy attenuation during dynamic excitation. On the other hand, once the seismic excitation has taken place, seismic waves appear to traveling through a soil mass. These wave amplitudes are reduced as waves propagate through an elastic medium. Such reduction is consequence of energy looses in the soil, and that is called “attenuation”.

Numerous explanations have been suggested as a measure of energy dissipation in geological materials of which many are dimensionless. These soils are idealized as isotropic, perfectly elastic, homogeneous, and are evaluated within a small range. In geotechnical earthquake engineering and soil dynamics the factor customarily used as a measure of energy dissipation is the material damping ratio, D. Damping is defined as the correlation concerning the energy dissipated during one cycle, and the maximum strain energy stored during that cycle.

Fields associated with soil dynamic, require the values of shear modulus and the damping ratio for analysis. Since a more thorough and rigorous study and application of geotechnical engineering, most of the practical geotechnical research has been focused on the

area of static behavior. Constitutive models have been accepted based on classical elasto-plastic theories assumptions a part of soil deformation under load is due to elastic deformation of the soil particles. The total deformation is a assumed to be the sum of the elastic and plastic deformations. This elastic distortion is only a small part of the total deformation of the soil. Elastic deformation is often obscured by deformation resulting from slippage, rearrangement, and crushing of particles. Classical elasto-plasticity assumes the elastic and plastic deformations as separated components, which can be experimentally achieved by loading and subsequent unloading process. The recoverable strain is supposed to be elastic, and the total magnitude is the sum of elastic and plastic strain (Takkabutr, 2006). However, in geo-materials, it is not entirely possible to separate the elastic strains by loading. Before exceeding the yield loci, the recovery of strain in soils is assumed to be a result of stored elastic energy; however, the recuperated strains are not always purely elastic. This strain recovery may be due to slippage at particle contacts points.

In soil, there is a variation in the shear modulus with the cyclic shear strain amplitude. The shear modulus is inversely proportional to the cyclic shear strain. Figure 2-2 depicts the stiffness of soil over a large range of strains, from very small to large, and distinguishes approximately between strain ranges. At very small strains, the shear modulus is nearly constant with strain. The shear modulus value conforming to this strain is known as the limiting value G_0 or G_{max}. For small strains, which are generally less than a subjective maximum of about 1%, the tangent shear modulus G is a non-linear function of strain. The large strain zone exceeds 1%, and the shear stiffness is very small as the soil approaches failure.

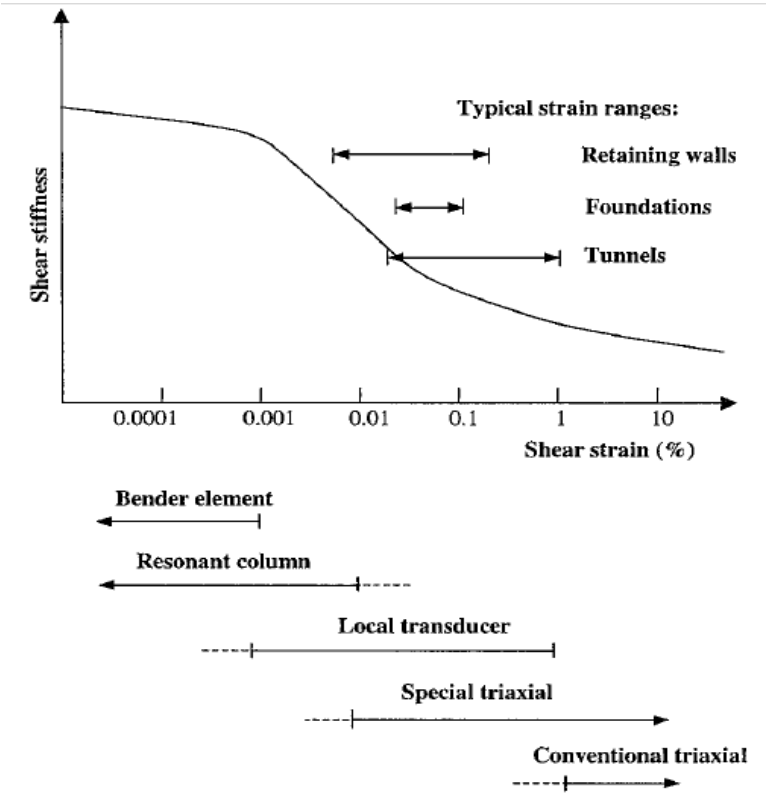

Figure 2.2 Deviation of soil stiffness with increasing shear strain (after Atkinson and Sallfors, 1991; Mair, 1993)

At very small strains, the stiffness is typically reduced and continuously decreases as the state nears the critical state line. The stiffness decreases smoothly in the intermediate small strain range with increasing strain.

2.3 Linear and non-linear behavior

Typically most soils become progressively nonlinear, after a shear strain of 0.001% is exceeded. There is no single reliable method for determining shear modulus and material damping at large shear strain magnitudes, the selected method must account for the level of cyclic strain variations.

The dynamic properties of soil can be sufficiently characterized with shear modulus and damping ratio, when ground motions consist of vertically propagating shear waves coupled with small soil displacements. The nonlinear portion of the stress-strain graph is typically expressed by the secant modulus and the damping correlated to the energy dissipation in one cycle of cyclic loading. Below, Figure 2-3 depicts one cycle of loading where the secant modulus is defined as the proportion concerning maximum stress and maximum strain. The damping ratio is relative to the area ΔE bounded by the hysteresis loop, and relates to the energy dissipated in one cycle of motion.

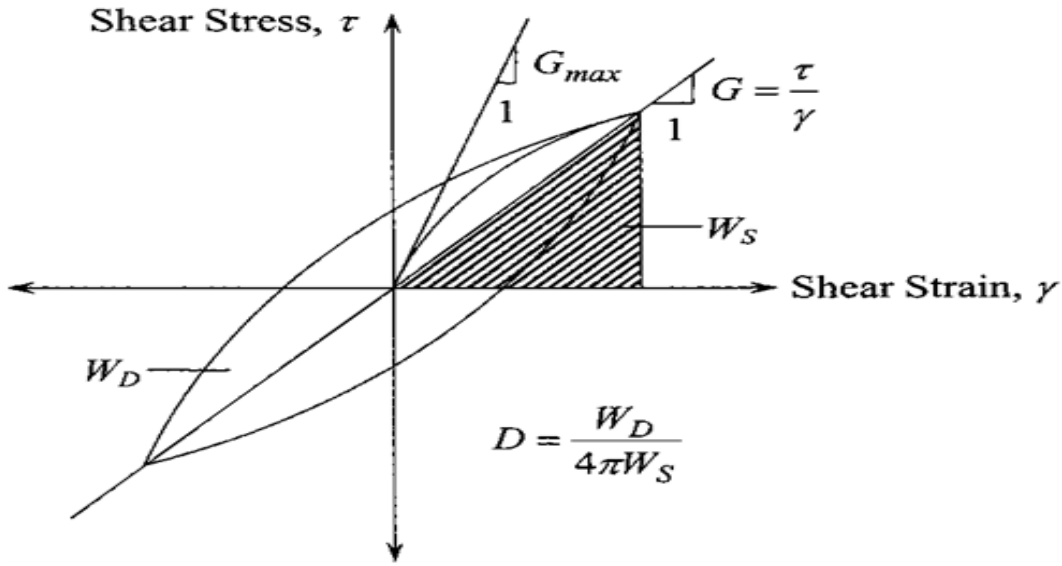

Figure 2.3 Cyclic Loading with varying strains (Assimaki and Kausel, 2000)

Material behavioral models of this style can be characterized by several, parallel elasto-plastic springs, characterized by response parameters attained by fitting the measured data to a best fit curve.

2.4 Techniques for measuring shear modulus in the laboratory

Numerous and varied laboratory techniques are currently used to assess shear wave velocities, shear modulus, and the material damping ratio of soils. Several methods directly calculate shear modulus while others first estimate the shear wave velocity by which shear modulus is calculated. In-situ techniques are used to quantify the dynamic properties of soils, while developing strains within the range of 10^{-3} thru 10^{-4} % and less. These field testing methods are able to achieve measurements at low strains; however, laboratory techniques are more able to manipulate the sample to a more desired precision and set to idealized boundary conditions.

This experiment is focused on laboratory methods for determining the dynamic response of soils; therefore, the following section is devoted to describing these techniques for estimating the dynamic response of soils.

2.4.1 Cyclic Triaxial Test

The Cyclic Triaxial device is used to measure the dynamic properties of soils beginning in the elastic range and continuing into the plastic range, 0.001% and 2% respectively. In order to achieve these strain levels, the loading system must have the ability to apply cyclic sinusoidal loads coupled with deformations ranging between 2 N (0.5 lbf) thru 225 N (50 lbf) coupled with 0.005 mm (0.0002 in.) and 2.5 mm (0.1 in.) of deformations respectively, at rates ranging between approximately 0.1 Hz and 1 Hz. The rates associated with the Cyclic Triaxial device are intended to mimic forces associated with wave action and earthquake analysis, respectively. Throughout testing, parameters such as changes in axial load, deformation and pore water pressure are measured and recorded.

The maximum shear modulus is estimated by carrying out three stages of sinusoidal fluctuating cyclic loading, at the recommended frequency, with five loading cycles being applied

in each stage. In the preliminary stage, the cyclic load applied is approximately ± 0.5 lbf (2 N). The cyclic load applied in subsequent stages is adjusted to obtain a uniform distribution of shear moduli data, G, versus shear strain amplitude, γ, up to a value of about $5x10^{-3}$ percent.

2.4.2 Resonant Column Test

Originally, the resonant column (RC) device was used to determine the dynamic response of rocks. The RC device has been continuously refined to make study the behavior of a multitude of geologic materials. In the 1970's Dr. Stokoe and his colleagues designed a variety of the RC devices. During the late 1970s, Prof. Stokoe and his co-workers developed a new version of resonant column device which had a fixed end. The Stokoe RC testing technique was standardized by the American Society for Testing and Materials (ASTM D 4015-92). This device is the most reliable testing methods used to estimate the shear modulus and damping ratio of soils. Later, Isenhower (1979) implemented a torsional shear appartus to the RC device. The dynamic properties of the soil are determined by applying a series of low frequency cycle to the sample in the torsional shear test.

The Stokoe RC test has a fixed end as well as a free end in which torque is applied. The natural frequency is found by sweeping the frequency spectrum to determine the frequency at which the sample experiences the greatest strain. After the frequency at resonance (f_r) is experimentally determined, the shear wave velocity (V_s) and therefore, the shear modulus (G) of the soil can be calculated. The damping ratio is assessed from the free decay curve or by the hysteresis loop at very low strains. The RC device is used to define the shear wave velocity, shear modulus and damping ratio of soil under varying isotropic pressure, void ratios, and shear strain amplitude, and number of cycles.

2.5 Fundamentals of Resonant Column Testing

Resonant Column (RC) devices have been used since the 1930's to examine soil and rock dynamic performance. Many different versions of the resonant column have been conceived by researches all over the world. The resonant column device was improved by Dr. Stokoe and his colleagues to be a fixed-free cyclic reaction test. It is derived from the one-dimensional wave propagation equation based on the theory of linear-elastic vibration. This limits the resonant column to medium and low strain amplitudes even when the apparatus is capable of measuring larger strains such as up 0.4% (Stokoe et al., 1978).

The resonant column is a fixed-free cyclic torsional device capable of testing solid cylindrical soil specimens or hollow cylindrical specimens. The bottom of the specimen is fixed and sits on a roughly textured base (the suction controlled device contains 3-ceramic disks which allows for water dissipation), while the top is free to rotate and does so by means of a motor (the suction controlled device has a porous stone for air entry or dissipation). The device is depicted below in Figure 2-5.

The test is carried out by applying torsional excitation to the top at constant amplitude and increasing frequency until the frequency at resonance is found, the frequency at which the maximum shear strain experienced by the cylindrical specimen is the frequency at resonance for the given soil as is shown in figure 2-6. This parameter is known as resonant frequency, f_r. According to Stokoe and Huoo-Ni (1985) typical values of resonant frequency for soil samples range from 6 to 150Hz.

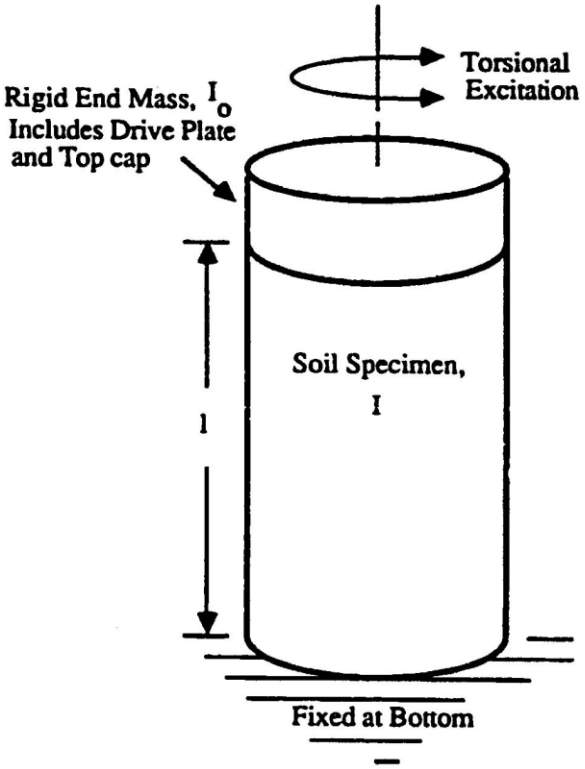

Figure 2.4 Fixed-free Resonant Column Device (from Huoo-Ni, 1987)

The dynamic properties of the soil specimen are derived as a function of the resonant frequency. The dynamic properties of the same soil specimen can change contingent on such variables as moisture content, density, weathering, voids ratio, as well as external variables that impact its variation such as confinement pressure and suction levels.

The damping ratio, D, is determined by the Half-Power Bandwidth, Free-Vibration Decay method, or Hysteresis Loop methods as will be discussed.

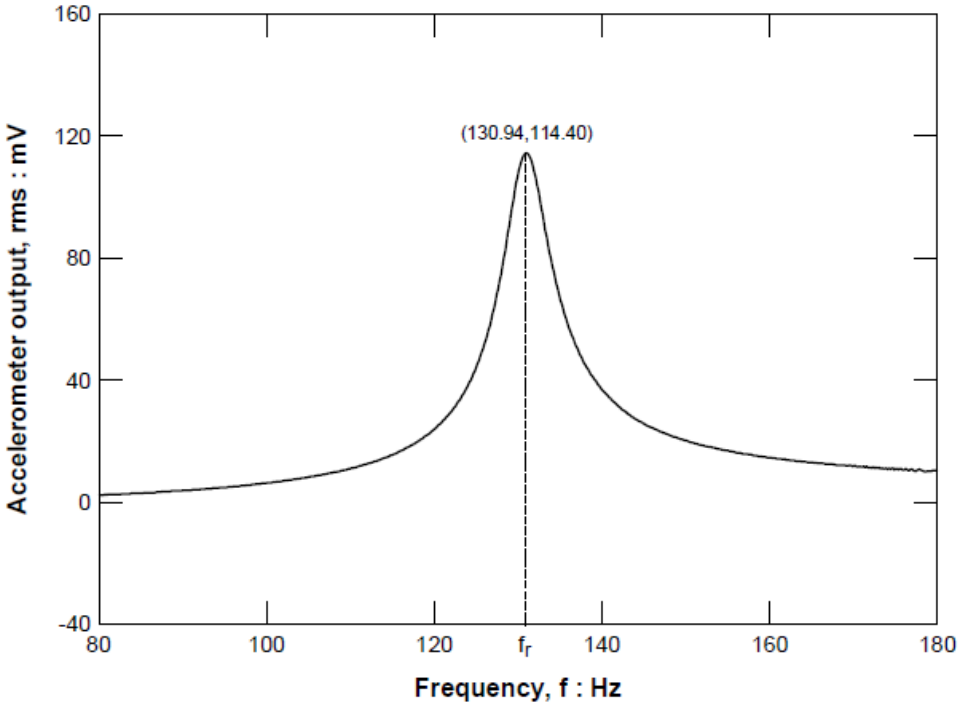

Figure 2.5 Frequency sweep curve from RC test (Takkabutr 2006)

2.6 *Determination of dynamic material properties*

2.6.1 Shear modulus (G)

The RC device is based on the elastic wave propagation theory in which the material is within the perfectly elastic region; therefore, these dynamic properties are assumed to be constant and independent of amplitude and frequency. The threshold limit is used to determine the peak shear strain at which the specimen can be subjected and still be within the elastic region. Dynamic soil parameters lower than this threshold limit, are taken to be independent of strain.

The frequency equation applied to obtain the shear wave velocity, V_S, of an elastic soil column is defined as,

$$\frac{\sum I}{I_o} = \frac{w_r}{V_s} \tan\left(\frac{w_r L}{V_s}\right) \qquad (2.2)$$

Where, $\sum I = I_s + I_m + I_w + \cdots$

I_s = mass moment of inertia of soil column,

I_m = mass moment of membrane,

I_o = mass moment of inertia of top rigid mass (top cap + spider),

I_w = mass moment of central wire (only for hollow samples)

W_r = natural frequency of soil (rad/sec),

L = length of soil sample.

Based on the theory of elasticity, shear modulus, G is then obtained as following:

$$G = \rho(V_s)^2 \qquad (2.3)$$

where,

Vs *is the shear wave velocity*

ρ *is the total mass density of the soils*

A streamlined method for estimating G from the resonant frequency, f_r and geometric characteristics, I_o of the system, was proposed by Richard (1975). He states that when the system is under resonance, equation 2.2 may be rewritten as,

$$\frac{I}{I_o} = \frac{\omega_r L}{V_s} \tan \frac{\omega_r L}{V_s} = \beta \tan \beta \qquad (2.4)$$

$$where,$$

$$\beta = \frac{\omega_r L}{V_s} \qquad (2.5)$$

$$V_s = \frac{\omega_r L}{\beta} = \frac{2\pi f_r L}{\beta} \qquad (2.6)$$

By substituting eq. 2.6. into 2.3

$$G = \rho(2\pi L)^2 \left[\frac{f_r}{\beta}\right]^2 \qquad (2.7)$$

.

$$\frac{I}{I_o} \ll 1$$

β = tan β and from equation 3.3:

$$\beta^2 = \frac{I}{I_o}$$

$$G = \rho(2\pi L)^2 \left[\frac{f_r}{\mathrm{F_r}}\right]^2 \qquad (2.8)$$

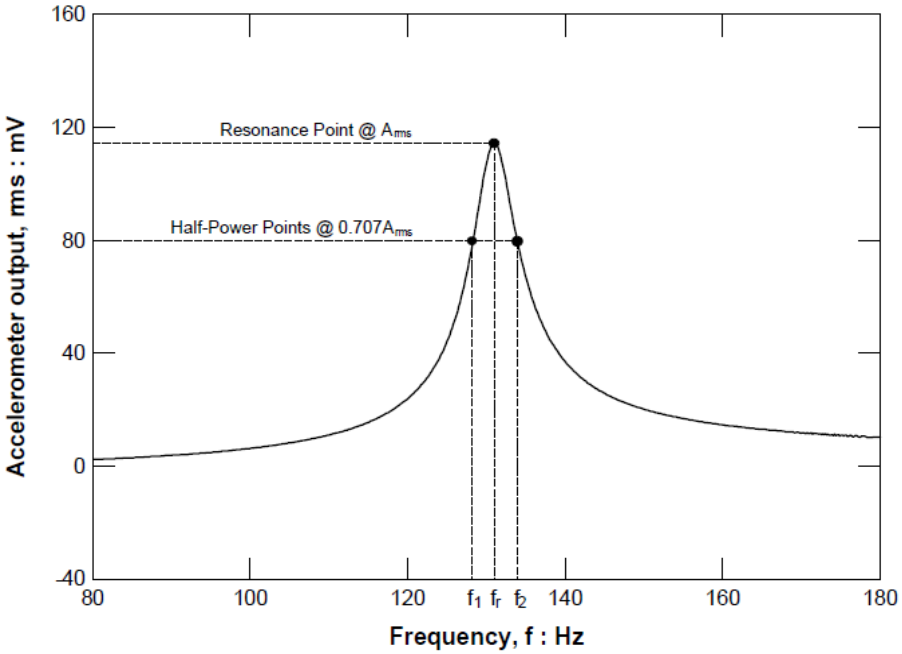

FIgure 2.6 Half-power Bandwidth Method for computation of material damping ratio, D.

F_r is a dimensionless frequency factor. Equation 2.8 was used to assess small-strain shear modulus, G.

2.6.2 Material Damping Ratio (D)

The Half-power Bandwidth Method and the Free Vibration-Decay method were used to estimate the material damping ratio, D_{min} of the soils. The Half-power Bandwidth method determines damping based on the resonant frequency curve. Where the frequencies

corresponding to $\frac{\sqrt{2}}{2} f_r$, both before, f_1 and after f_2 of the frequency at resonance, as depicted in Figure 2-7.

From this curve and following this step, the material damping ratio (D) can be estimated as:

$$\mathrm{D}\ (\%)\ = \frac{1}{2}\ \frac{\mathrm{f}_2 - \mathrm{f}_1}{\mathrm{f}_\mathrm{r}} \qquad (2.9)$$

where,

fr *is the resonant frequency of the system*

The material damping ratio can also be calculated as a function of the decay rate under free vibrations. This technique is known as the Free Vibration-Decay method. As described in Huoo-Ni (1987) and Craig (1981), the free vibration response of soil specimens in the resonant column test normally exhibits under-damped behavior and the general solution to this case is,

$$\theta\ (\mathrm{x}, \mathrm{t}) = \mathrm{Ce}^{-\mathrm{Dw_n t}} \sin(\ w_d t + \ \phi) \sin\left(\frac{w_n L}{V_s}\right) \qquad (2.10)$$

where,

$C\ =\ constant$

$D\ = \frac{c w_n}{2G}$

ϕ *is the phase shift between excitation and the response of the system*

$$w_d\ =\ w_n \sqrt{1 - \ D^2} \qquad (2.11)$$

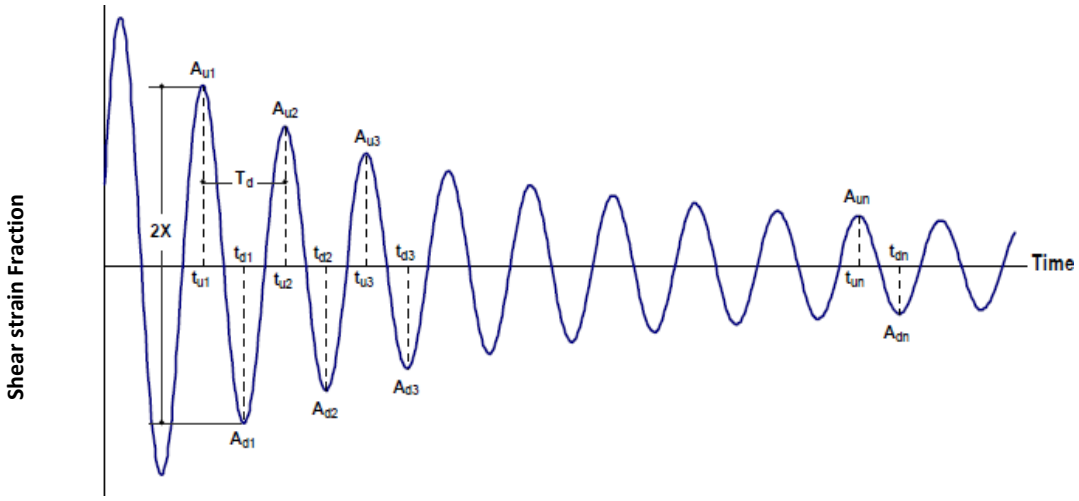

Figure 2.7 Damping ratio using the Free Vibration Decay curve

The relationship between two peaks as depicted in figure 2-8 is given as:

$$\frac{x_n}{x_{n+1}} = e^{-w_n D(t_n - t_{n+1})} = e^{\frac{2\pi D}{\sqrt{1-D^2}}} \qquad (2.12)$$

where,

$$t_n + 1 = t_n + \frac{2\pi}{w_d}$$

δ, *is found by taking the natural logarithm of equation* 2.12.

$$\Delta = \ln \frac{x_n}{x_{n+1}} = \frac{2\Pi d}{\sqrt{1-D^2}} \qquad (2.1)$$

$The\ Damping\ ratio\ is\ now\ calculated\ as$:

$$D = \sqrt{\frac{\delta^2}{4\pi + \delta^2}} \qquad (2.14)$$

Equations 2.13 and 2.14 were used in this work to calculate the material damping ratio, D.

2.6.3 Shear strain (γ)

The shear strain of a solid cylindrical specimen in the resonant column device is a function of the angle of deformation, the distance from the axis, and of the height from the fixed base. The shear strain fluctuates from zero at the center of the longitudinal axis to a maximum value at its outside face as shown in figure 2-9.

The shear strain, γ is determined as follows:

$$\gamma(r) = \frac{r\,\theta_{max}}{h} \qquad (2.15)$$

$where,$

$r\ is\ radial\ distance\ from\ the\ soil\ column\ axis$

$\theta_{max}\ is\ the\ maximum\ angle\ of\ twist$

$h\ =\ height\ of\ the\ specimen.$

An equivalent shear strain, $\gamma_{eq,}$ is required to represent the average shear strain, since the shearing strain is not constant.

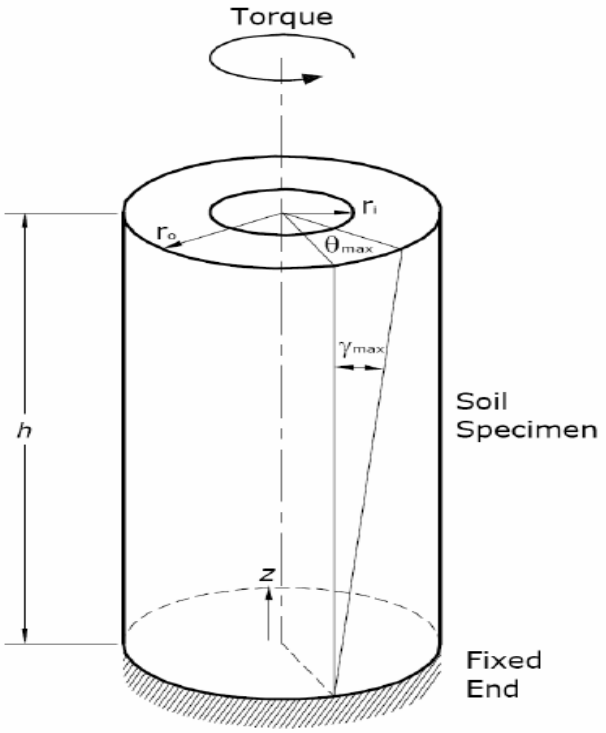

Figure 2.8 Shear strain model for the Resonant Column device, γ. (GCTS RC manual, 2009)

2.7 Essentials of Unsaturated Soil Mechanics

Traditional soil mechanics characterizes the behavior of soils based on saturated or dry conditions. These conventional idealizations estimates positive pore water pressures for those materials beneath the water table and represents the soil as being under fully dry conditions for those soils above water. The shear strength of saturated soils employs Terzaghi's effective stress theory. Yet, the variations in soil strength and volume change are greatly affected by soil suction inherent in unsaturated soils and the effective stress conditions which the unsaturated soil alters. A vast percentage of soils in the field are under partially saturated conditions, and

this behavior must be taken into account. In this section, suction properties, and soil water characteristic curves are detailed.

Saturated soil mechanics has received additional attention recently and there have been many refinements in its modeling and understanding. Some of these changes are related to an increased focus on to the unsaturated soil zone (Vadose zone), which is in a region immediately above the ground water table (Fredlund and Rahardjo, 1993), yet refinement in the understanding of unsaturated soil mechanics has been comparatively slow in contrast to the gained understanding of the behavior of saturated soil mechanics. The concepts for understanding unsaturated soil behavior, are slowly established (Bishop, 1959). Early on, a majority of the focus related to unsaturated soils was associated with to capillary flow (Black and Croney, 1957; Williams, 1957; Bishop et al., 1960; and Atchison, 1967). Their research gave rise to a modeling of effective stress equations for unsaturated soils. In 1977, Fredlund and Morgenstern defined the unsaturated soil with two independent normal stress variables, which are net normal stress ($\sigma_{net} = \sigma - u_a$) and matric suction ($\psi = u_a - u_w$).

The water content in unsaturated soil is a function of the suction in the soil and this relationship can be modeled in a plot of volumetric water content versus suction curve that is known as the soil-water characteristic curve (SWCC). These profiles can be used to understand changes in void and saturation levels in unsaturated expansive soils that are subjected to increased moisture content. Therefore, a more refined understanding of this behavior will lead to a better description in the mechanisms that cause the soil to swell and shrink. Sections 2.6.1, 2.6.2, and 2.6.3 describe various properties of unsaturated soils, suction measurement techniques, and fundamentals of soil-water characteristic curve, respectively.

2.7.1 *Partially saturated soil profile*

The unsaturated region can be separated into three subzones: the capillary fringe, the intermediate (Vadose) zone, and the soil water zone as depicted in Figure 2-12. The unsaturated zone can vary contingent on the type of soil encountered. The saturated zone is located below the ground water table in coarse materials, and the saturated zone can reach higher levels than the ground water table in soils consisting of fine material due to capillary forces (Bear, 1979). The precise extent of the capillary zone hinges on such parameters as the grain size distribution, the soil density, and the soil stratigraphy. The unsaturated (Vadose) zone is located above the saturated part of the capillary zone (Bear, 1979).

2.7.2 Matric suction

The matric suction is defined as the difference between the pore-air pressure, known as u_a, and the pore-water pressure, u_w (Fredlund and Rahardjo, 1993). The suction, signified as (u_a-u_w) is linked to tension in the capillary spaces of the pore water, and water absorption forces of the soil particles. These forces of them related to the geometric arrangement of the soil (Department of the Army USA, 1983; Lu and Likos, 2004). The matric suction may change dependent on fluctuations in weather and surrounding ecological variations. Therefore, the dry and wet seasons create changes in the suction profile, mainly close to the surface (Fredlund and Rahardjo, 1993). Furthermore, field factors such as ground surface conditions, environmental conditions, vegetation, water table, and permeability of soil play an important role on the suction variation into the soil profile.

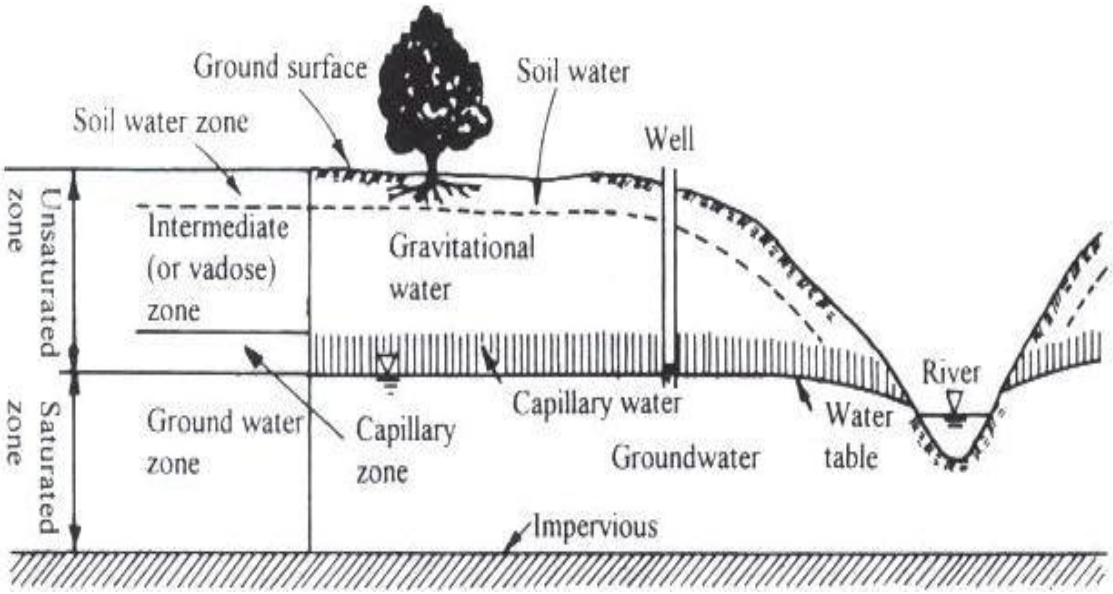

Figure 2.9 Unsaturated soil profile (Bear, 1979)

Ground surface condition: Dry and wet seasons cause changes in the ground water table and in turn the suction, particularly near the ground surface. In field conditions, suction beneath a covered ground surface is more constant with time than beneath an uncovered surface (Fredlund and Rahardjo, 1993).

Vegetation: The existence of plants on the ground surface may cause tension to develop in the pore-water as much as 1-2 MPa because of the evapotranspiration process. Evapotranspiration removes water from the soil near the surface and consequently leads to an increase in the matric suction. The evapotranspiration rate is the function of climate, the type of vegetation, and the depth of the root zone (Fredlund and Rahardjo, 1993).

Water table: The depth of the ground water table affects the scale of the matric suction. The deeper the water table, the higher the possible matric suction (Fredlund and Rahardjo, 1993).

Permeability of the soil profile: The hydraulic permeability of the soil denotes its capacity to drain and conduct water. This indicates the ability of the soil to change matric suction as the environment changes (Fredlund and Rahardjo, 1993).

2.8 Previous Works

There have been numerous studies which are focused on modeling the dynamic response of soils (e.g., Richart et al. 1970; Seed and Idriss 1970; Hardin and Drnevich 1972b; Iwasaki et al. 1978; Lee and Finn 1978; Zen et al. 1978; Kokusho et al. 1982; Seed et al.1986; Ni 1987; Sun et al. 1988; Vucetic and Dobry 1991; Ishibashiand Zhang 1993; Rollins et al. 1998; Vucetic et al. 1998; Stokoe et al. 1999; 2001). This research agreed that the overriding element tied to G/G_{max} includes mean effective confining stress (σ'), soil type, shear strain magnitude γ, and plasticity index (PI). Other elements contributing to changes in G/G_{max} include: degree of saturation, frequency of loading, overconsolidation ratio, void ratio, grain characteristics, and number of loading cycles (Darendeli 2001).

Much of the research that has been conducted on unsaturated soils has been focused on gaining a clearer understanding of the influence of both degree of saturation and capillarity on the small-strain stiffness properties. Recently, Mancuso et al. (2002) and Vasallo et al. (2007) performed a series of suction-controlled resonant column/torsional shear tests on unsaturated silty soil using a RC. This apparatus was developed at the University of Napoli, Italy. The matric suction, was induced by the axis-translation technique, while the torsional torque was progressively increased to study soil stiffness response at small, mid, and high-shear strain amplitude levels.

The literature review will focus on three papers which are most closely related to the current research. These papers include: ‘Effects of Net Stress and Suction history on the

Small Strain Stiffness of a Compacted Clayey Silt' (Vassallo et al. 2007); 'Small Strain behavior of a Silty Sand in Controlled-Suction Resonant Column – Torsional Shear Tests' (Mancuso et al. 2002); and 'Development of a Suction-Controlled Resonant Column Apparatus with Self-Contained Bender Elements' (Suescun 2010).

The work of Mancuso et al. (2002) was conducted in an attempt to model the effect of moisture content on a sample subjected various suctions. Shear stiffness measurements had also been taken during constant-suction tests.

Additional research on unsaturated soil was conducted by Vassallo et al. (2007) which modeled the small strain stiffness response of unsaturated soil based on the consolidation ratio of a clayey soil. This work attempted to model the effect of suction and compaction variables on the initial shear modulus of soil and volumetric state. This research work included suction controlled triaxial and resonant column devices. This study also found that the sample undergoes a significant increase of irreversible strains when it is subjected to a suction beyond the maximum past value.

The work of Suescun (2010) has led to a clearer understanding of the effect of varying suction on compacted silty sand. His work introduced a suction controlled proximitor resonant column device with bender elements. His research also compared the dynamic properties found from the proximitor RC test with results in a traditional accelerometer based resonant column device, as well as the results from the bender elements found on the proximitor RC device. Before initiating the series of tests on this new device, Suescun calibrated the proximitor RC device. This same equipment was used for the present research project; therefore, the resonant column device did not require additional calibration. This device utilizes a pressure control panel which allows for individual application and simultaneous measurement of both pore-water and pore-air pressure, which allows for implementation of the axis translation technique. This apparatus features a set of self-contained bender elements for simultaneous testing of small-

strain stiffness properties under both techniques, though the current research project did not utilize this feature.

Suescun's work also included the same soil that was used for the current research work. A comprehensive series of pressure plate, resonant column, and bender element tests undertaken in his research work have been used to devise empirical correlations between small-strain stiffness properties, such as shear modulus and material damping, and key environmental factors, such as matric suction state and net mean stress, for compacted silty sandy soil.

The current research project differed from previous works in that the effects of the stress/suction history of the soil on the G/G_{max} and D/D_{min} were studied. The range of experimental variables selected in this work, as well as the scope of the experimental program, has been intended to reproduce in situ stress states and loading paths at pre- and post-construction stages in shallow foundation and subgrade systems that remain under partially saturated conditions throughout any given year.

CHAPTER 3

TEST SOIL AND RESONANT COLUMN APPARATUS

3.1 Introduction

This chapter details the properties of the soil used in the current research. This soil was previously analyzed by Suescun and was classified as yellow compacted silty sand. The characteristics of the soil are detailed, including the general engineering properties of the soil, as well as the soil water characteristic curve. This chapter also contains a detailed description of the proximitor based-resonant column. All main components such as main cell, driver system, measurement digital sensors, and software capabilities are presented. Each feature is meticulously described and categorized. Further in this chapter, steps for sample preparation will be discussed. As previously mentioned, this device had previously been calibrated and therefore did not necessitate further adjustment.

3.2 Properties of Test Soil

3.2.1 Basic engineering properties

The test soil used in this effort was classified as fine-grained silty sand which has a dark rusty yellow color. The soil classifies as A-2-4 and SM according to the AASHTO and USCS, respectively.

The sieve analysis specified particle sizes varying between 11mm and 0.08mm, which indicates that the soil has the behavior of a granular soil. The fine percentages ranged between 25% and 35%, whereas the percentage of sand varied from 65% to 75%. The normal water content ranged from between 24% and 29%, with an average of 26.5%, a liquid limit (LL) of 26.4%, and a plasticity index (PI) of 6.2%. The total unit weight was 16.7 kN/m^3, and the dry unit

weight was 13.1 KN/m^3. The specific gravity was estimated between 2.71 and 2.72, and the void ratio was estimated within a range of 1.0 to 1.10 for the soil at this density.

Table 3.1 General Soil Properties and Classification

Property	Value / Result
Color	yellow
Moisture content (%)	26.5
Passing No.200 sieve (%)	30
Specific gravity (G_s)	2.71
Liquid limit, LL (%)	26.4
Plastic Index, PI (%)	6.2
Total unit weight, γ (kN/m^3)	16.7
Void ratio	1.05
AASHTO classification	A-2-4
USCS classification	SM

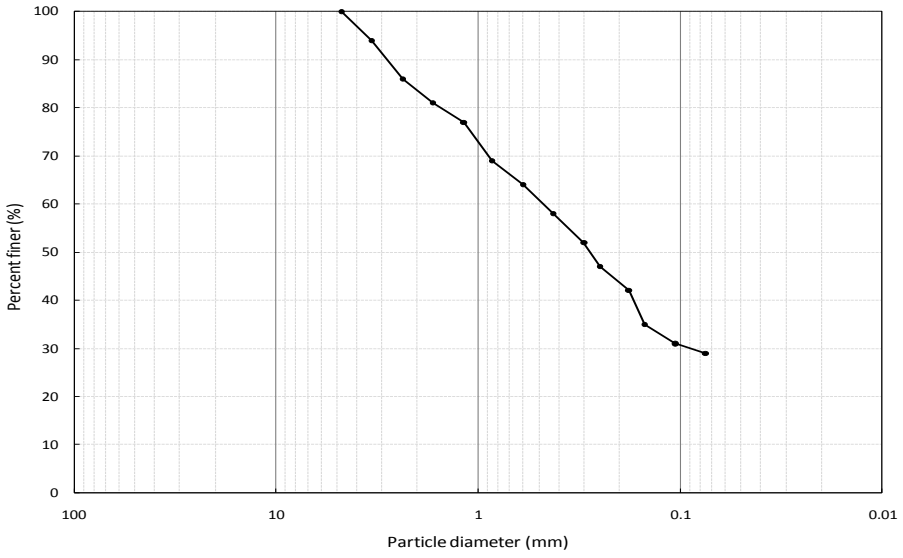

Figure 3.1 Particle-size distribution curve for SM soil

3.2.2 Soil water characteristic curve

The soil water characteristic curve of a soil correlates the moisture content with the associated matric suction in the soil (Fredlund and Rahardjo, 1993). The graph was reported by Suescun (2010), and was used in this research in which precisely the same soil was used. Suescun obtained the SWCC for the soil via a pressure plate extractor device by applying axis translation technique. Nine (9) samples of identical dimensions and weights were placed inside the pressure plate vessel and over the ceramic plate. The experimental points of the SWCC curve were deduced by applying nine different suction levels. The values of matric suction varied between 0 and 800 kPa, as shown in figure 3-2.

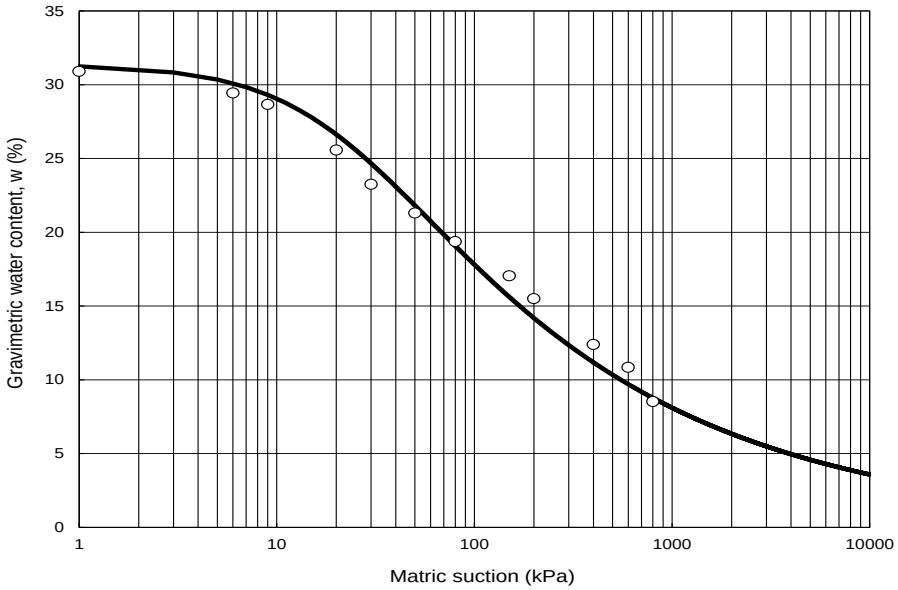

Figure 3.2 SWCC of silty sand

The selected range of matric suction states used for testing SM soil is from 50 kPa to 400 kPa, due primarily to two factors : the air-entry value of the ceramic disk being approximately equal to 15 kPa; the residual volumetric water content corresponding to the suction value was nearly 6000 kPa,.

3.3 Components of Proximitor-Based Resonant Column device

The Proximitor-based Resonant Column Device that was used for the current research has been refined to a point that the testing is fully automated. Testing is made possible by the use of highly sensitive and advanced sensors as well as digitized electronics and computer software programs make testing an automated process.

The device applies a cyclic torsion to the free end of the cylindrical sample by means of a computer controlled torsional motor. The load applied is a harmonic torque with constant amplitude. This load is applied at varying frequencies while the specimen's response is measured. The shear wave velocity is a function of the frequency at resonance, which is the frequency which causes the greatest shear strain. Thereafter, shear modulus was attained from the velocity of the shear wave and the density of the soil. As discussed in chapter 2, the material damping ratio can also be obtained by two different methods. The material damping ratio can be determined both by using the logarithmic decay curve, which measures energy attenuation once the torque is no longer applied, or by the Half-Power bandwidth method. The Hysteresis loop method for determining material damping can only be utilized when the specimen is subject to small-strains.

This system has the capacity of measuring the shear modulus ranging from very low strains to high strains. Figure 3-3 depicts the Proximitor-based RC used in the current research. The Proximitor-based RC testing system has five main components: (a) main cell, (b) servo

controller and acquisition system, (c) resonant column software, (d) gauge deformation sensor, and (e) computer unit.

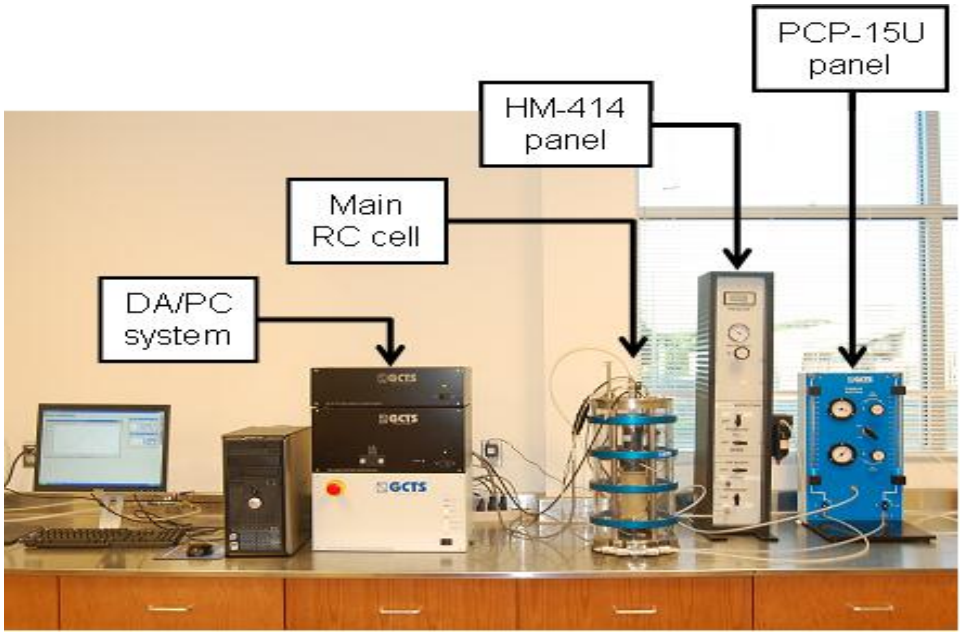

Figure 3.3 General layout of the proximitor-based RC device

3.3.1 Resonant Column main cell

The principal assembly for the main cell used four stainless steel columns, of which two were used as the base shaft for the gauge displacement sensor and motorized drive system. The cell consists of a ¾ inch thick transparent reinforced acrylic plastic. The cell wall has a 1,000 kPa maximum isotropic confining pressure capacity. Numerous connections bridge the specimen to the computer for the application of torque and for data acquisition. The top and bottom of the main cell have a drainage system, which will be discussed subsequently in this chapter. These connections were arranged to regulate the flow of water out of the specimen,

and to allow for isotropic pressure, and to allow for direct air pressure into the sample. The main cell assembly is depicted below in Figure 3-4.

Figure 3.4 Proximitor-based RC Main cell

The proximitor measures the internal angular displacement that the specimen experiences due to harmonic torsional loading. The Proximitor was mounted by means of a stainless steel guide which was fixed to the top cap of the main cell. The circular ‘target’ was fixed to the free end of the specimen top cap and spins slightly back and forth along with the cyclic torsional loading.

3.3.2 Proximitor Mount

The signal is sent to the digital servo-controlled and acquisition system which processes these angular changes to assess the shear strain. The proximitor is a SR-DF-FO-250 fiber optics

deformation sensor with dual range output +/- 0.1 mm low range and +/-6.0 mm high range with 0-15 kHz flat frequency response. The Proximitor mount is shown in Figure 3-5 below.

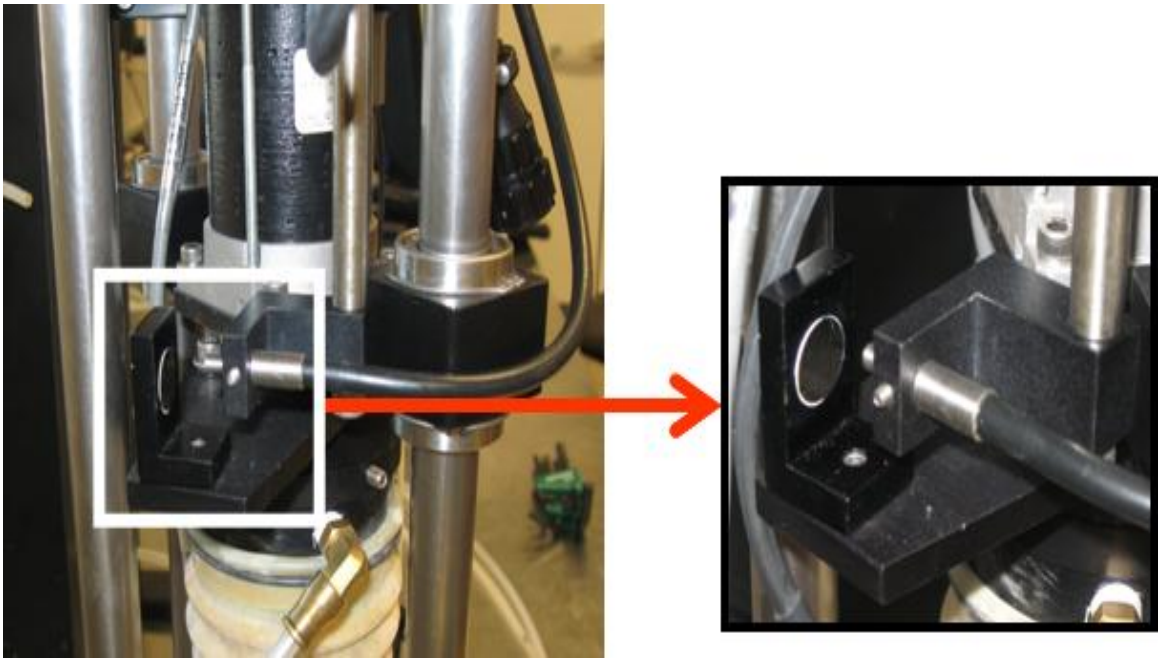

Figure 3.5 Detailed picture of Proximitor mounting (internal angular displacement transducer.

3.3.3 Digital servo controller and acquisition system

The digital servo-controlled and acquisition system (also known as GCTS SCON-1500 Digital System Controller) comprises numerous digital electronics. The settings and configurations are operated by the software. The system is capable of controlling, activating, and storing, angular and vertical displacement data.

The SCON-1500 model DA/PC contains a microprocessor based digital servo controller, data acquisition, function generator, and a digital I/O unit. There is also software for data

reduction and monitoring the performance of the resonant column tests which allow for the automatic calculation of shear strain, shear modulus, and damping ratio at shear strains ranging from 10% to 10^{-4}%. The signal conditioning mother board accepts up to eight universal signal conditioning module slots.

3.3.4 Resonant column software

The Proximitor-based RC software is compatible with numerous resonant column devices. The software has the capability of determining the dynamic response of the soil specimens. It does so by graphically assessing the resonant frequency and by determining the damping from the free vibration decay data. The system is named CATS-RC.

The following are results that were measured by CATS-RC.

a) Resonant frequency (Hz)
b) Shear wave velocity (m/s)
c) Shear modulus (MPa)
d) Maximum shear strain (fraction)
e) Damping ratio-Free vibration decay (%)
f) Predominant frequency from Free vibration data FFT Analysis
g) Damping ratio-Half power bandwidth (%)
h) Natural frequency –from resonant frequency and free vibration decay (Hz)
i) Natural frequency –from resonant frequency and phase shift (Hz)
j) Natural frequency –from FFT frequency and free vibration decay (Hz)

Figure 3-6 below depicts a typical Windows software application environment. The starting frequency, stop frequency, cycles until steady state is reached, coupled with soil and specimen properties are input into the software. These are the only input data required to allow

for automatic calculation of the above parameters without user intervention. When the testing is completed, the CATS-RC calculates the parameters and the user can import and save a substantial data set for each test. The software also provides the forced vibration data, as well as the free vibration data of the specimen, from which the damping was determined.

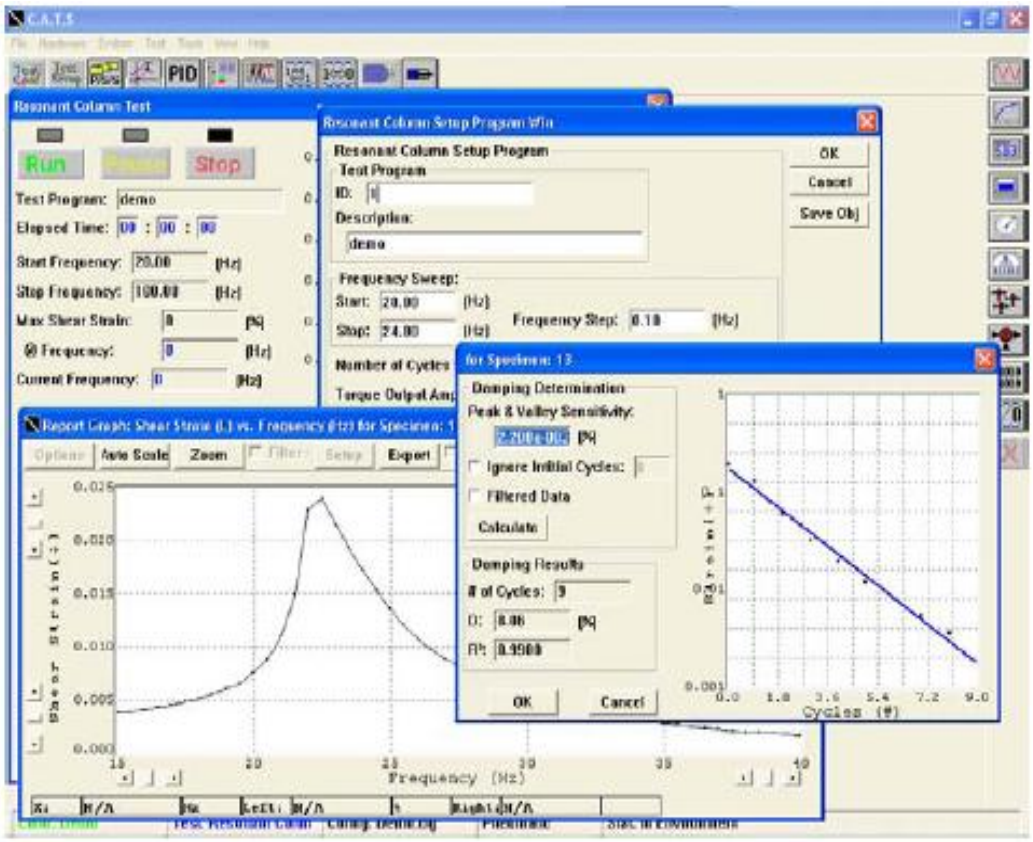

Figure 3.6 CATS-RC Windows sofware display

3.4 Pressure control monitoring system

3.4.1 Pore-air pressure control

The external and pore-air pressure conditioning of the sample are regulated by two pressure panels: The HM-414 and thePCP-15U. The HM-414 model pressure panel controls

the external confining pressure and is depicted on the left in Figure 3-7. The pressurized air is introduced by the inlet air-pressure port which is positioned on the cover plate of the main cell. As previously mentioned the acrylic cell was designed to withstand a maximum air pressure of 1000 kPa.

The PCP-15U model pressure control panel, depicted on the right in Figure 3-7, is used for application of pore-air pressure u_a at the top of the soil specimen via dual pressure regulators and gauges for the application of the matric suction; $s = (u_a - u_w)$; $u_w = 0$. The panel has a flushing mechanism to remove the air that has diffused into the compartment underneath the 5-bar HAVE ceramics located on the bottom pedestal.

Figure 3.7 Pressure control panels

3.4.2 Pore-water monitoring system

The pore water pressure is allowed to dissipate via three ceramic disks mounted within the rough surfaced bottom pedestal, shown in Figure 3-8a. Three coarse porous stones are also located on the top cap (Figure 3-8b) and are used to introduce air pressure into the specimen,

which in turn induces a target matric suction in the unsaturated soil specimen. This is done so by increasing the air pressure while keeping the pore=-pressure under atmospheric conditons. This technique is termed the axis translation technique. The choice of an air entry value for the HAE (High-Air-Entry) ceramic disk for testing unsaturated soils is principally based on the maximum value of matric suction expected to be applied during that test. In this work, the samples were subjected to a maximum suction of 200 kPa; therefore, 7.65mm height, 16.95 mm diameter, 5-bar HAVE ceramics, manufactured by GCTS was chosen for this experiment.

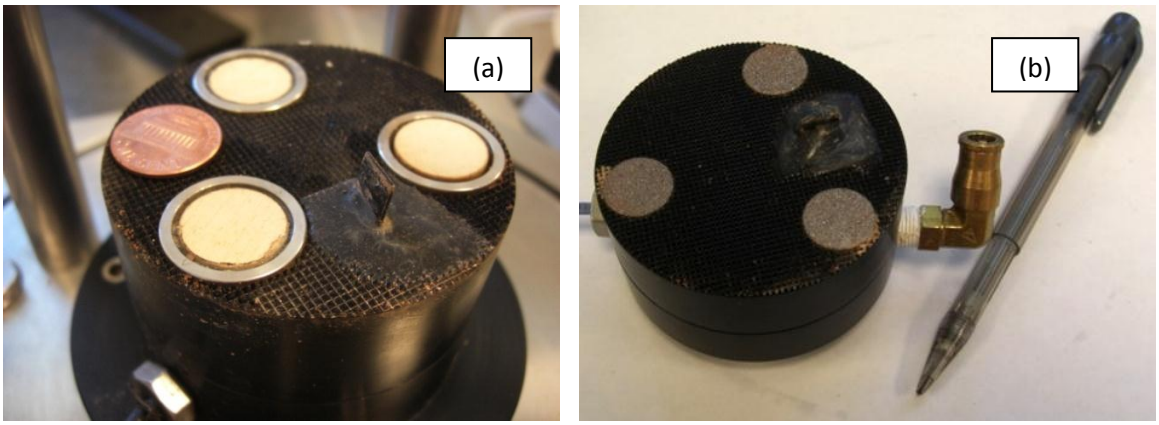

Figure 3.8 Bottom pedestal and top cap: (a) HAE ceramic disk at bottom pedestal, and (b) porous stones and tubing conector at top cap.

3.5 Sample preparation

Samples were statically compacted into a 130-mm height, 70-mm diameter, split mold. A monotonic force was delivered via a triaxial loading frame. Samples were prepared by using three lifts with a constant compaction displacement rate of 1.0 mm/min (Venkatarama and Jagadih 1995).

The sample was prepared by using a cylindrical stainless steel mold shown in Figure 3-9. The mold was filled with 902 g of silty sand, which was added in three layers, then placed on

the triaxial loading base as depicted in Figure 3-9. A steel cap is placed on top of the specimen and leveled, and finally the load is applied.

Figure 3.9 Cylindrical mold mounted on Triaxial Loading Frame

Once the sample is compacted, the mechanism was stopped and was allowed to sit for one minute to minimize a rebound effect. The specimen was then extruded from the stainless steel mold and placed within the resonant column main cell to be tested.

CHAPTER 4

EXPERIMENTAL PROGRAM I: VARIABLES, PROCEDURES AND RESULTS

4.1 Introduction

The initial series of testing sought to assess the dynamic response of compacted silty sand while reproducing the effect of the soil first being subjected to loading (e.g. a machine foundation) then being subjected to an increase in suction due to a loss in moisture. This moisture loss can be attributed to drying from seasonal moisture variations. One of the intents of the research project was to assess how the small strain stiffness properties of the soil were affected by the stress/suction history (hydro-mechanical path). An overview of the stress paths are depicted below in Figure 4-1. The ranges of the experimental variables are summarized in table 4-1.

4.2 Test procedure and stress/suction paths prior to RC testing

The testing began with the assembly of the resonant column device, after which isotropic pressure was applied using the HM-414 panel. The initial suction in the compacted soil begins at approximately 20kPa at moisture content of 26.5% (see Figure 3-2); therefore, a confinement (p) that is greater than the initial suction was required outside of the specimen for the first series of testing. The axial deformation is monitored to assess whether the specimen is set for another pressure increase. Once the sample has achieved 90% consolidation, the next pressure increment is added. The pore-air pressure at that point was increased with the PCP-15U panel until the desired suction state is attained (Fig. 4-1). The external confinement was adjusted accordingly for the purposes of maintaining the constant desired net confining pressure, (p_a-u_a).

When the chosen stress/suction state was attained, the pore fluids are then allowed to equalize. This process took an average of 8-days to complete for each test. The dynamic response of the soil was then tested by using 1-pfs (100 N·m cyclic torque); thereby, assuring that the specimen's elastic boundary has not been exceeded, which could lead to misrepresentative data in subsequent stress/suction states induced on the same sample. The frequency of the cyclic torque was swept from 75 H_z (on average) sweeping to 250 H_z (on average). This was done to obtain the frequency response curve. These curves are depicted as the change of the shear strain fraction (cm/cm) as a function of the frequency (H_z) with given constant torque amplitude.

As the test terminates, the cyclic torque is cut off and the free torsional vibration of the specimen was plotted, thus obtaining the logarithmic decay curve for the assessment of material damping. The attenuation of shear strain was presented in terms of shear strain fraction (cm/cm) as a function of time (sec).

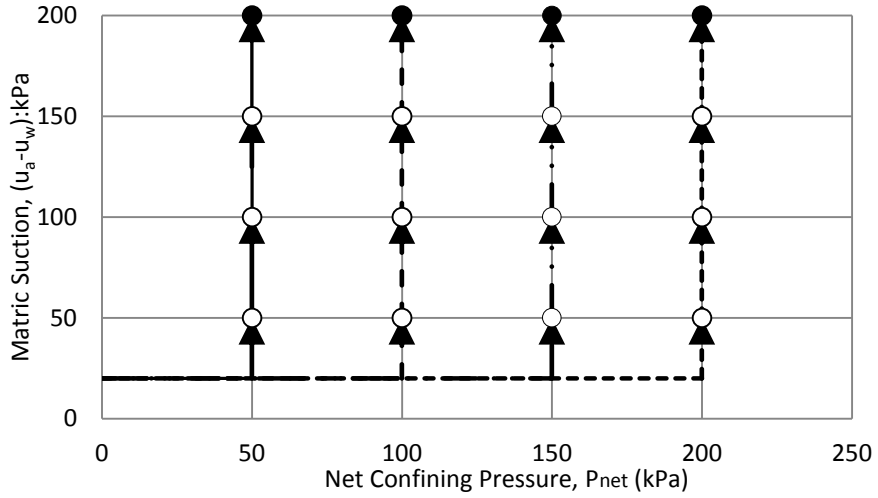

Figure 4.1 Stress paths induced on silty sand specimen during Experimental Program I prior to RC tests.

In the final stage of testing (matric suction = 200kPa) for each constant net confinement pressure testing series, the non-linear dynamic response of the specimen is assessed for various torque amplitudes ranging from 1-10pfs (100 N·m to 1000 N·m). This ensures that the load path has breached the elastic boundary for each subsequent testing phase, thus necessitating the preparation of a new sample for the next series of testing.

Table 4.1 Experimental variables used for RC Testing during Experimental Program I

Variable description	**Number of variables**
Soil type	Silty Sand (SM)
Confining pressure, p	50 kPa 100 kPa 150 kPa 200 kPa 250 kPa 300 kPa 400 kPa
Net confining pressure, ($p-u_a$)	50 kPa 100 kPa 150 kPa 200 KPa
Matric suction (u_a-u_w)	50 kPa 100 kPa 150 kPa 200 kPa

The same test procedure was repeated for suction states, $s = (u_a - u_w) = 50$, 100, 150, and 200kPa, on the same sample, at constant net confining pressure, $(p - u_a)$. This identical test sequence was followed in testing SM soil samples at constant net confining pressures of $(p\text{-}u_a) = 50$, 100, 150, and 200kPa, as illustrated in Fig. 4.1. The following sections summarize all the experimental results from Experimental Program I.

4.3 Test Results from Experimental Program I

Figs. 4.2 through 4.5 show the frequency response curves and free-vibration decay curves from RC tests conducted at matric suction, s = 50, 100, 150, and 200kPa, respectively, under a constant net confining pressure, $(p\text{-}u_a)$ = 50kPa. All tests were conducted with a 1-pfs input torque.

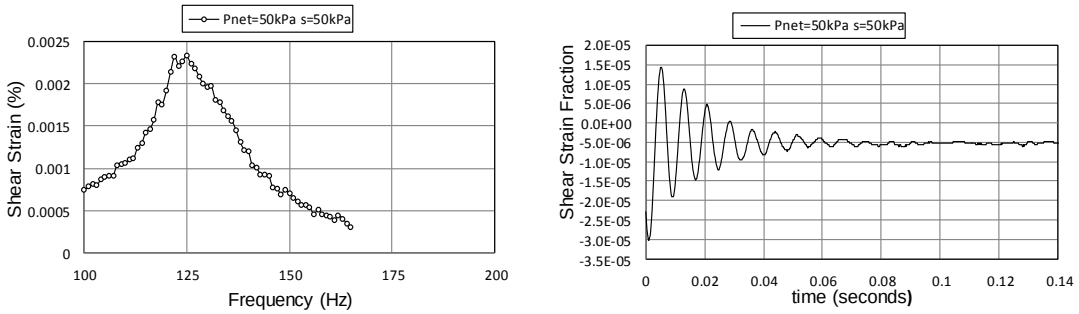

Figure 4.2 SM Soil Response at 1-pfs torque: $(p\text{-}u_a)$ = 50kPa, s = 50kPa

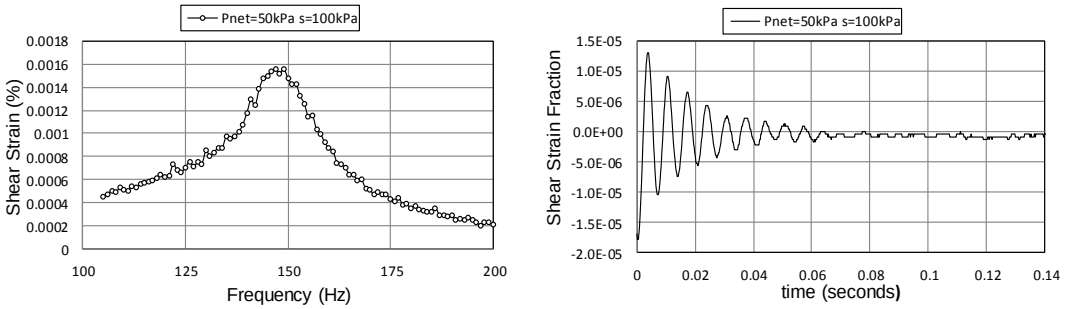

Figure 4.3 SM Soil Response at 1-pfs torque: $(p\text{-}u_a)$ = 50kPa, s = 100kPa

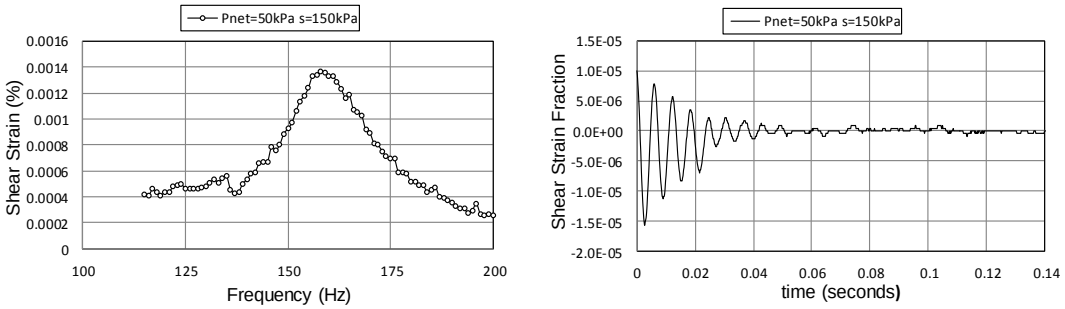

Figure 4.4 SM Soil Response at 1-pfs torque: $(p\text{-}u_a)$ = 50kPa, s = 150kPa

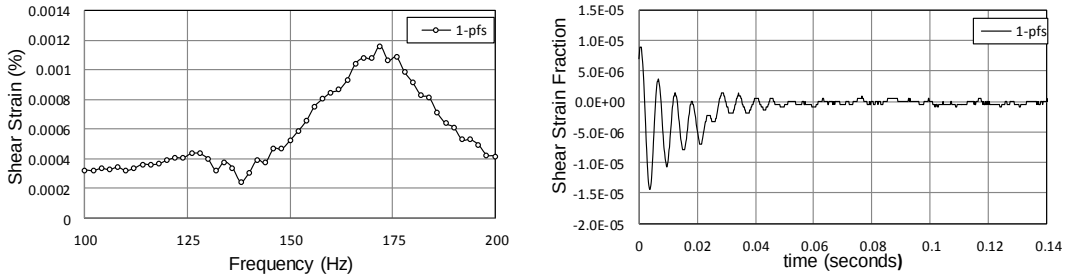

Figure 4.5 SM Soil Response at 1-pfs torque: (p-ua) = 50kPa, s = 200kPa

It can be observed that the resonant frequency increases with increasing matric suction. Qualitatively, this ensures an increasing shear modulus with increasing suction, as the resonant frequency is directly proportional to shear modulus in shear modulus calculations. This can be attributed to an increase in tensile forces between soil particles from increased matric suction, thereby causing closer contact between soil particles and stiffer material.

Figs. 4-6 through 4-14 show the frequency response curves and free-vibration decay curves from RC tests conducted at matric suction, s = 200kPa, net confining pressure, $(p\text{-}u_a)$ = 50kPa, and 2, 3, 4, 5, 6, 7, 8, 9, and 10-pfs input torque, respectively.

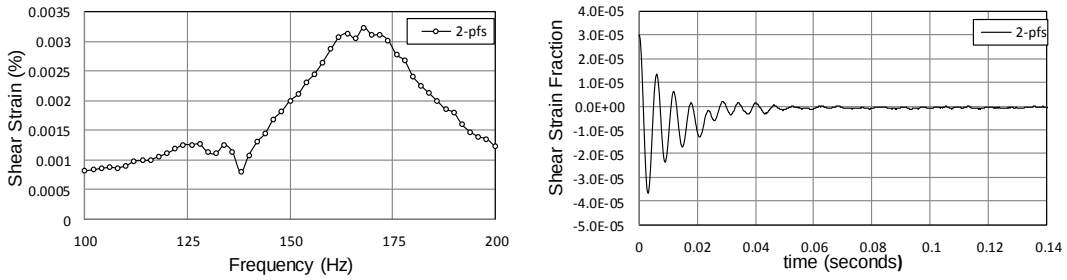

Figure 4.6 SM Soil Response at 2-pfs torque: $(p\text{-}u_a)$ = 50kPa, s = 200kPa

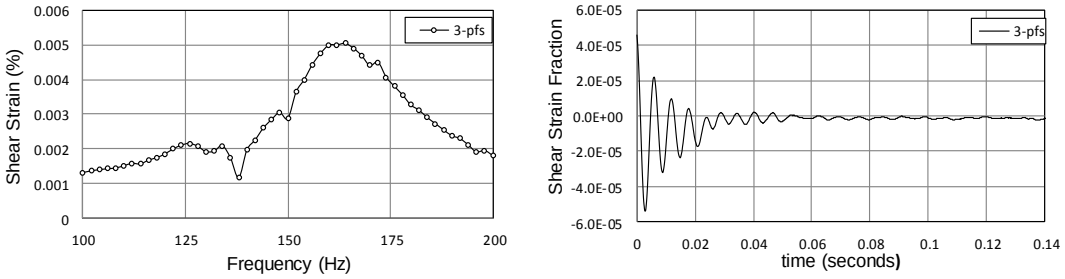

Figure 4.7 SM Soil Response at 3-pfs torque: $(p\text{-}u_a)$ = 50kPa, s = 200kPa

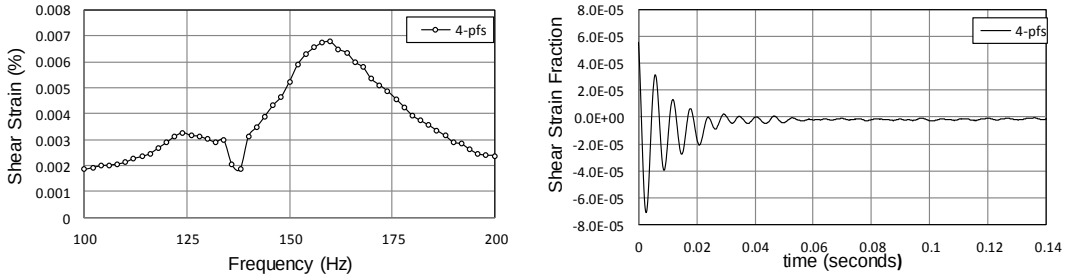

Figure 4.8 SM Soil Response at 4-pfs torque: $(p\text{-}u_a)$ = 50kPa, s = 200kPa

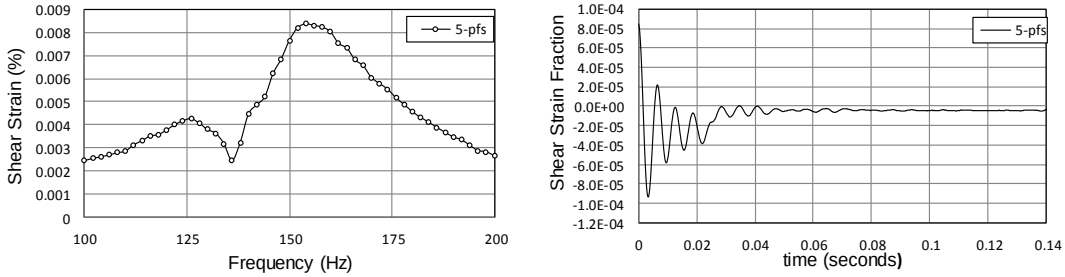

Figure 4.9 SM Soil Response at 5-pfs torque: $(p\text{-}u_a)$ = 50kPa, s = 200kPa

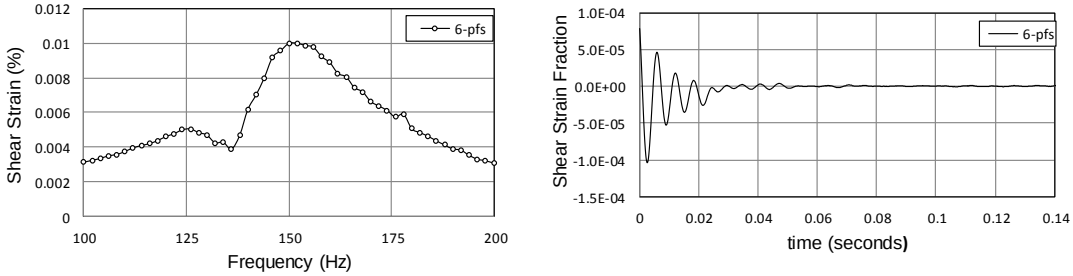

Figure 4.10 SM Soil Response at 6-pfs torque: $(p\text{-}u_a)$ = 50kPa, s = 200kPa

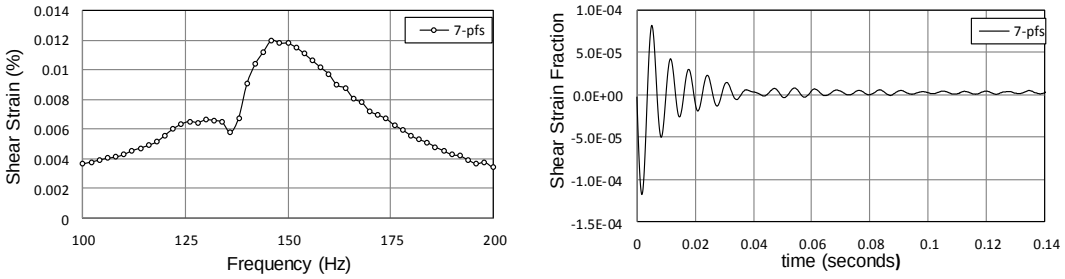

Figure 4.11 SM Soil Response at 7-pfs torque: $(p\text{-}u_a)$ = 50kPa, s = 200kPa

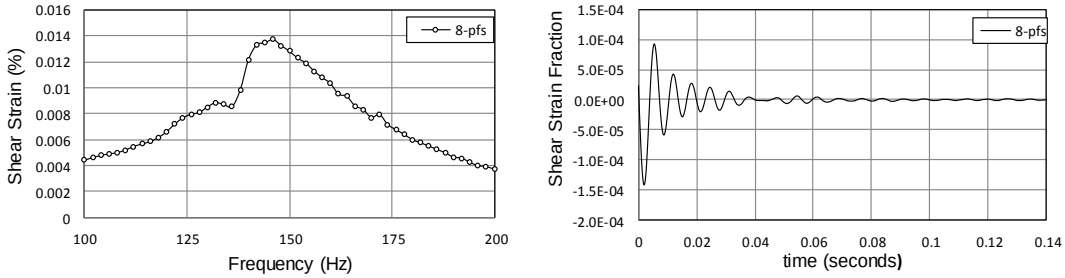

Figure 4.12 SM Soil Response at 8-pfs torque: $(p\text{-}u_a)$ = 50kPa, s = 200kPa

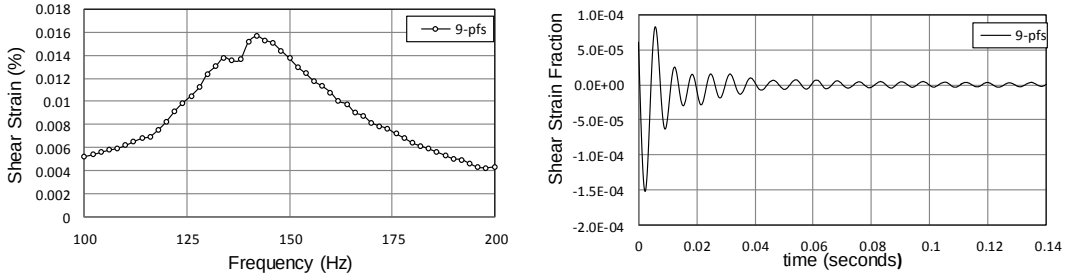

Figure 4.13 SM Soil Response at 9-pfs torque: $(p\text{-}u_a)$ = 50kPa, s = 200kPa

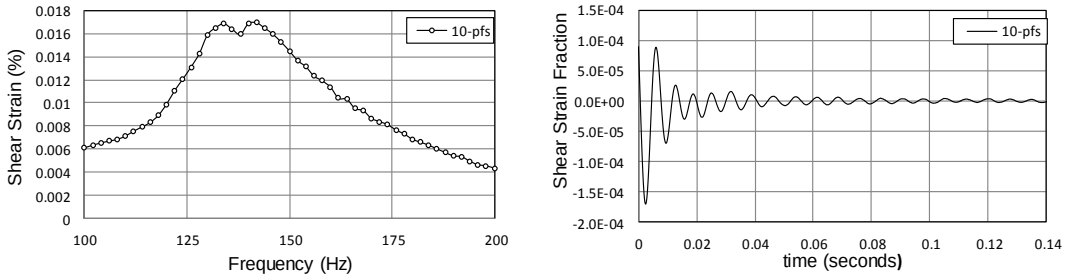

Figure 4.14 SM Soil Response at 10-pfs torque: $(p\text{-}u_a)$ = 50kPa, s = 200kPa

It can be observed that the resonant frequency decreases with increasing cyclic torque. There is a well-defined, linearly decreasing resonant frequency, with increasing input torque. This can be attributed to the initial yield loci being exceeded, bringing the soil specimen into the elasto-plastic region.

Fig. 4.15 depicts the frequency response curves for input cyclic torques of 1 through 10-pfs on one single graph for $(p-u_a)$ = 50kPa and s=200kPa. The linearly decreasing resonant frequency for increasing input torque (i.e., back-bone curve) can be clearly observed in this graph.

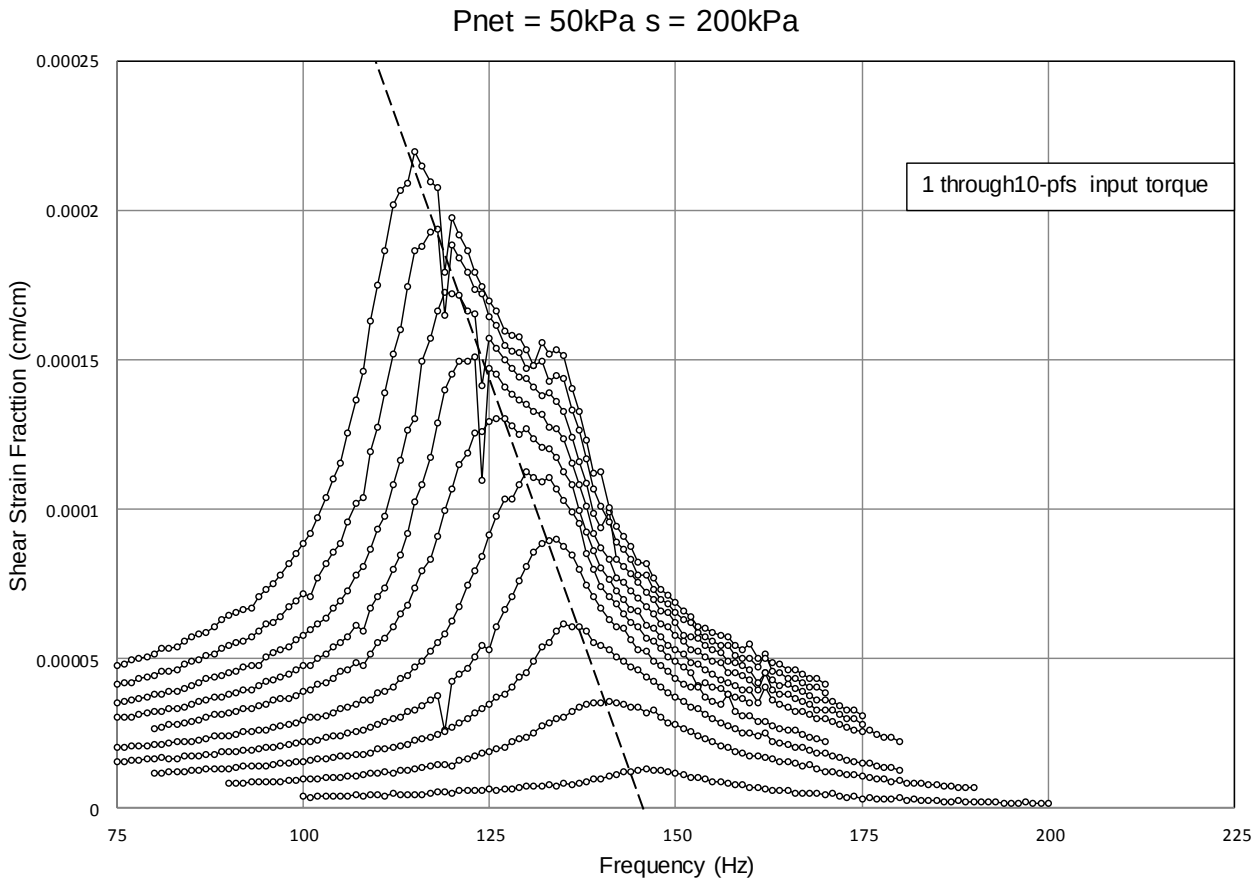

Figure 4.15 SM Soil Backbone Curve at 1 through 10-pfs

Figs. 4-16 through 4-19 show the frequency response curves and free-vibration decay curves from RC tests conducted at matric suction, s = 50, 100, 150, and 200kPa, respectively, under a constant net confining pressure, $(p\text{-}u_a)$ = 100kPa. All tests were conducted with a 1-pfs input torque.

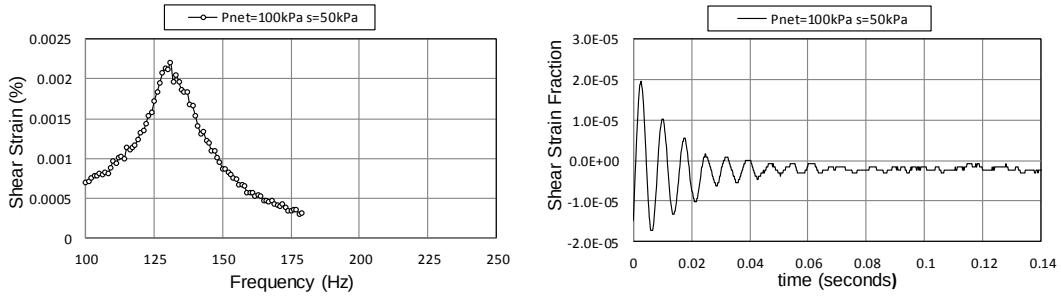

Figure 4.16 SM Soil Response at 1-pfs torque: $(p\text{-}u_a)$ = 100kPa, s = 50kPa

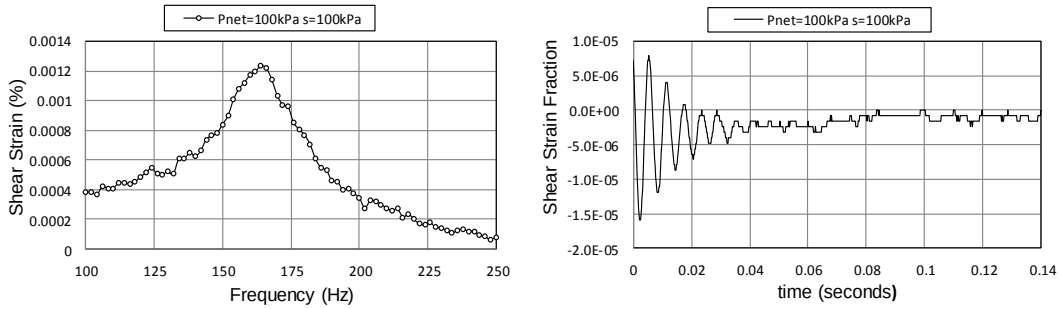

Figure 4.17 SM Soil Response at 1-pfs torque: $(p\text{-}u_a)$ = 100kPa, s = 100kPa

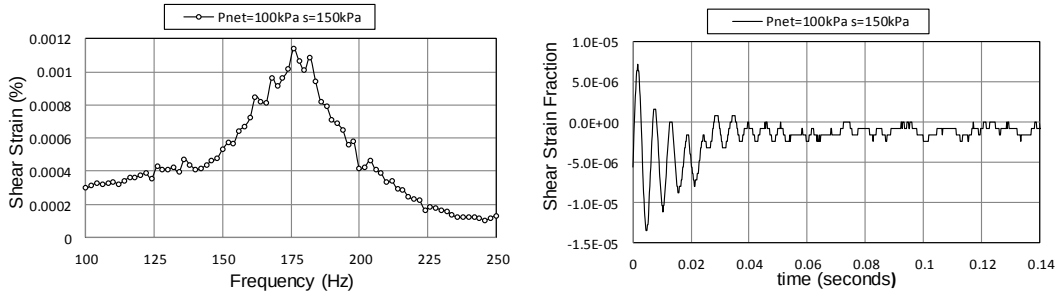

Figure 4.18 SM Soil Response at 1-pfs torque: $(p\text{-}u_a)$ = 100kPa, s = 150kPa

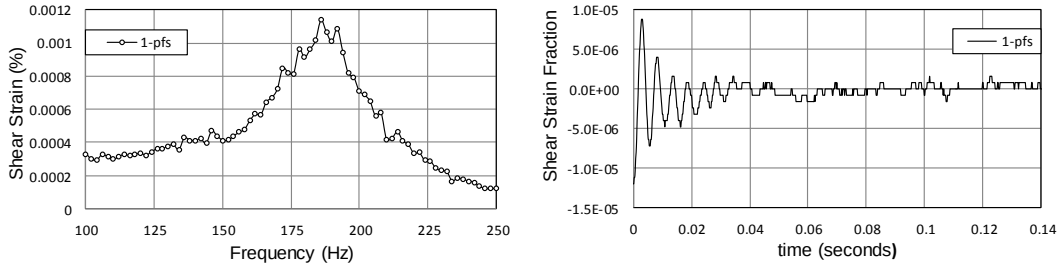

Figure 4.19 SM Soil Response at 1-pfs torque: $(p\text{-}u_a)$ = 100kPa, s = 200kPa

It can be observed that the resonant frequency increases with increasing matric suction. Qualitatively, this ensures an increasing shear modulus with increasing suction, as the resonant frequency is directly proportional to shear modulus in shear modulus calculations. This can be attributed to an increase in tensile forces between soil particles from increased matric suction, thereby causing closer contact between soil particles and stiffer material.

Figs. 4.20 through 4.28 show the frequency response curves and free-vibration decay curves from RC tests conducted at matric suction, s = 200kPa and $(p\text{-}u_a)$ = 100kPa. With 2, 3, 4, 5, 6, 7, 8, 9, and 10-pfs input torque, respectively.

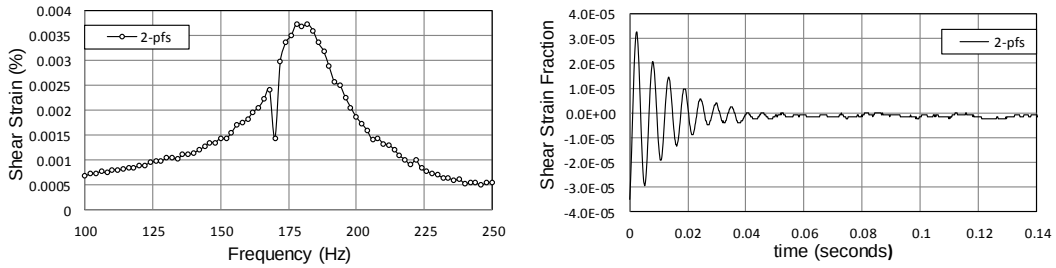

Figure 4.20 SM Soil Response at 2-pfs torque: $(p\text{-}u_a)$ = 100kPa, s = 200kPa

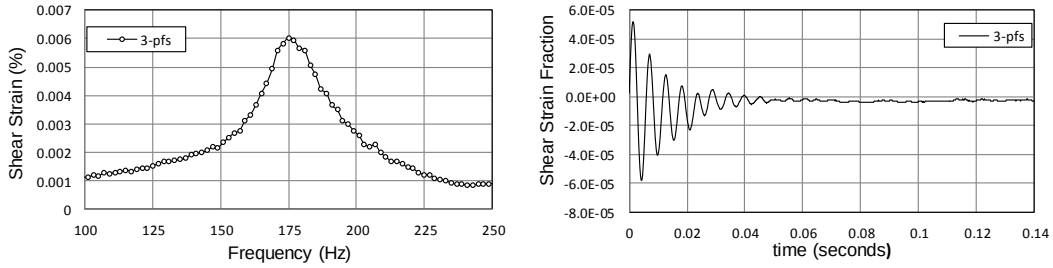

Figure 4.21 SM Soil Response at 3-pfs torque: $(p\text{-}u_a)$ = 100kPa, s = 200kPa

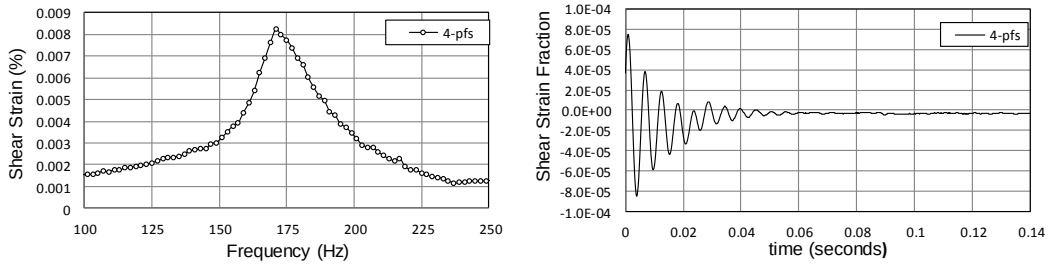

Figure 4.22 SM Soil Response at 4-pfs torque: $(p\text{-}u_a)$ = 100kPa, s = 200kPa

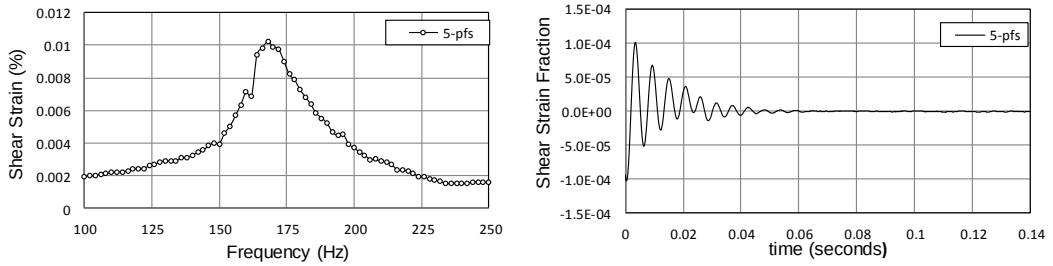

Figure 4.23 SM Soil Response at 5-pfs torque: $(p\text{-}u_a)$ = 100kPa, s = 200kPa

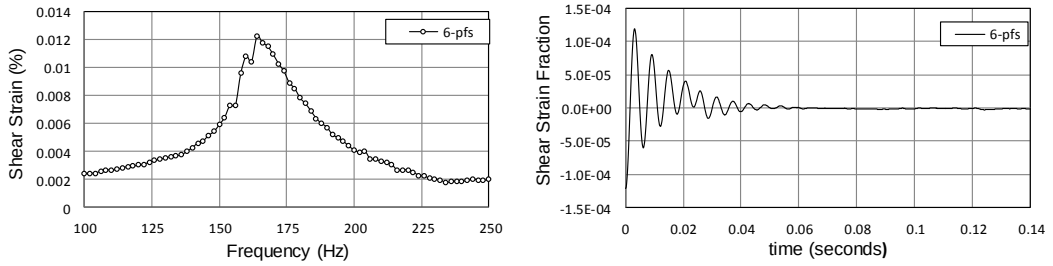

Figure 4.24 SM Soil Response at 6-pfs torque: $(p\text{-}u_a)$ = 100kPa, s = 200kPa

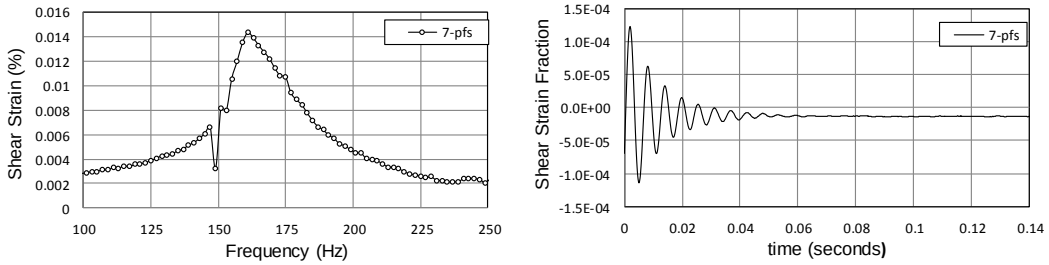

Figure 4.25 SM Soil Response at 7-pfs torque: $(p\text{-}u_a)$ = 100kPa, s = 200kPa

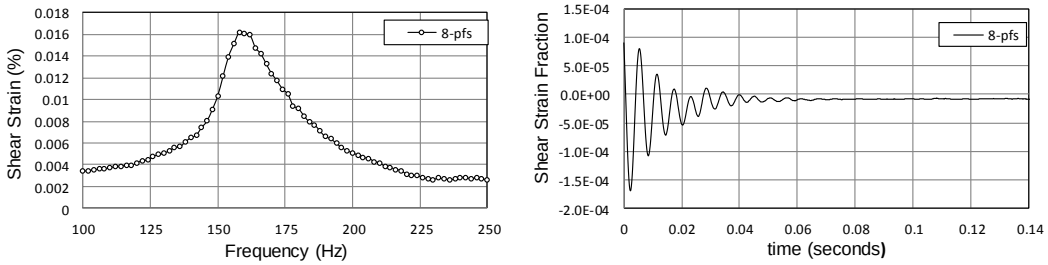

Figure 4.26 SM Soil Response at 8-pfs torque: $(p\text{-}u_a)$ = 100kPa, s = 200kPa

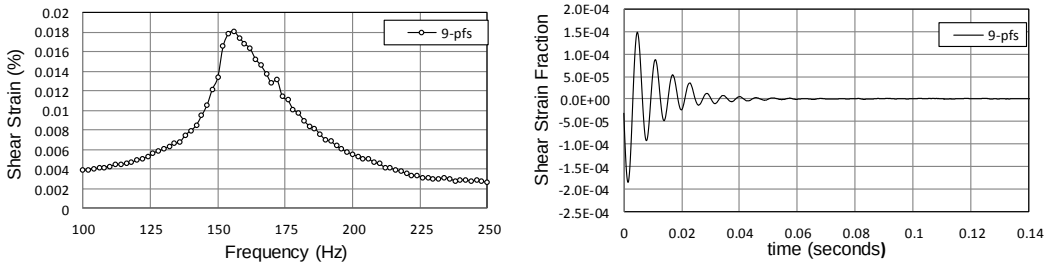

Figure 4.27 SM Soil Response at 9-pfs torque: $(p\text{-}u_a)$ = 100kPa, s = 200kPa

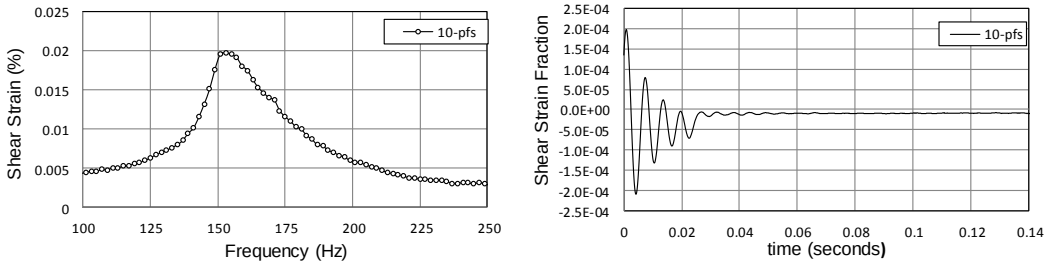

Figure 4.28 SM Soil Response at 10-pfs torque: $(p\text{-}u_a)$ = 100kPa, s = 200kPa

It can be observed that the resonant frequency decreases with increasing cyclic torque. There is a well-defined, linearly decreasing resonant frequency, with increasing input torque. This can be attributed to the initial yield loci being exceeded, bringing the soil specimen into the elasto-plastic region.

Fig. 4.29 depicts the frequency response curves for input cyclic torques of 1 through 10-pfs on one graph for $(p\text{-}u_a)$ = 100kPa and s=200kPa. The linearly decreasing resonant frequency for increasing input torque (i.e., back-bone curve) can be clearly observed in this graph.

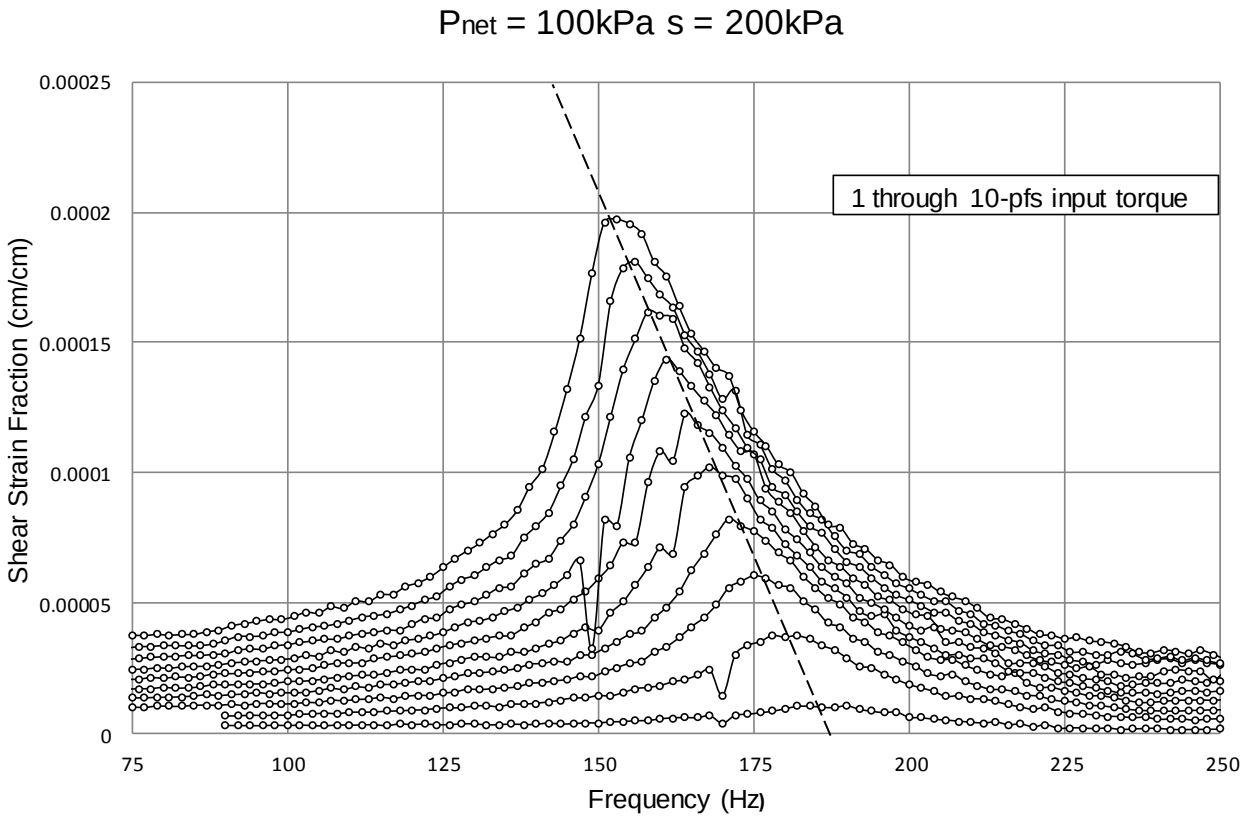

Figure 4.29 SM Soil Backbone Curve at 1 through 10-pfs

Figs. 4.30 through 4.33 show the frequency response curves and free-vibration decay curves from RC tests conducted at matric suction, s = 50, 100, 150, and 200kPa, respectively, under a constant net confining pressure of, $(p\text{-}u_a)$ = 150kPa. All tests were conducted with a 1-pfs input torque.

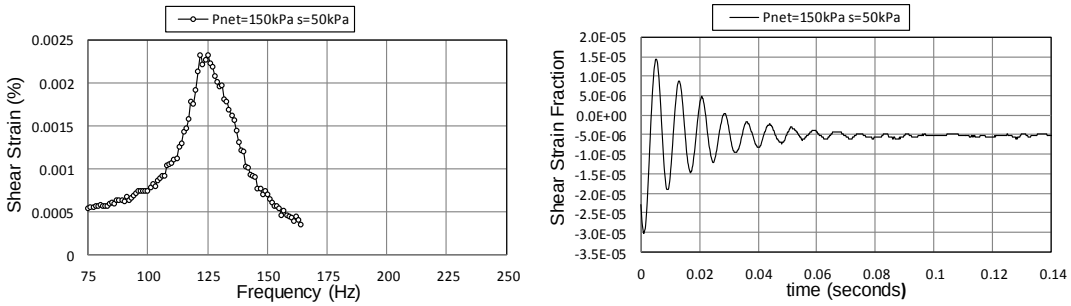

Figure 4.30 SM Soil Response at 1-pfs torque: $(p\text{-}u_a)$ = 150kPa, s = 50kPa

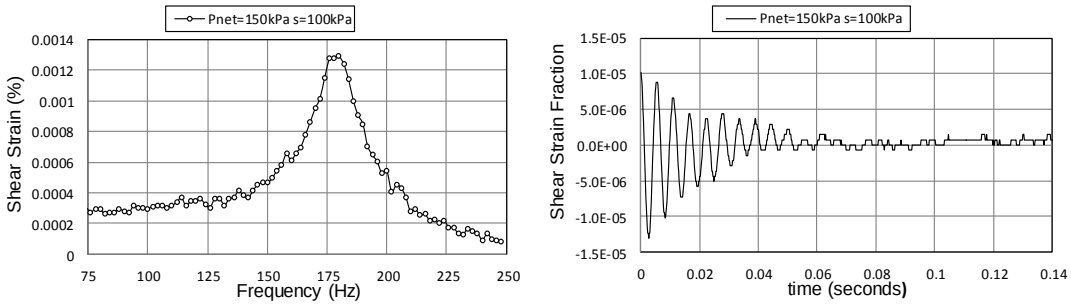

Figure 4.31 SM Soil Response at 1-pfs torque: $(p\text{-}u_a)$=150kPa, s=100kPa

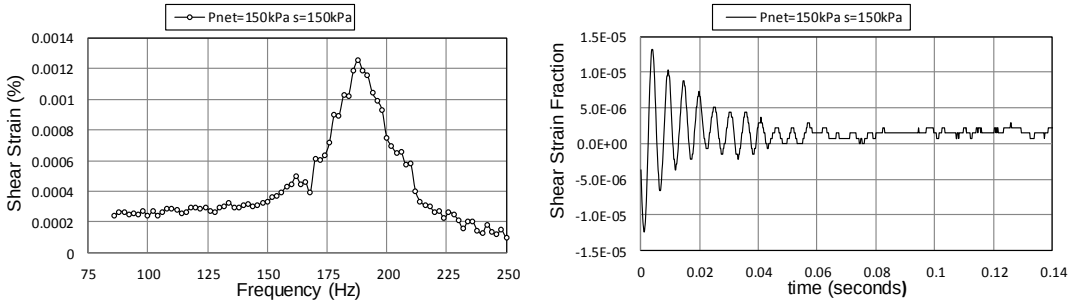

Figure 4.32 SM Soil Response at 1-pfs torque: $(p\text{-}u_a)$=150kPa, s=150kPa

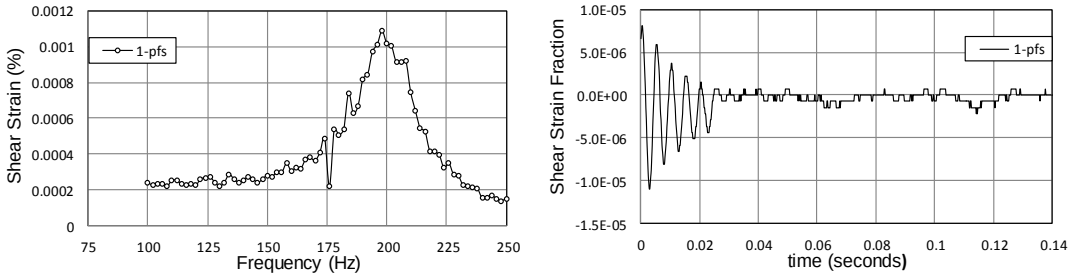

Figure 4.33 SM Soil Response at 1-pfs torque: $(p\text{-}u_a)$=150kPa, s=200kPa

It can be observed that the resonant frequency increases with increasing matric suction. Qualitatively, this ensures an increasing shear modulus with increasing suction, as the resonant frequency is directly proportional to shear modulus in shear modulus calculation. This can be attributed to an increase in tensile forces between soil particles from increased matric suction, thereby causing closer contact between soil particles and stiffer material.

Figs. 4.34 through 4.42 show the frequency response curves and free-vibration decay curves from RC tests conducted at matric suction, s = 200kPa and $(p\text{-}u_a)$ = 100kPa. With 2, 3, 4, 5, 6, 7, 8, 9, and 10-pfs input torque, respectively.

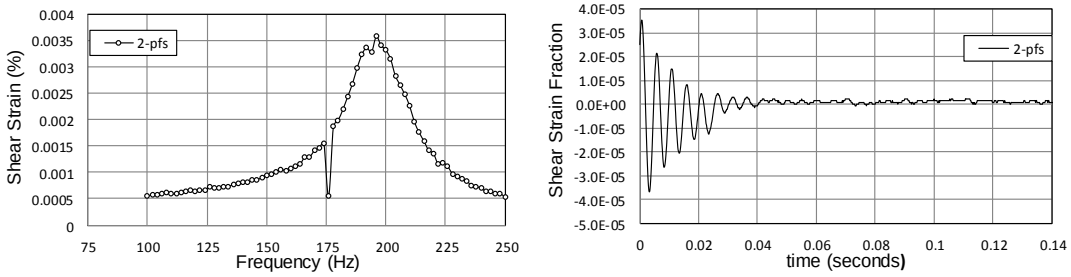

Figure 4.34 SM Soil Response at 2-pfs torque: $(p\text{-}u_a)$ = 150kPa, s = 200kPa

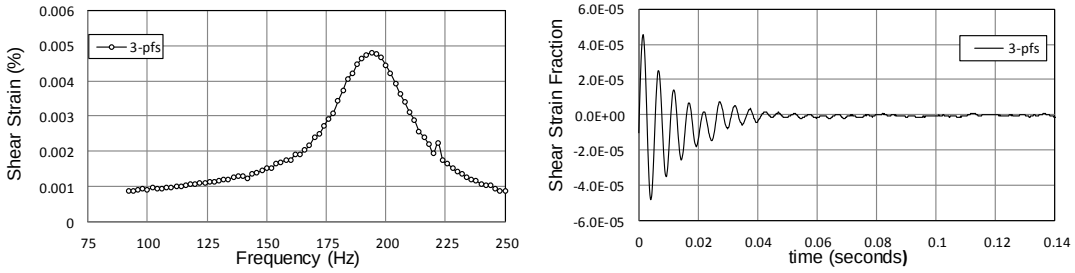

Figure 4.35 SM Soil Response at 3-pfs torque: $(p\text{-}u_a)$ = 150kPa, s = 200kPa

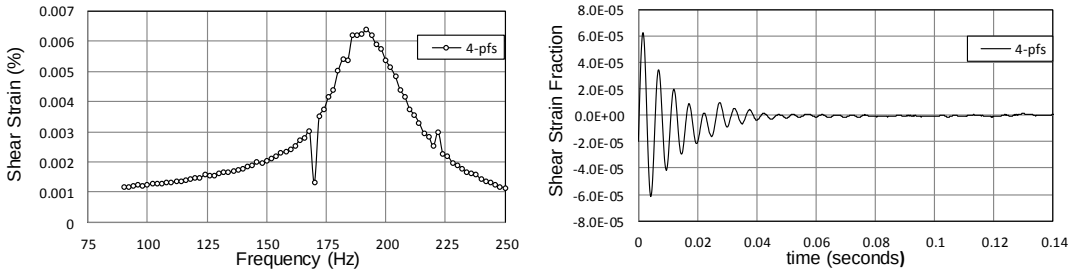

Figure 4.36 SM Soil Response at 4-pfs torque: $(p\text{-}u_a)$ = 150kPa, s = 200kPa

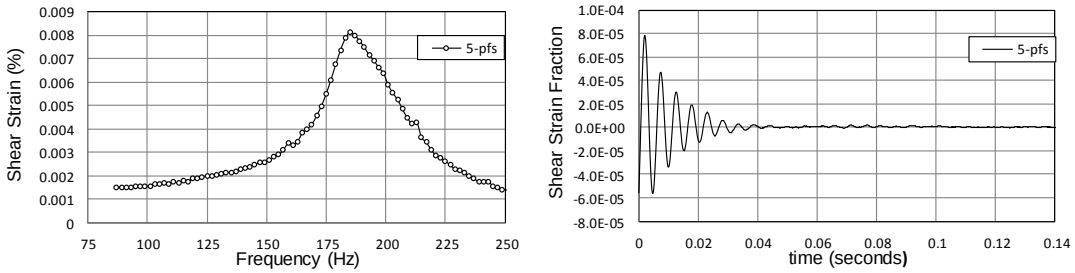

Figure 4.37 SM Soil Response at 5-pfs torque: $(p\text{-}u_a)$ = 150kPa, s = 200kPa

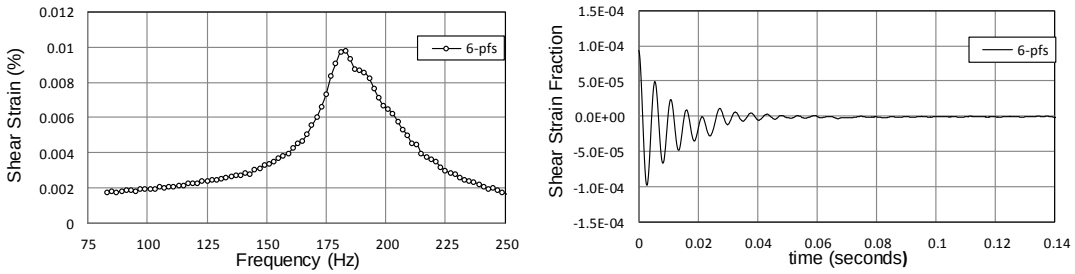

Figure 4.38 SM Soil Response at 6-pfs torque: $(p\text{-}u_a)$ = 150kPa, s = 200kPa

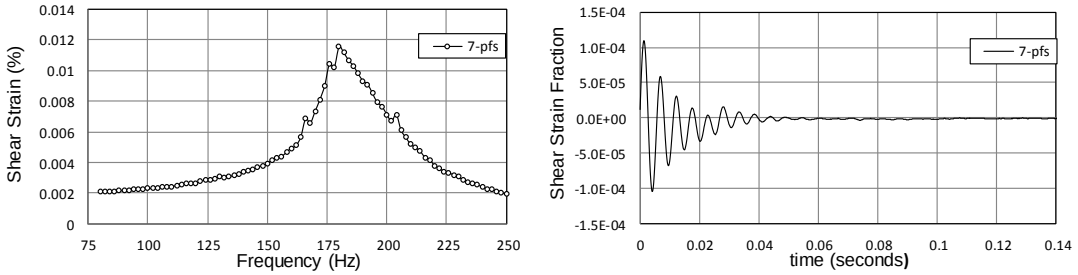

Figure 4.39 SM Soil Response at 7-pfs torque: $(p\text{-}u_a)$ = 150kPa, s = 200kPa

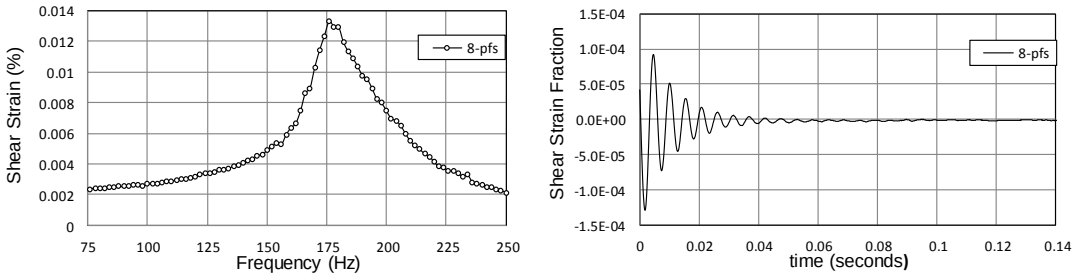

Figure 4.40 SM Soil Response at 8-pfs torque: $(p\text{-}u_a)$ = 150kPa, s = 200kPa

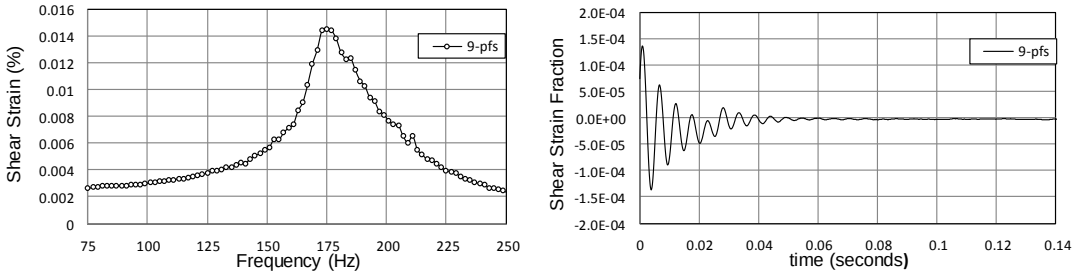

Figure 4.41 SM Soil Response at 9-pfs torque: $(p\text{-}u_a)$ = 150kPa, s = 200kPa

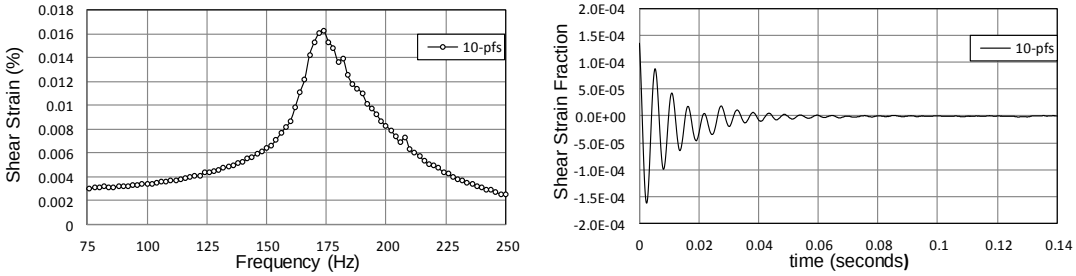

Figure 4.42 SM Soil Response at 10-pfs torque: $(p\text{-}u_a)$ = 150kPa, s = 200kPa

It can be observed that the resonant frequency decreases with increasing cyclic torque. There is a well-defined, linearly initial creasing resonant frequency, with increasing input torque. This can be attributed to thein yield loci being exceeded, bringing the soil specimen into the elasto-plastic region.

Fig. 4.43 depicts the frequency response curves for input cyclic torques of 1 through 10-pfs on one graph for $(p-u_a)$ = 150kPa and s=200kPa. The linearly decreasing resonant frequency for increasing input torque (i.e., back-bone curve) can be clearly observed in this graph.

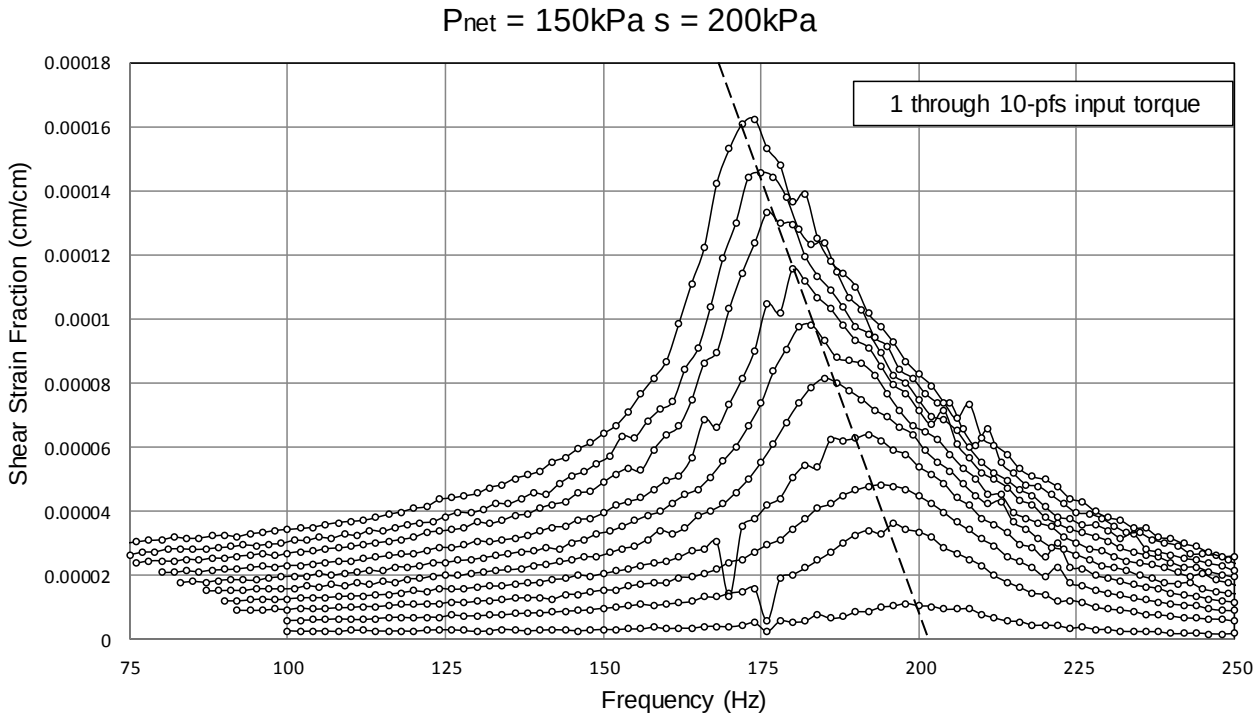

Figure 4.43 SM Soil Backbone Curve at 1 through 10-pfs

Figs. 4.44 through 4.47 show the frequency response curves and free-vibration decay curves for RC tests conducted at matric suction, s=50, 100, 150, and 200kPa, respectively, under a constant net confining pressure of, $(p\text{-}u_a)$ = 200kPa. All tests were conducted with a 1-pfs input torque.

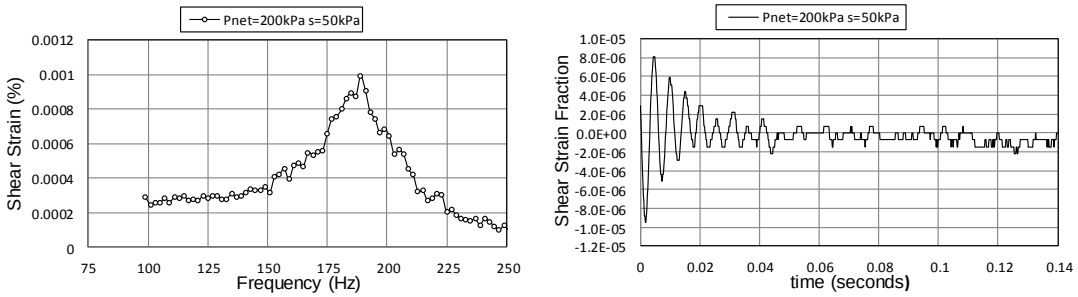

Figure 4.44 SM Soil Response at 1-pfs torque: $(p\text{-}u_a)$=200kPa, s=50kPa

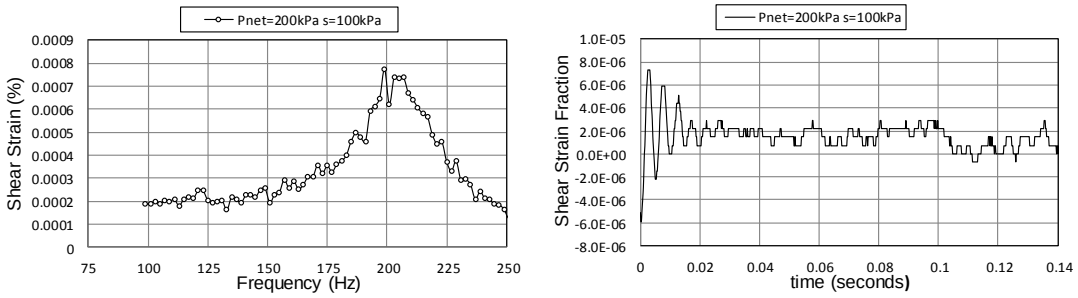

Figure 4.45 SM Soil Response at 1-pfs torque: $(p\text{-}u_a)$=200kPa, s=100kPa

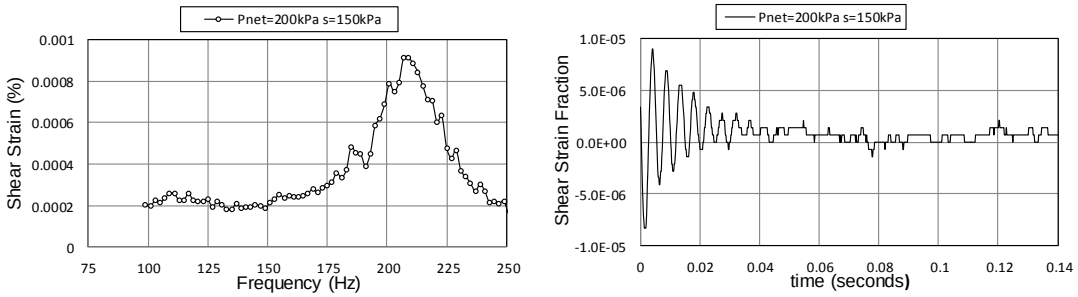

Figure 4.46 SM Soil Response at 1-pfs torque: $(p\text{-}u_a)$=200kPa, s=150kPa

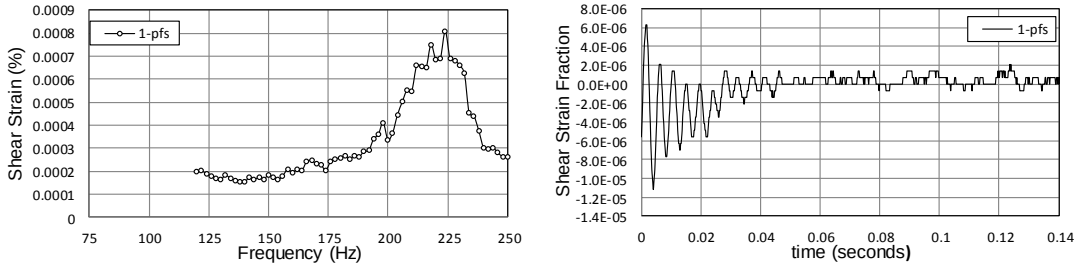

Figure 4.47 SM Soil Response at 1-pfs torque: $(p\text{-}u_a)$=200kPa, s=200kPa

It can be observed that the resonant frequency increases with increasing matric suction. Qualitatively, this ensures an increasing shear modulus with increasing suction, as the resonant frequency is in the denominator for shear modulus calculations. This can be attributed to an increase in tensile forces between soil particles from increased matric suction, thereby causing closer contact between soil particles.

Figs. 4.48 through 4.56 show the frequency response curves and free-vibration decay curves from RC tests conducted at matric suction, s = 200kPa and $(p\text{-}u_a)$ = 200kPa. With 2, 3, 4, 5, 6, 7, 8, 9, and 10-pfs input torque, respectively.

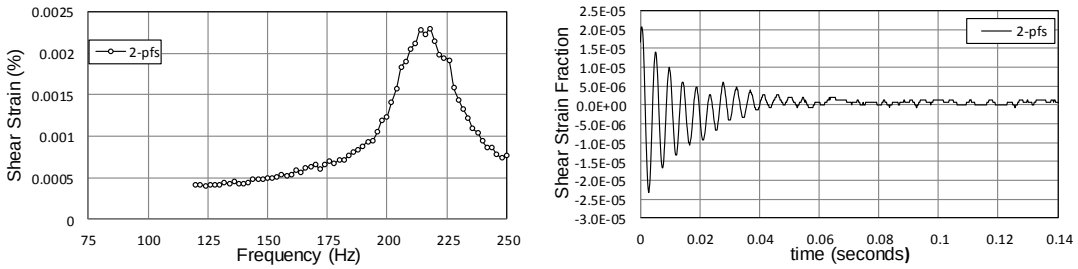

Figure 4.48 SM Soil Response at 2-pfs torque: $(p\text{-}u_a)$=200kPa, s=200kPa

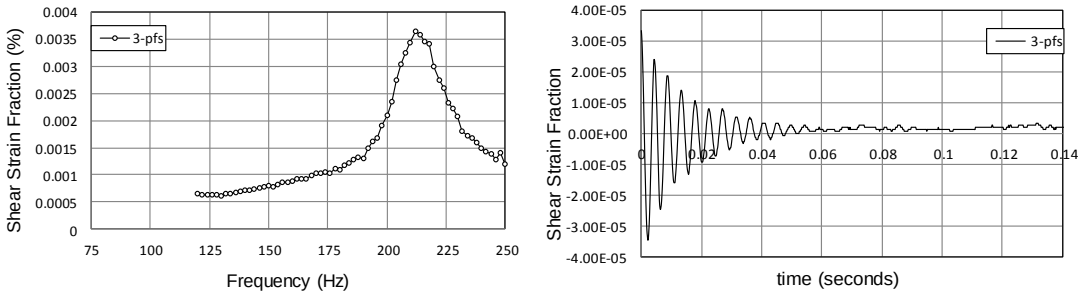

Figure 4.49 SM Soil Response at 3-pfs torque: $(p\text{-}u_a)$=200kPa, s=200kPa

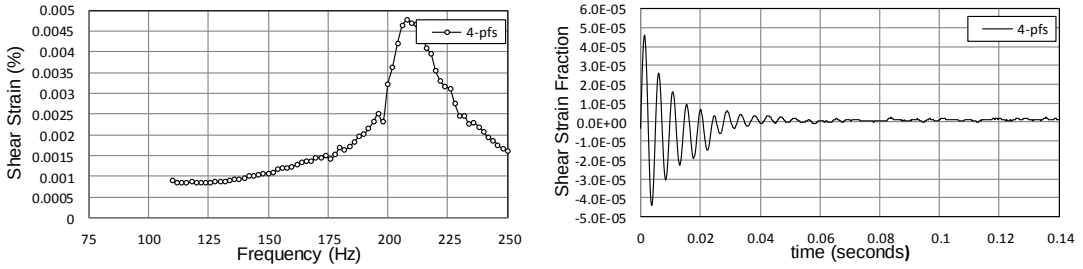

Figure 4.50 SM Soil Response at 4-pfs torque: $(p\text{-}u_a)$=200kPa, s=200kPa

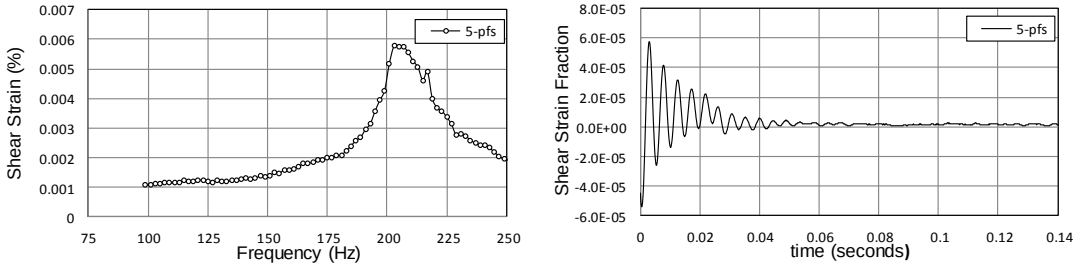

Figure 4.51 SM Soil Response at 5-pfs torque: $(p\text{-}u_a)$=200kPa, s=200kPa

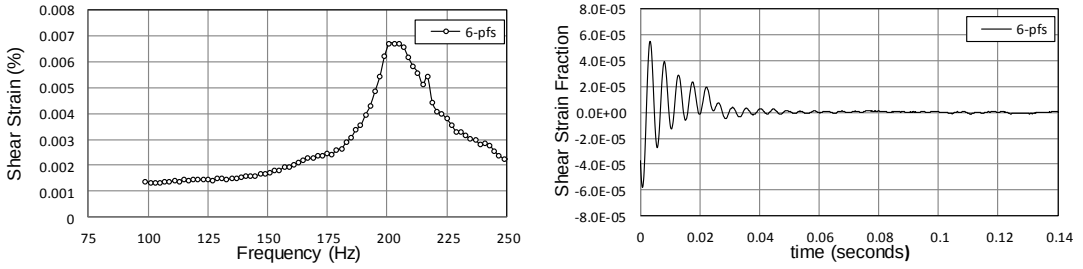

Figure 4.52 SM Soil Response at 6-pfs torque: $(p\text{-}u_a)$=200kPa, s=200kPa

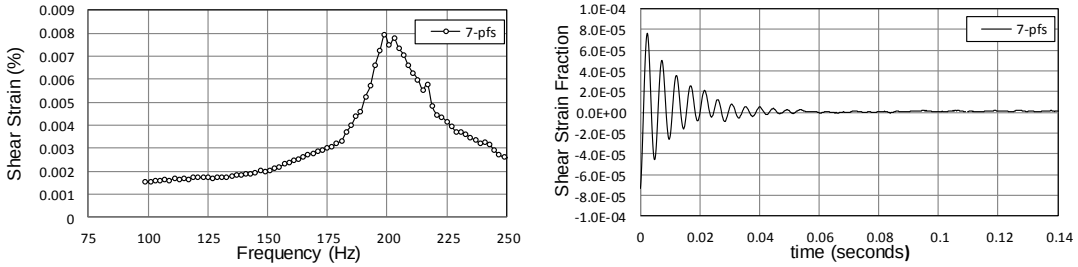

Figure 4.53 SM Soil Response at 7-pfs torque: $(p\text{-}u_a)$=200kPa, s=200kPa

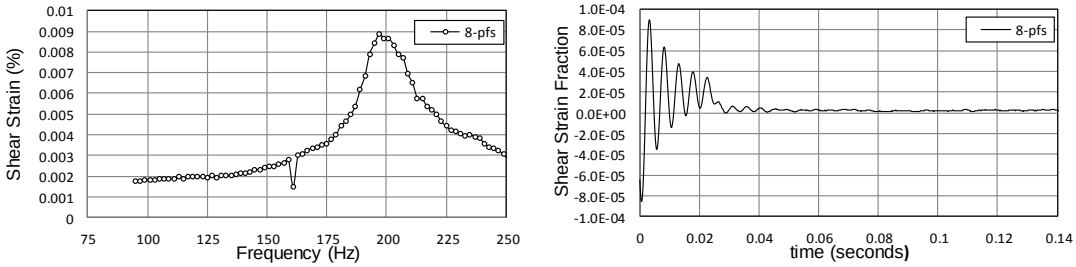

Figure 4.54 SM Soil Response at 8-pfs torque: $(p\text{-}u_a)$=200kPa, s=200kPa

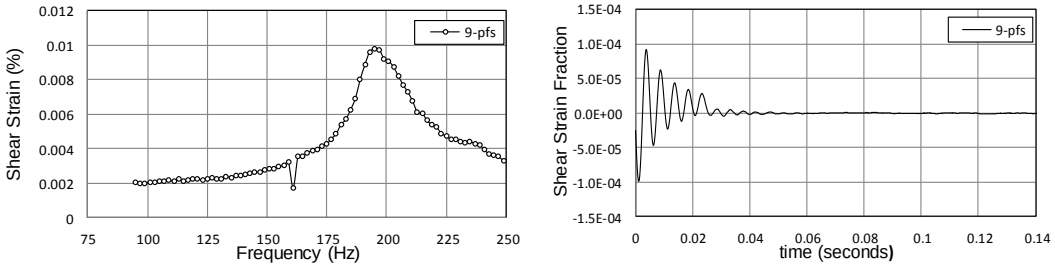

Figure 4.55 SM Soil Response at 9-pfs torque: $(p\text{-}u_a)$=200kPa, s=200kPa

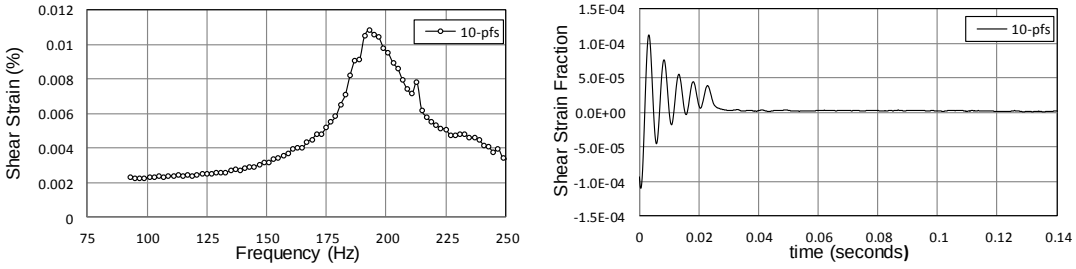

Figure 4.56 SM Soil Response at 10-pfs torque: $(p\text{-}u_a)$=200kPa, s=200kPa

It can be observed that the resonant frequency decreases with increasing cyclic torque. There is a well-defined, linearly decreasing resonant frequency, with increasing input torque. This can be attributed to the yield loci being exceeded, bringing the soil specimen into the elasto-plastic region.

Fig. 4.57 depicts the resonant response curves for input cyclic torques of 1 through 10-pfs on one graph for $(p\text{-}u_a)$ = 200kPa and s=200kPa. The linearly decreasing resonant frequency for increasing input torque can be clearly observed in this graph.

Figs. 4.58 and 4.59, whichfollow the backbone curve, depict the normalized shear modulus (G/G_{max}) and normalized damping (D/D_{min}) as a function of shear strain, for varying matric suctions. It can be observed that the normalized shear modulus decreased with increasing shear strain. There is no observable correlation of varying net confinement with respect to normalized shear modulus. The normalized damping ratio increases with increasing shear strain. There is no clear relationship for varying net confinement with respect to normalized damping ratio from this graph. Both curves suggest that the net confinement does not play a crucial role in the definition of threshold strain, γ_{th}, at matric suction states of 200 kPa or higher.

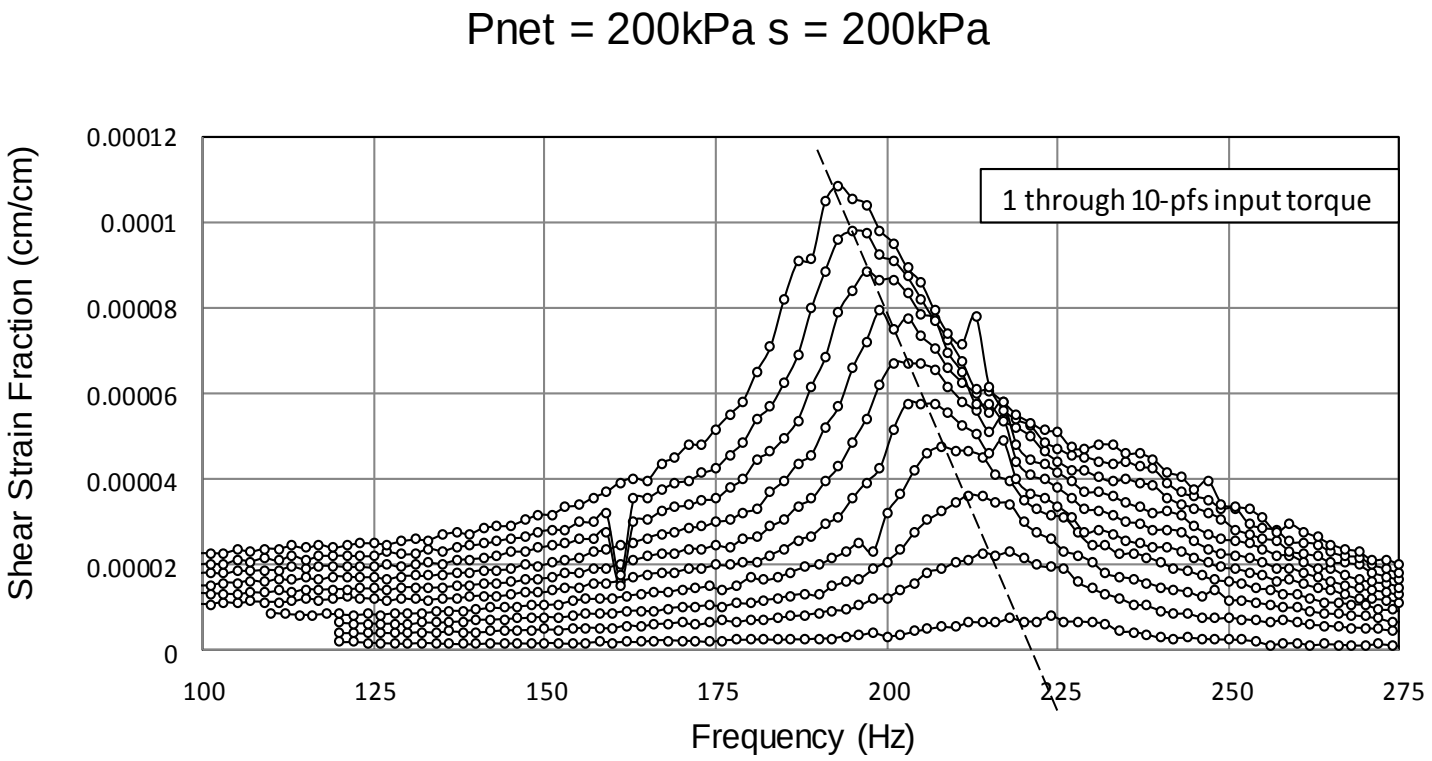

Figure 4.57 SM Soil Backbone Curve at 1 through 10-pfs

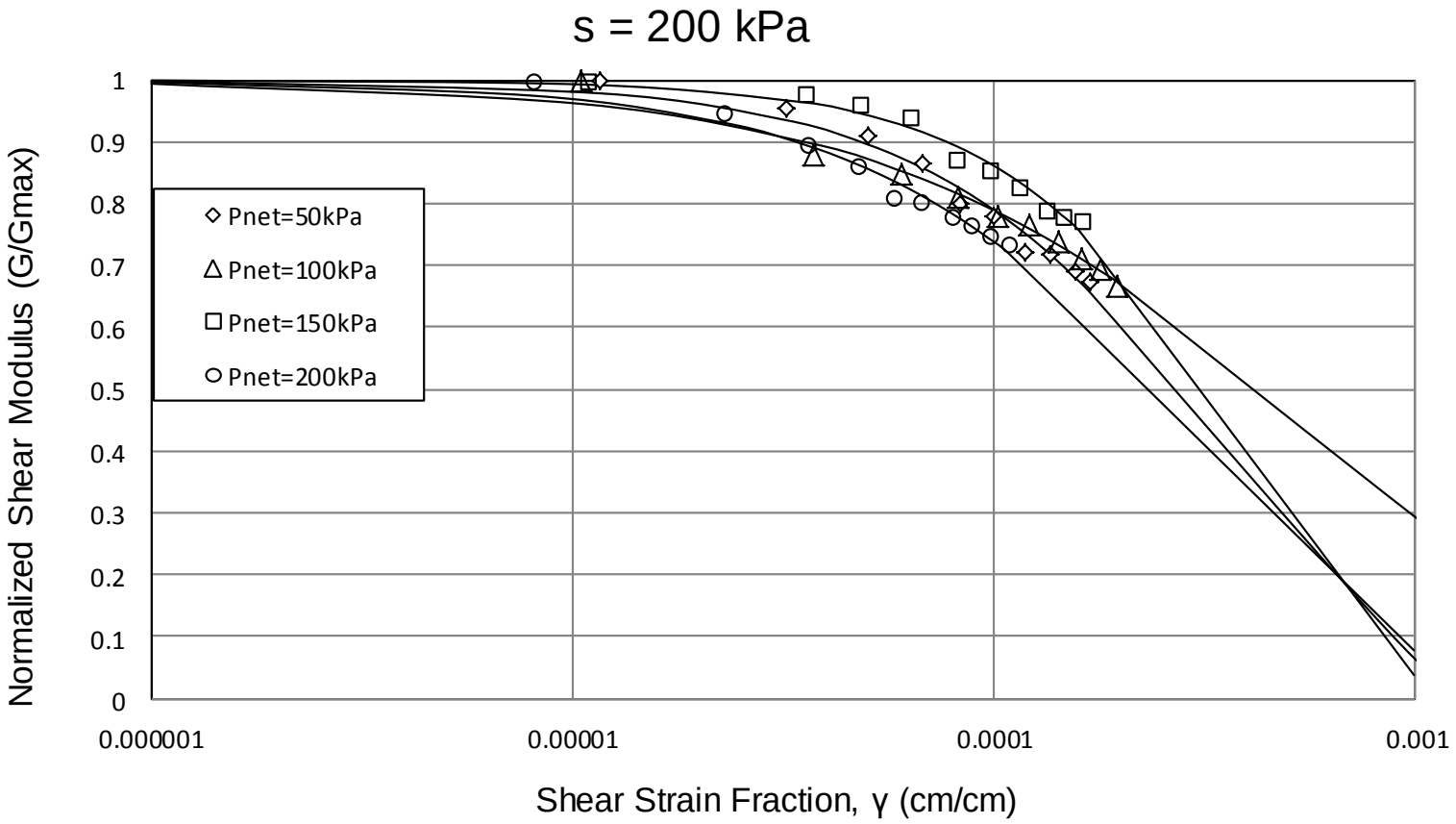

Figure 4.58 Normalized Shear Modulus as a function of Shear Strain

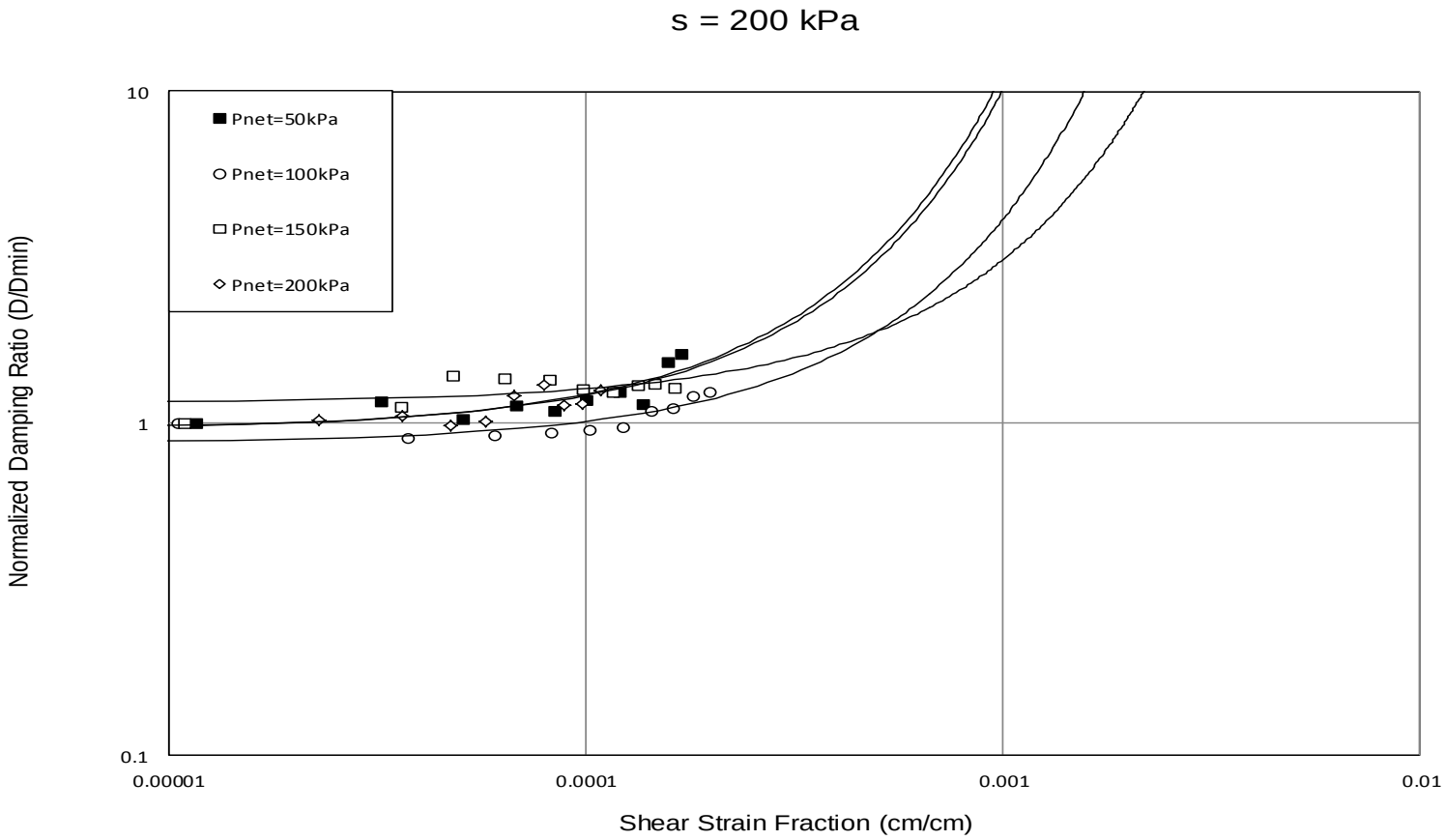

Figure 4.59 Normalized Damping Ratio as a function of Shear Strain

Figs. 4.60 through 4-63 show the cyclic hysteresis stress-strain loops for net confining pressures of $(p\text{-}u_a)$ = 50, 100, 150, and 200kPa, respectively; each with constant matric suctions of s = 200kPa. The general pattern indicates a general decrease in the proportional area enclosed by the loops as the input torque increases. This inclination indicates to a decrease in material damping ratio, as this parameter is directly related to the area of the hysteretic loop. The overall observed trend shows that the material damping ratio increases with increased net confining pressure.

P_{net} = 50 kPa, s = 200 kPa

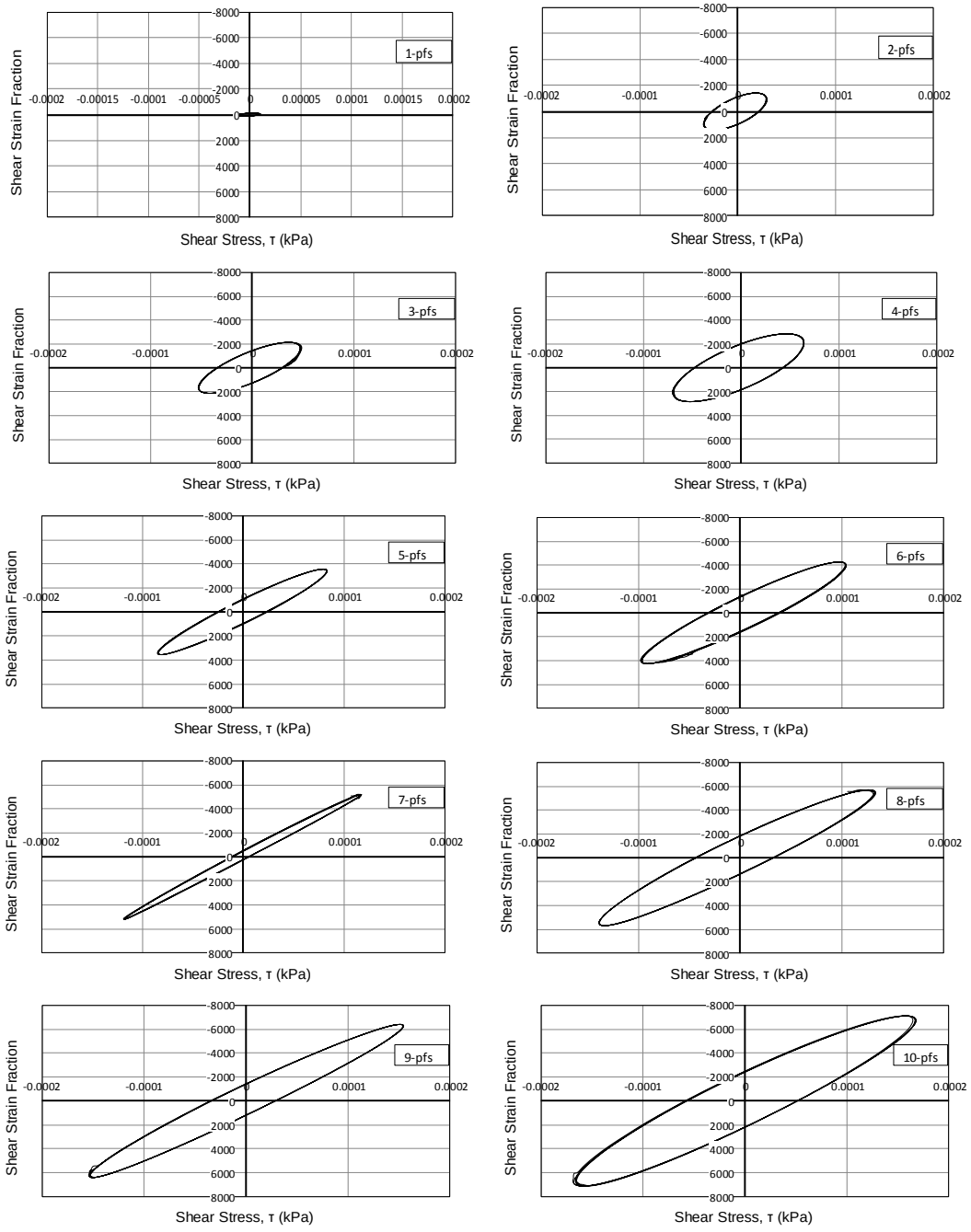

Figure 4.60 Cyclic hysteretic stress-strain loops: $(p\text{-}u_a)$ = 50 kPa, s = 200 kPa

P_{net} = 100 kPa, s = 200 kPa

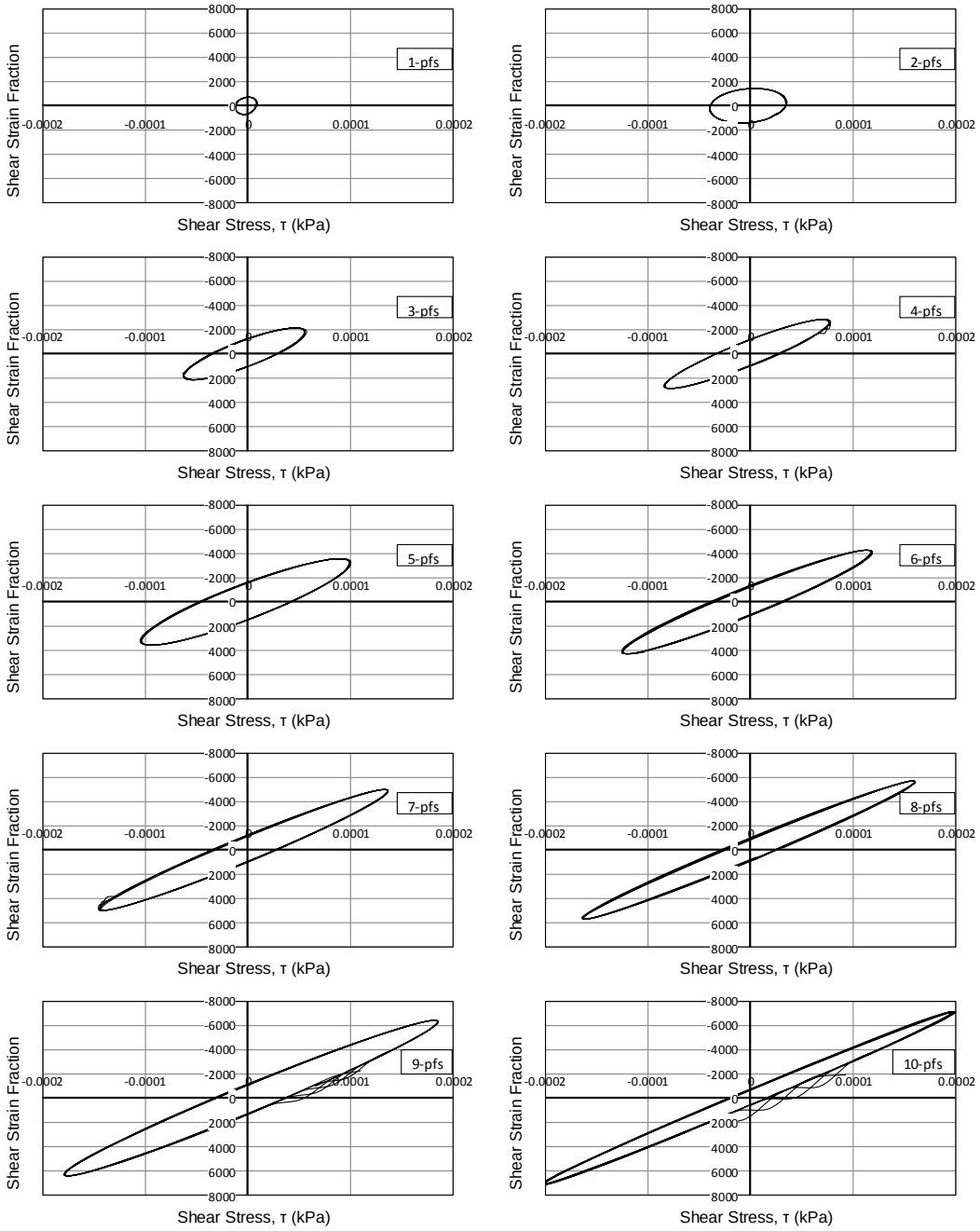

Figure 4.61 Cyclic hysteretic stress-strain loops: (p-ua) = 100 kPa, s = 200 kPa

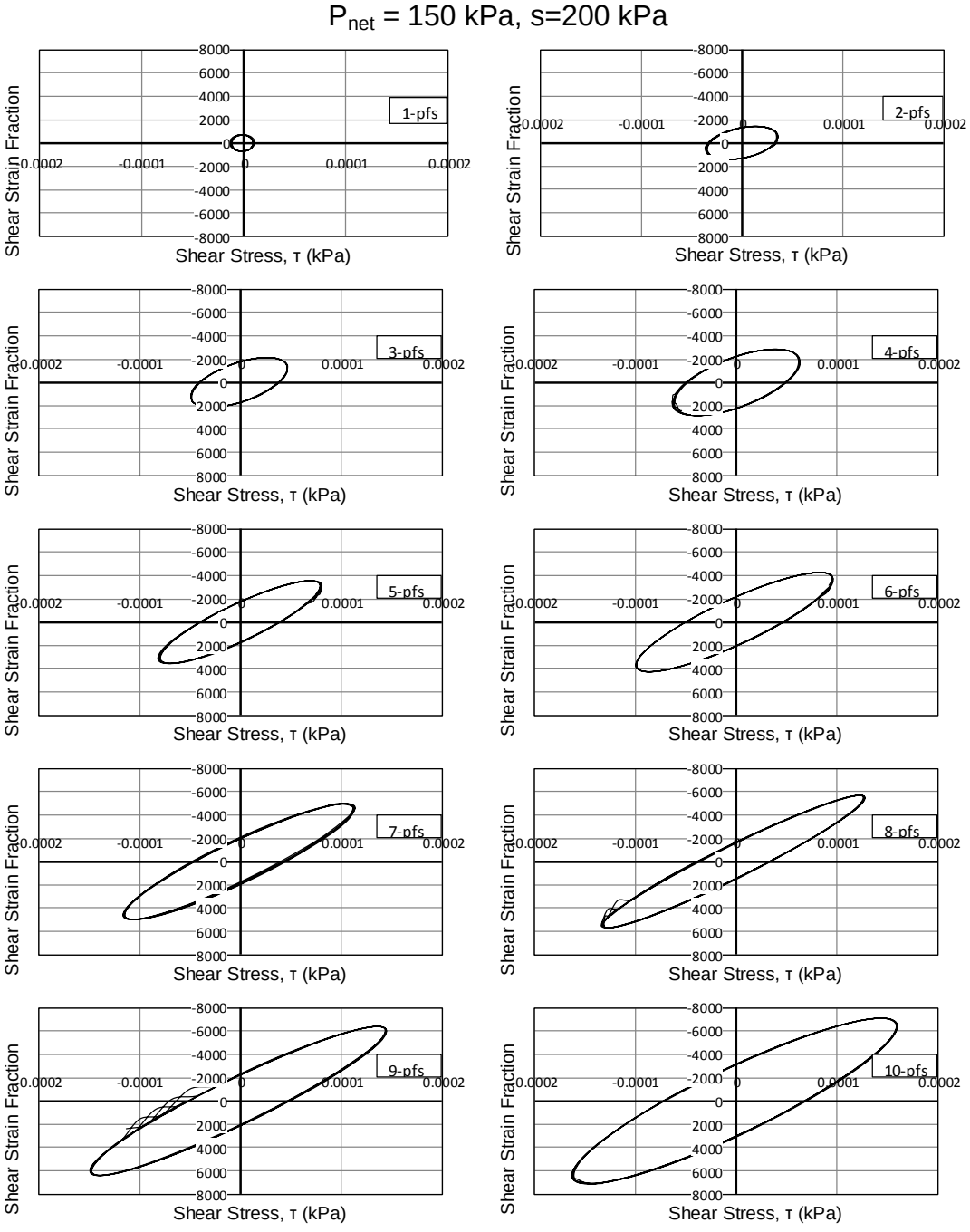

Figure 4.62 Cyclic hysteretic stress-strain loops: (p-ua) = 150 kPa, s = 200 kPa

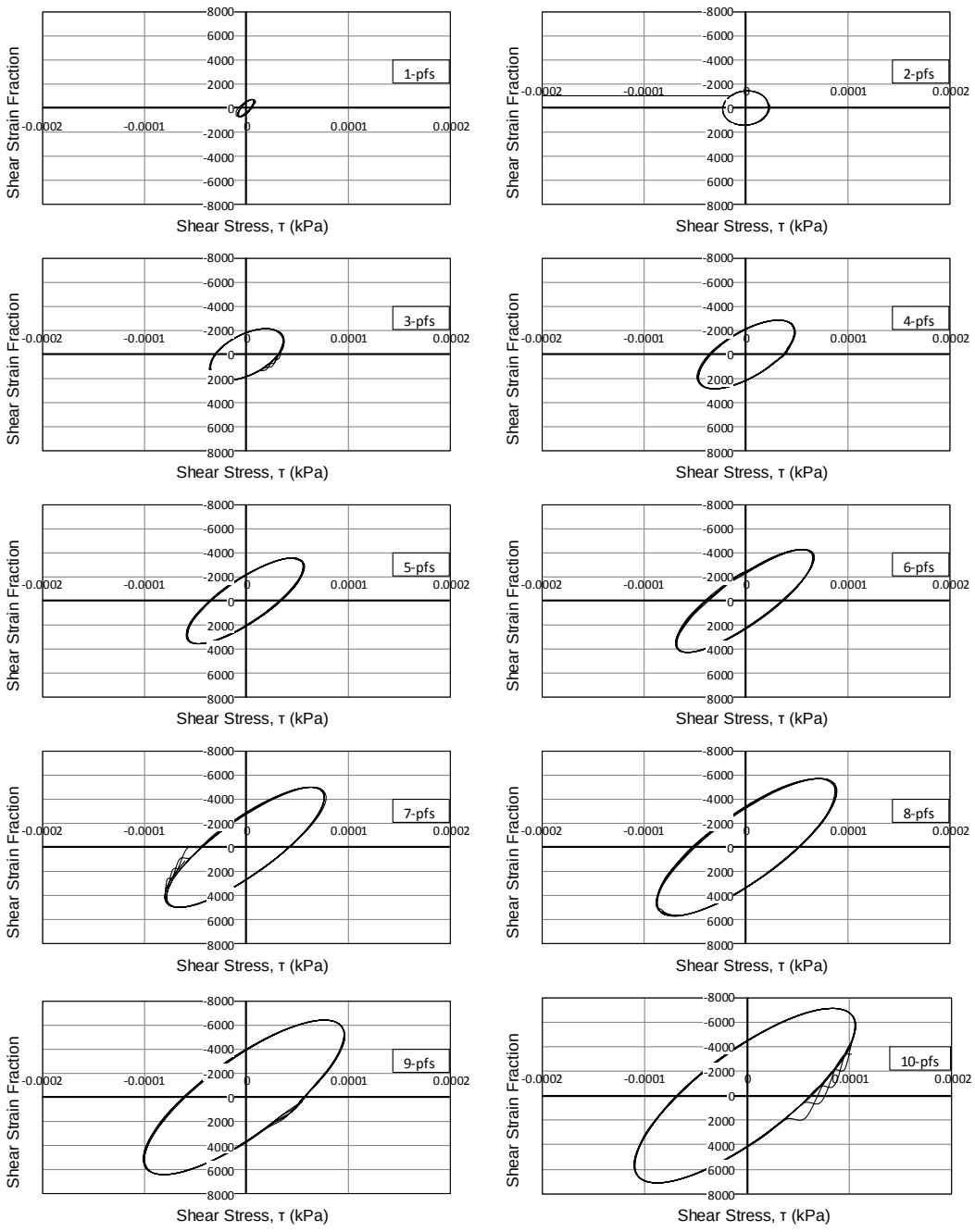

Figure 4.63 Cyclic hysteretic stress-strain loops: (p-ua) = 200 kPa, s = 200 kPa

Figs. 4-64 and 4-65 show the shear modulus as a function of confining pressure with varying matric suction states; and shear modulus as a function of matric suction with varying net confining pressures, respectively. It can be observed that there is an increase in shear modulus for increasing net confining pressures and increasing matric suction states.

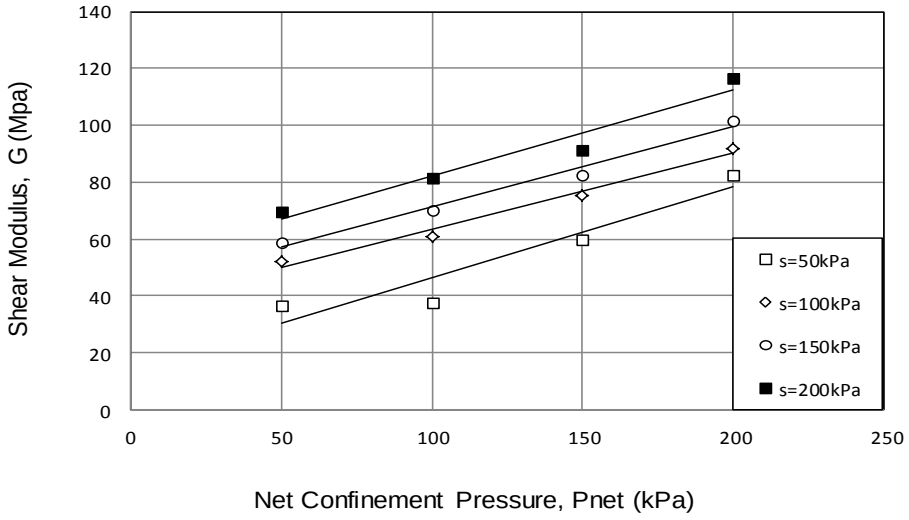

Figure 4.64 Shear Modulus as a function of Net Confining Pressure

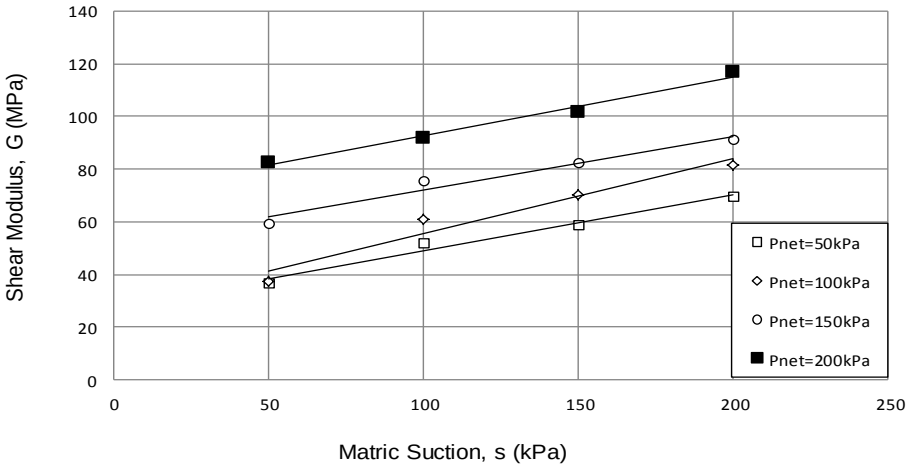

Figure 4.65 Shear Modulus as a function of Matric Suction

Figs 4-66 and 4-67 show the material damping ratio as a function of net confining pressure with varying matric suction states; and material damping ratio as a function of matric suction with varying net confining pressure, respectively. It can be observed that the material damping decreases with an increase in net confining pressure and increasing matric suction.

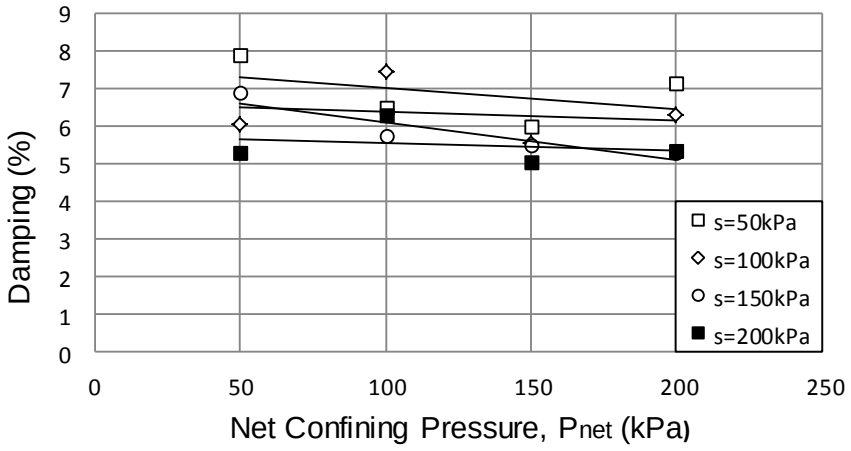

Figure 4.66 Damping as a function of Net Confining Pressure

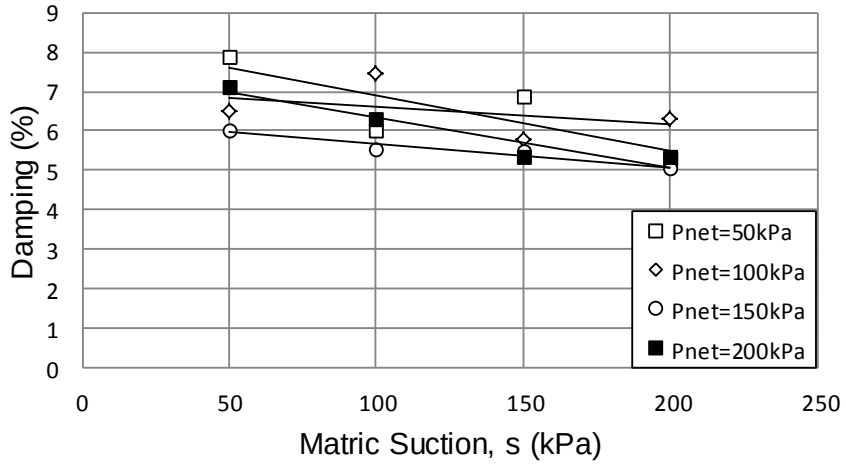

Figure 4.67 Damping as a function of Matric Suction

CHAPTER 5

EXPERIMENTAL PROGRAM II: VARIABLES, PROCEDURES, AND RESULTS

5.1 Introduction

The initial series of testing sought to assess the dynamic response compacted of silty sand while reproducing the effect of the soil first being subjected an increase in suction due to a loss in moisture, then being subjected loading (e.g., a machine foundation). This moisture loss can be attributed to drying from seasonal moisture variations. One of the intents of the research project was to assess how the small strain stiffness properties of the soil were affected by the stress/suction history (hydro-mechanical path). An overview of the stress paths are depicted below in Figure 5-1.The range of the experimental variables are summarized in Table 5-1.

5.2 Test procedure and stress paths prior to RC testing

The testing began with the assembly of the resonant column device, after which isotropic pressure was applied using the HM-414 panel. The initial suction in the compacted soil begins at approximately 20kPa at moisture content of 26.5% (see Figure 3-2); therefore, a confinement (p) that is greater than the initial suction was required outside of the specimen for the first series of testing. The axial deformation is monitored to assess whether the specimen is set for another pressure increase. Once the sample has achieved 90% consolidation, the next pressure increment is added. The pore-air pressure at that point was increased with the PCP-15U panel until the desired suction state is attained (Fig. 5-1). The external confinement was adjusted accordingly for the purposes of maintaining the constant desired net confining pressure, $(p\text{-}u_a)$.

When the chosen stress/suction state was attained, the pore fluids are then allowed to equalize. This process took an average of 8-days to complete for each test. The dynamic

response of the soil was then tested by using 1-pfs (100 N·m cyclic torque); thereby, assuring that the specimen's elastic boundary has not been exceeded, which could lead to misrepresentative data in subsequent stress/suction states induced on the same sample. The frequency of the cyclic torque was swept from 75 H_z (on average) sweeping to 250 H_z (on average). This was done to obtain the frequency response curve. These curves are depicted as the change of the shear strain fraction (cm/cm) as a function of the frequency (H_z) with given constant torque amplitude.

As the test terminates, the cyclic torque is cut off and the free torsional vibration of the specimen was plotted, thus obtaining the logarithmic decay curve for the assessment of material damping. The attenuation of shear strain was presented in terms of shear strain fraction (cm/cm) as a function of time (sec).

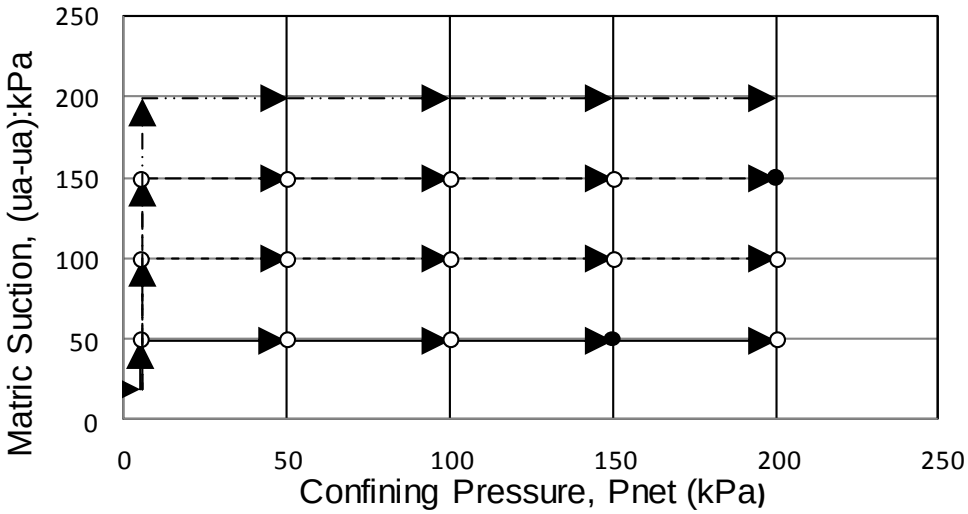

Figure 5.1 Stress paths induced on silty sand specimen prior to RC test

In the final stage of testing (Net Confinement Pressure = 200kPa) for each constant matric suction testing series, the non-linear dynamic response of the specimen is assessed for various torque amplitudes ranging from 1-10pfs (100 N·m to 1000 N·m). This ensures that the load path has breached the elastic boundary for each subsequent testing phase, thus necessitating the preparation of a new sample for the next series of testing.

Table 5.1 Experimental variables used for RC Testing during Experimental Program II

Variable description	**Number of variables**
Soil type	Silty Sand (SM)
Confining pressure, p	50 kPa 100 kPa 150 kPa 200 kPa 250 kPa 300 kPa 400 kPa
Net confining pressure, $(p-u_a)$	50 kPa 100 kPa 150 kPa 200 kPa
Matric suction, (u_a-u_w)	50 kPa 100 kPa 150 kPa 200 kPa

The same test procedure was repeated for net confining pressure, $p_{net} = (p - u_w) = 50$, 100, 150, and 200kPa, on the same sample at constant matric suction, $s = (u_a-u_w)$. This identical testing sequence was followed in testing SM soil samples at constant matric suction of $(u_a-u_w) = 50$, 100, 150, and 200kPa, as illustrated in Fig. 5-1. The following sections summarize all the experimental results from Experimental Program II.

5.3 Test Results from Experimental Program II

Figs. 5-2 through 5-5 show the frequency response curves and free-vibration decay curves from RC tests conducted at net confining pressures, p_{net} = 50, 100, 150, and 200kPa, respectively, under a constant matric suction, s= (u_a-u_w) = 50kPa. All tests were conducted with a 1-pfs input torque.

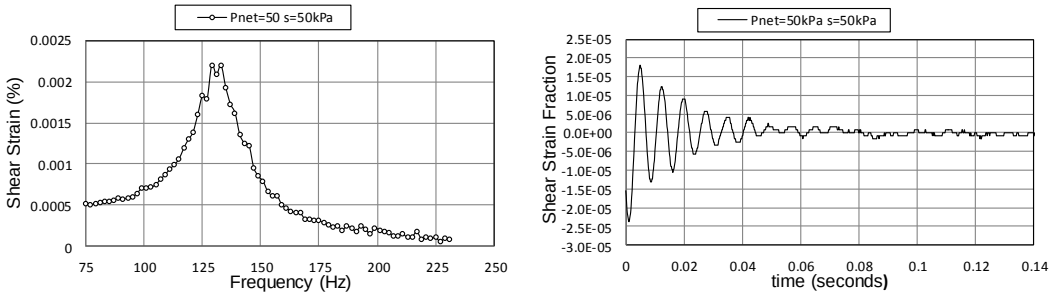

Figure 5.2 SM Soil Response at 1-pfs torque: (p-u_a) = 50kPa, s = 50kPa

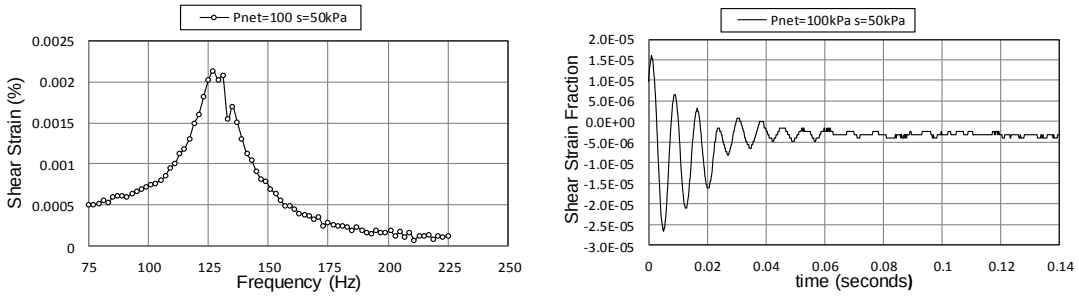

Figure 5.3 SM Soil Response at 1-pfs torque: (p-u_a) = 100kPa, s = 50kPa

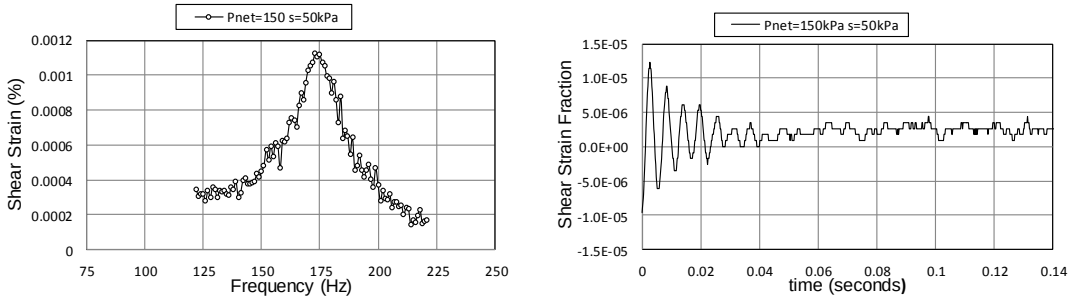

Figure 5.4 SM Soil Response at 1-pfs torque: (p-u_a) = 150 kPa, s = 50kPa

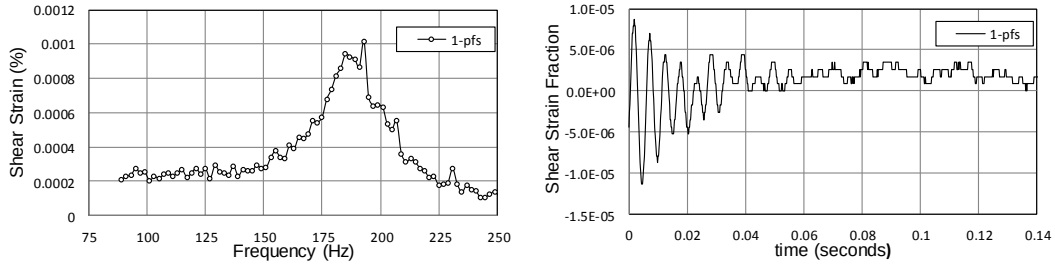

Figure 5.5 SM Soil Response at 1-pfs torque: $(p\text{-}u_a)$ = 200 kPa, s = 50kPa

It can be observed that the resonant frequency increases with increasing net confining pressure, although the data from the first two tests do not follow this pattern. Qualitatively, this ensures an increasing shear modulus with increasing net confining pressure, as the resonant frequency is directly proportional to shear modulus in shear modulus calculations. This can be attributed to an increase in tensile forces between soil particles from increased matric suction, thereby causing closer contact between soil particles and stiffer material.

Figs. 5-6 through 5-13 show the frequency response curves and free-vibration decay curves from RC tests conducted at net confining pressure, $(p\text{-}u_a)$ = 200 kPa and s = 50 kPa. With 2, 3, 4, 5, 6, 7, 8, 9, and 10-pfs input torque, respectively.

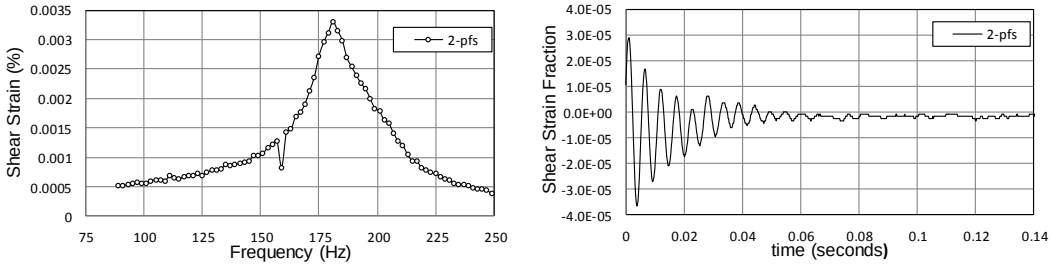

Figure 5.6 SM Soil Response at 2-pfs torque: $(p\text{-}u_a)$ = 200 kPa, s = 50 kPa

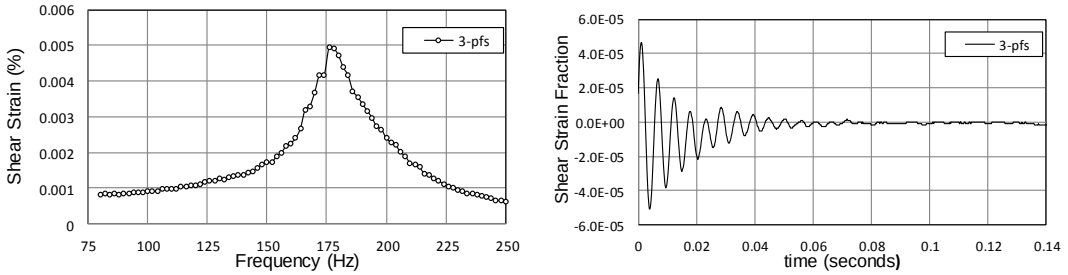

Figure 5.7 SM Soil Response at 3-pfs torque: (p-ua) = 200 kPa, s = 50 kPa

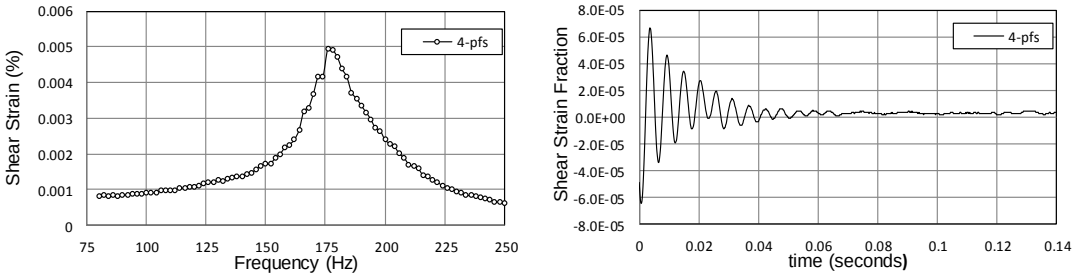

Figure 5.8 SM Soil Response at 4-pfs torque: (p-ua) = 200 kPa, s = 50 kPa

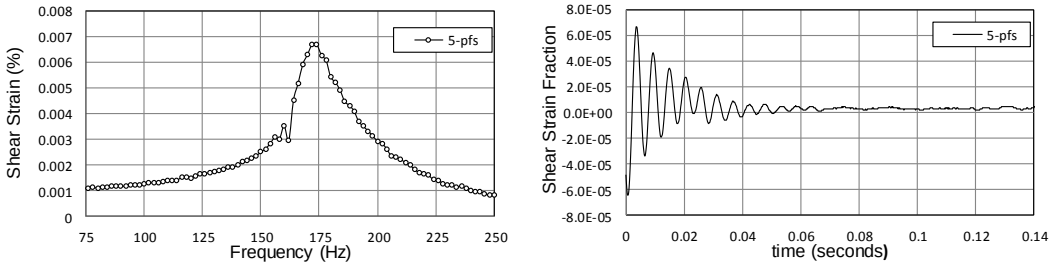

Figure 5.9 SM Soil Response at 5-pfs torque: (p-ua) = 200 kPa, s = 50 kPa

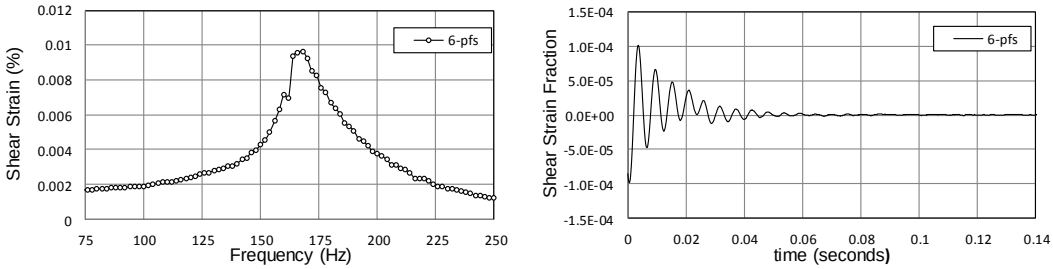

Figure 5.10 SM Soil Response at 6-pfs torque: (p-ua) = 200 kPa, s = 50 kPa

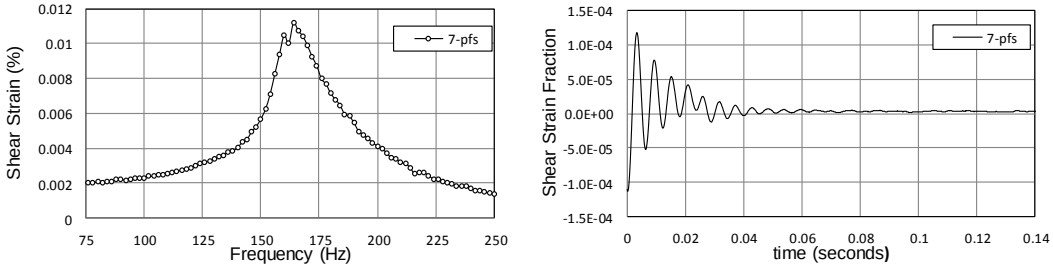

Figure 5.11 SM Soil Response at 7-pfs torque: (p-ua) = 200 kPa, s = 50 kPa

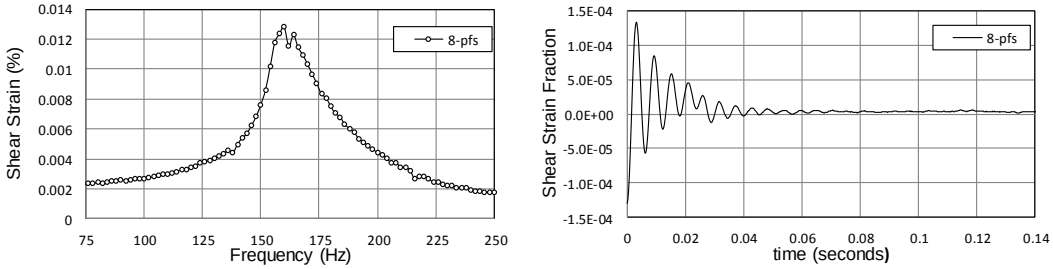

Figure 5.12 SM Soil Response at 8-pfs torque: (p-ua) = 200 kPa, s = 50 kPa

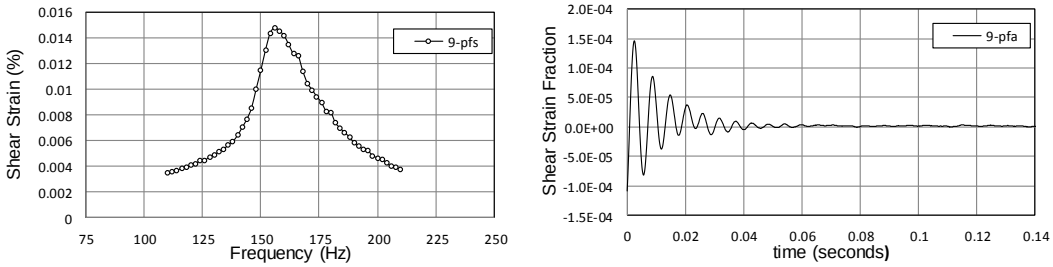

Figure 5.13 SM Soil Response at 9-pfs torque: (p-ua) = 200 kPa, s = 50 kPa

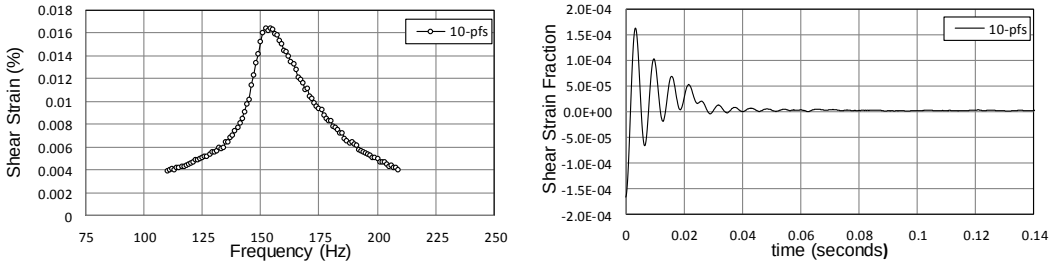

Figure 5.14 SM Soil Response at 10-pfs torque: (p-ua) = 200 kPa, s = 50 kPa

It can be observed that the resonant frequency decreases with increasing cyclic torque. There is a well-defined, linearly decreasing resonant frequency, with increasing input torque. This can be attributed to the initial yield loci being exceeded, bringing the soil specimen into the elasto-plastic region.

Fig. 5.15 depicts the frequency response curves for input cyclic torques of 1 through 10-pfs on one single graph ($p-u_a$) =200kPa, and for s = 50kPa. The linearly decreasing resonant frequency for increasing input torque (i.e., back-bone curve) can be clearly observed in this graph.

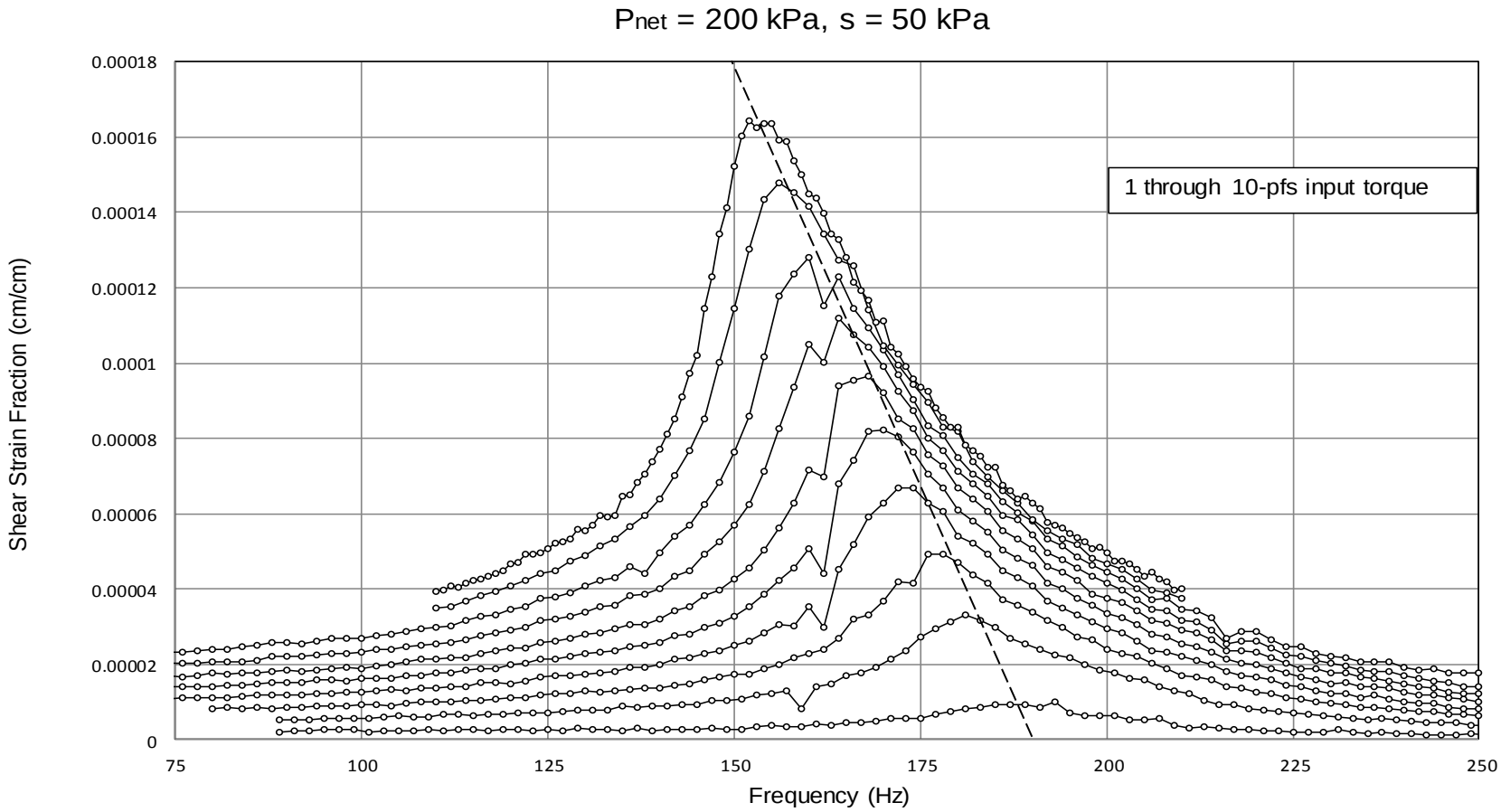

Figure 5.15 SM Soil Backbone Curve at 1 through 10-pfs

Figs. 5-15 through 5-18 show the frequency response curves and free-vibration decay curves from RC tests conducted at net confining pressures, pnet = 50, 100, 150, and 200kPa, respectively, under a constant matric suction, s= (ua-uw) = 100 kPa. All tests were conducted with a 1-pfs input torque.

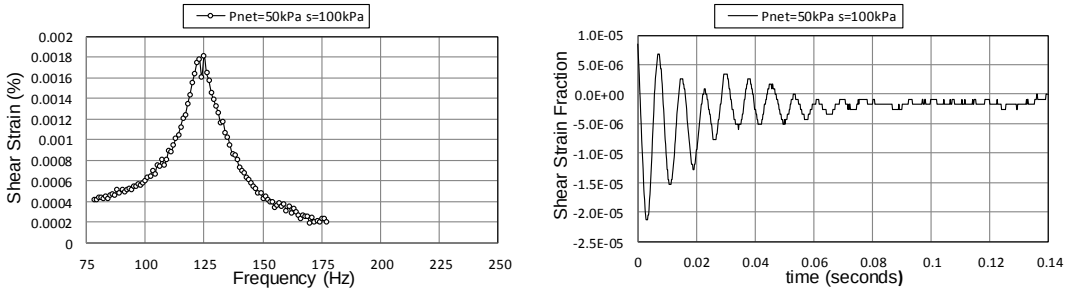

Figure 5.16 SM Soil Response at 1-pfs torque: $(p\text{-}u_a)$ = 50 kPa, s = 100 kPa

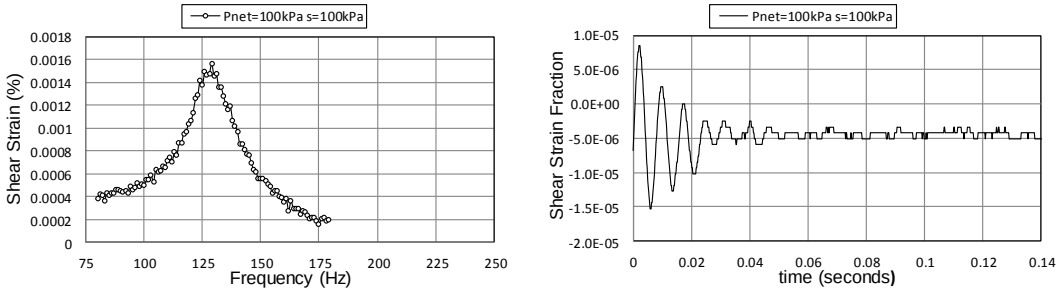

Figure 5.17 SM Soil Response at 1-pfs torque: $(p\text{-}u_a)$ = 100 kPa, s = 100 kPa

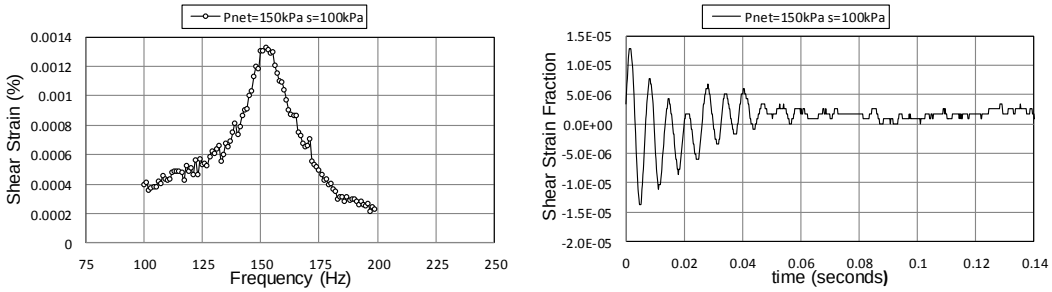

Figure 5.18 SM Soil Response at 1-pfs torque: $(p\text{-}u_a)$ = 150 kPa, s = 100 kPa

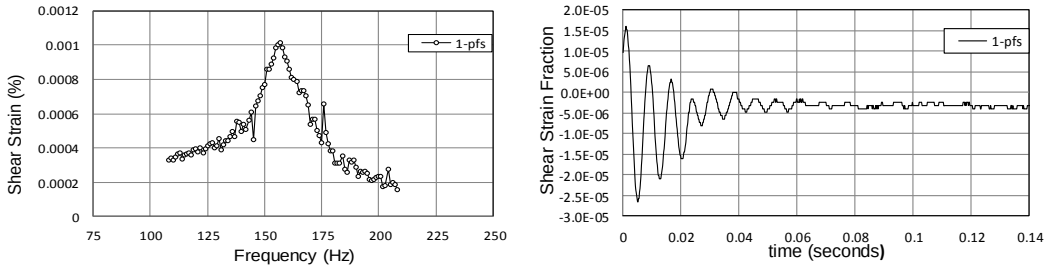

Figure 5.19 SM Soil Response at 1-pfs torque: $(p\text{-}u_a)$ = 200 kPa, s = 100 kPa

It can be observed that the resonant frequency increases with increasing net confining pressure. Qualitatively, this ensures an increasing shear modulus with increasing net confining pressure, as the resonant frequency is in the denominator for shear modulus calculations.

Figs. 5-19 through 5-27 show the frequency response curves and free-vibration decay curves from RC tests conducted at matric suction, $(p\text{-}u_a)$ = 200kPa and s=100kPa. With 2, 3, 4, 5, 6, 7, 8, 9, and 10-pfs input torque, respectively.

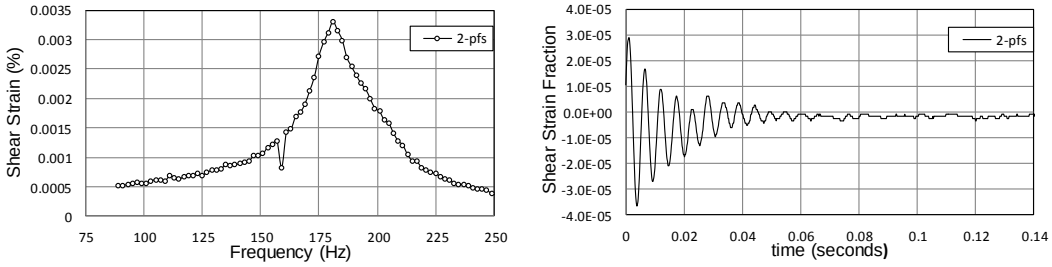

Figure 5.20 SM Soil Response at 2-pfs torque: $(p\text{-}u_a)$ = 200 kPa, s = 100 kPa

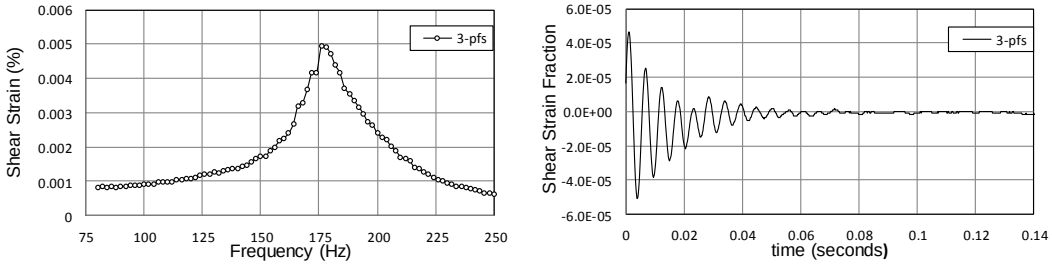

Figure 5.21 SM Soil Response at 3-pfs torque: $(p\text{-}u_a)$ = 200 kPa, s = 100 kPa

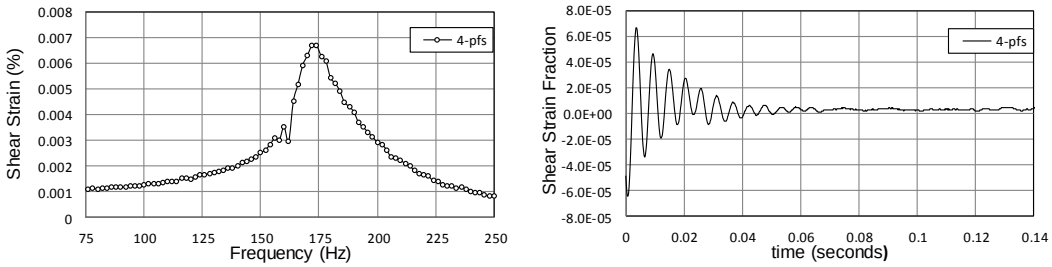

Figure 5.22 SM Soil Response at 4-pfs torque: $(p\text{-}u_a)$ = 200 kPa, s = 100 kPa

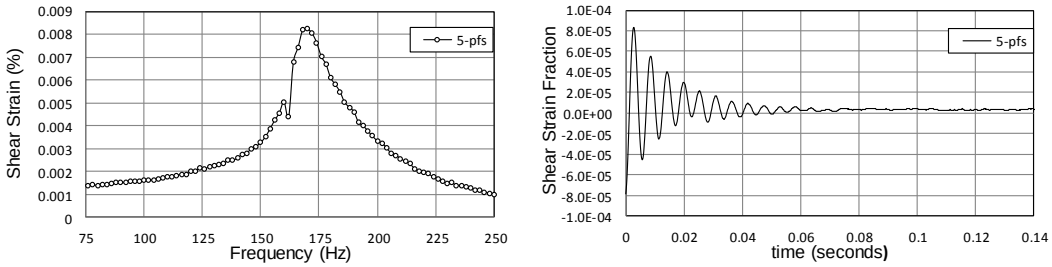

Figure 5.23 SM Soil Response at 5-pfs torque: $(p\text{-}u_a)$ = 200 kPa, s = 100 kPa

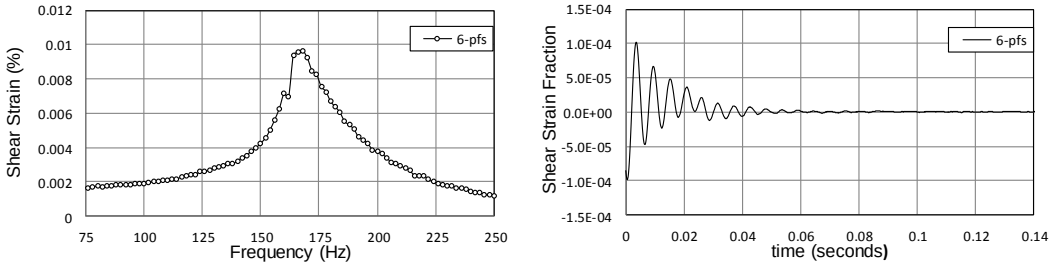

Figure 5.24 SM Soil Response at 6-pfs torque: $(p\text{-}u_a)$ = 200 kPa, s = 100 kPa

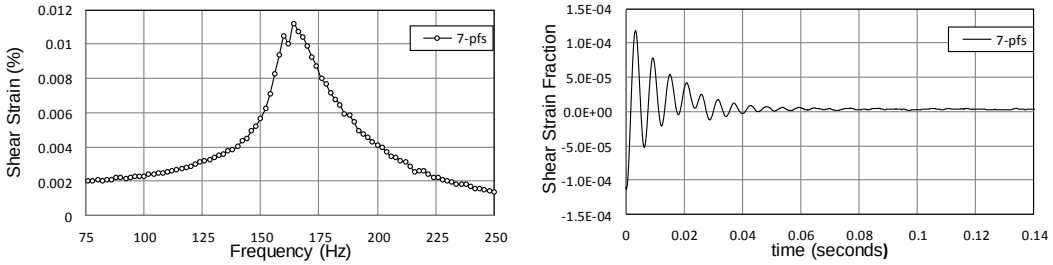

Figure 5.25 SM Soil Response at 7-pfs torque: ($p\text{-}u_a$) = 200 kPa, s = 100 kPa

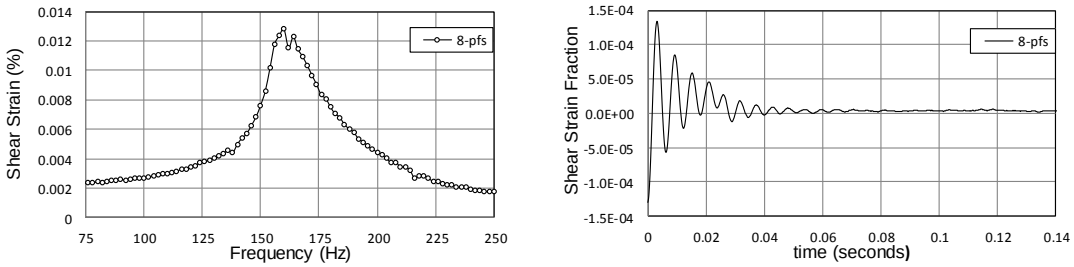

Figure 5.26 SM Soil Response at 8-pfs torque: ($p\text{-}u_a$) = 200 kPa, s = 100 kPa

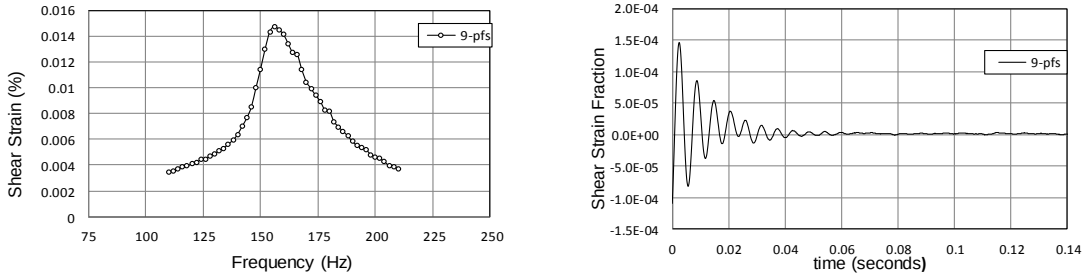

Figure 5.27 SM Soil Response at 9-pfs torque: ($p\text{-}u_a$) = 200 kPa, s = 100 kPa

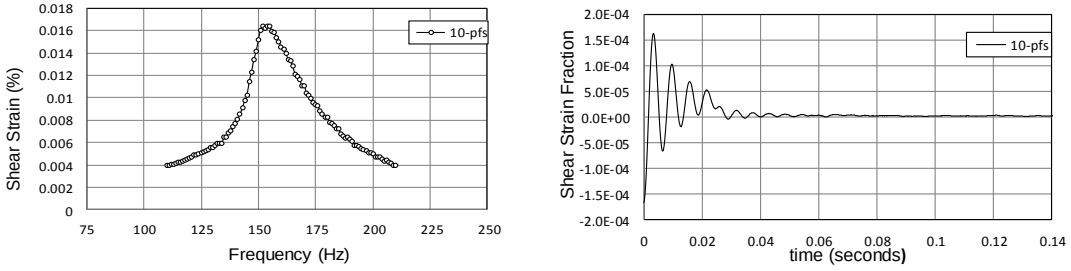

Figure 5.28 SM Soil Response at 10-pfs torque: ($p\text{-}u_a$) = 200 kPa, s=100 kPa

It can be observed that the resonant frequency decreases with increasing cyclic torque. There is a well-defined, linearly decreasing resonant frequency, with increasing input torque. This can be attributed to the initial yield loci being exceeded, bringing the soil specimen into the elasto-plastic region.

Fig. 5.29 depicts the frequency response curves for input cyclic torques of 1 through 10-pfs on one single graph for $(p-u_a)$ =200kPa, and s = 100kPa. The linearly decreasing resonant frequency for increasing input torque (i.e., back-bone curve) can be clearly observed in this graph.

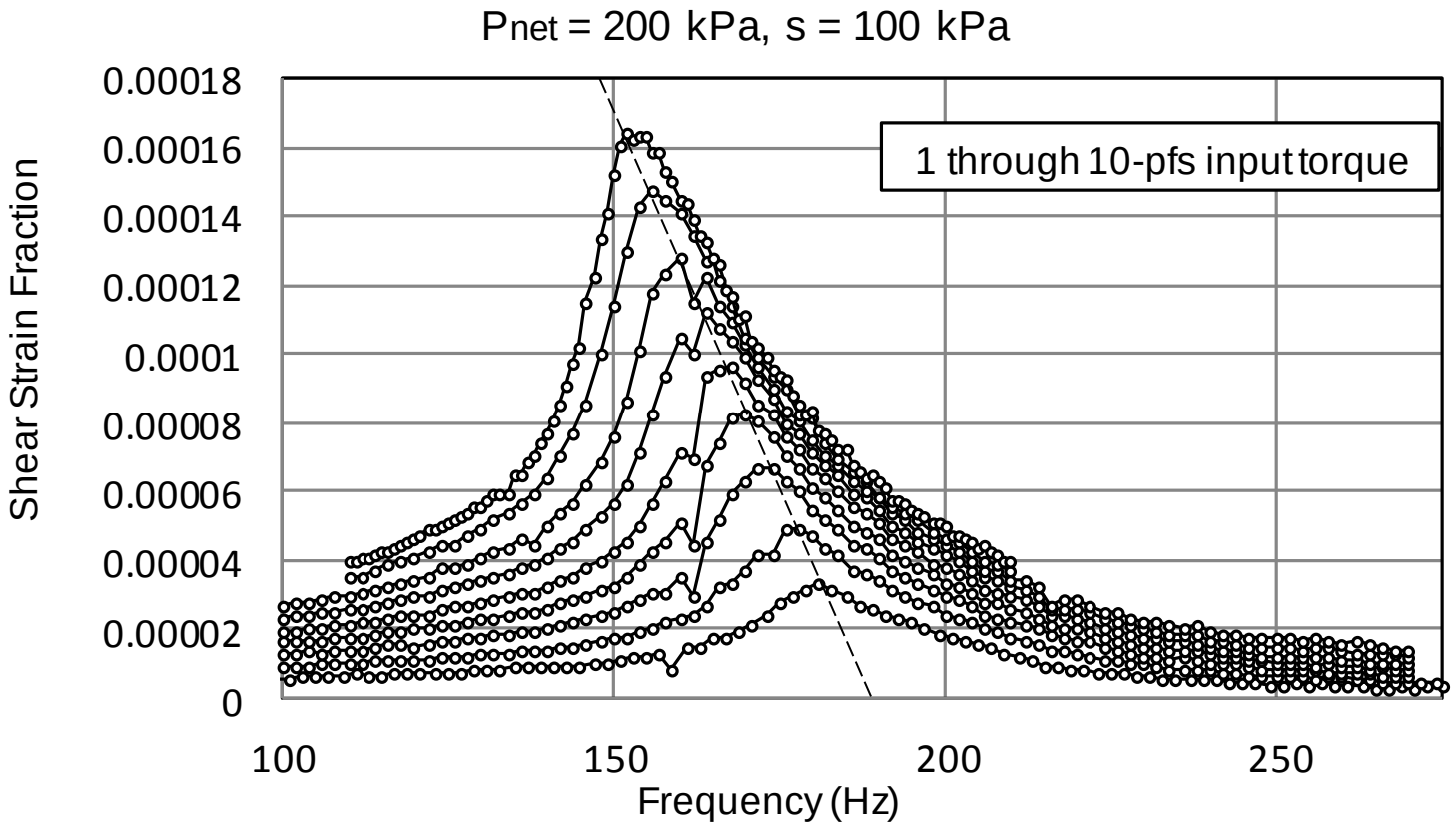

Figure 5.29 SM Soil Backbone Curve at 1 through 10-pfs

Figs. 5.30 through 5.33 show the frequency response curves and free-vibration decay curves for RC tests conducted at net confining pressures, p_{net} = 50, 100, 150, and 200 kPa, respectively, under a constant matric suction, s = (u_a-u_w) = 150 kPa. All tests were conducted with a 1-pfs input torque.

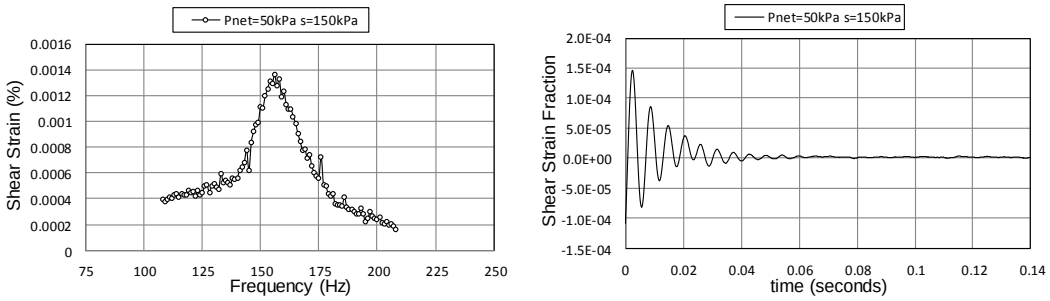

Figure 5.30 SM Soil Response at 1-pfs torque: (p-u_a) = 50 kPa, s =150 kPa

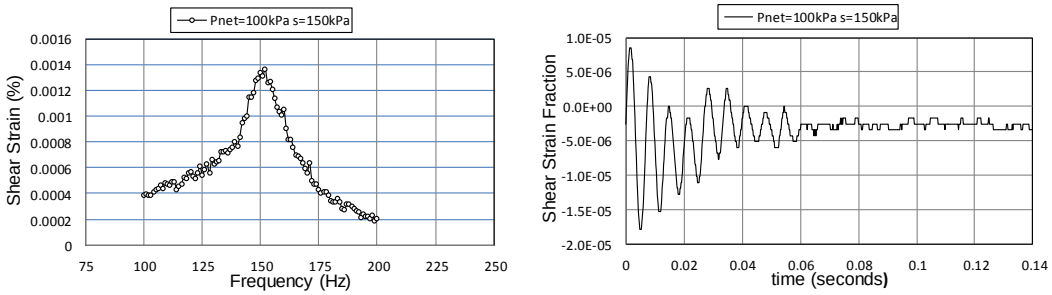

Figure 5.31SM Soil Response at 1-pfs torque: (p-u_a) = 100 kPa, s = 150 kPa

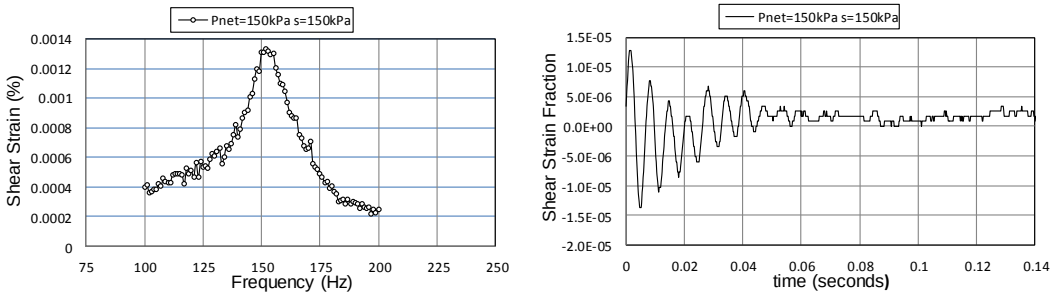

Figure 5.32 SM Soil Response at 1-pfs torque: (p-u_a) = 150 kPa, s = 150 kPa

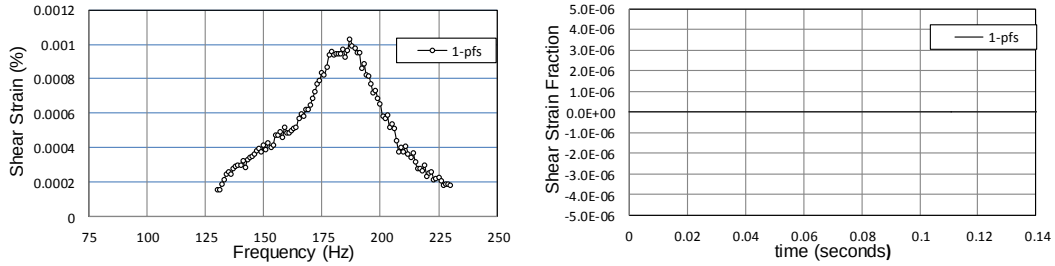

Figure 5.33 SM Soil Response at 1-pfs torque: $(p\text{-}u_a)$ = 200 kPa, s = 150 kPa

It can be observed that the resonant frequency remains approximately constant for the first three (3) tests, then increases for the remaining test.

Figs. 5-33 through 5-41 show the frequency response curves and free-vibration decay curves from RC tests conducted at matric suction, $(p\text{-}u_a)$ = 200 kPa and s=150 kPa. With 2, 3, 4, 5, 6, 7, 8, 9, and 10-pfs input torque, respectively.

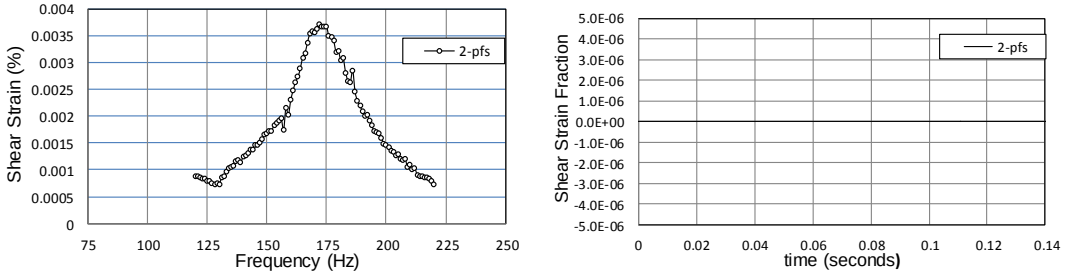

Figure 5.34 SM Soil Response at 2-pfs torque: $(p\text{-}u_a)$ = 200kPa, s = 150 kPa

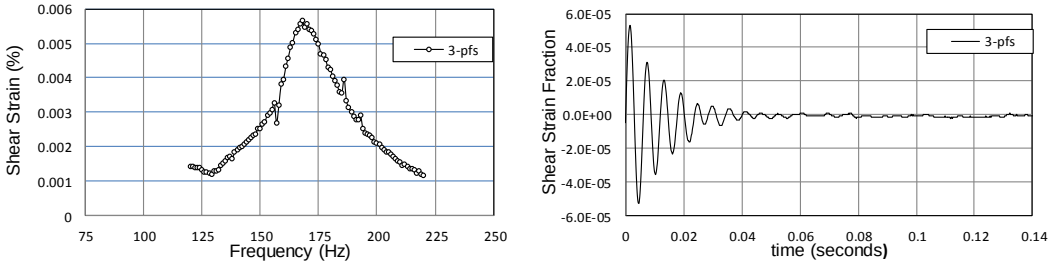

Figure 5.35 SM Soil Response at 3-pfs torque: $(p\text{-}u_a)$ = 200 kPa, s = 150 kPa

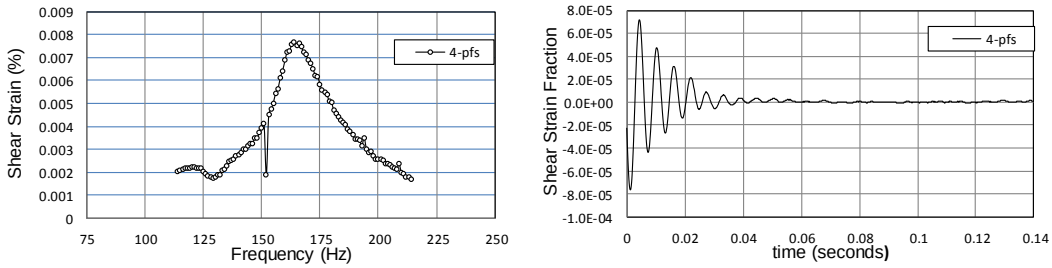

Figure 5.36 SM Soil Response at 4-pfs torque: $(p\text{-}u_a)$ = 200 kPa, s = 150 kPa

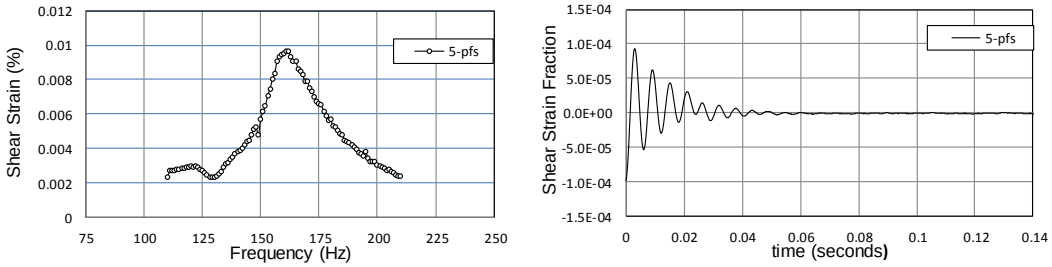

Figure 5.37 SM Soil Response at 5-pfs torque: $(p\text{-}u_a)$ = 200 kPa, s = 150 kPa

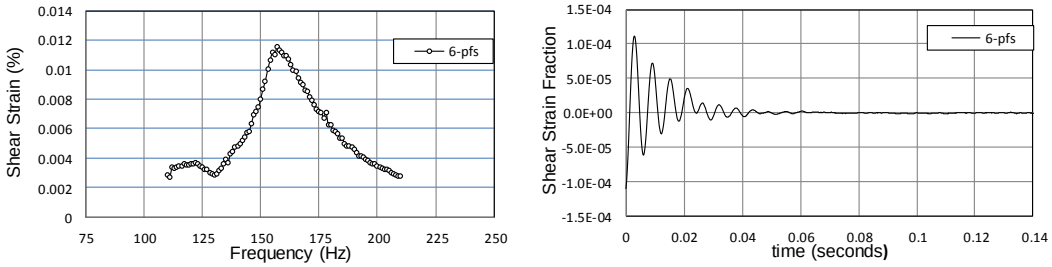

Figure 5.38 SM Soil Response at 6-pfs torque: $(p\text{-}u_a)$ = 200 kPa, s = 150 kPa

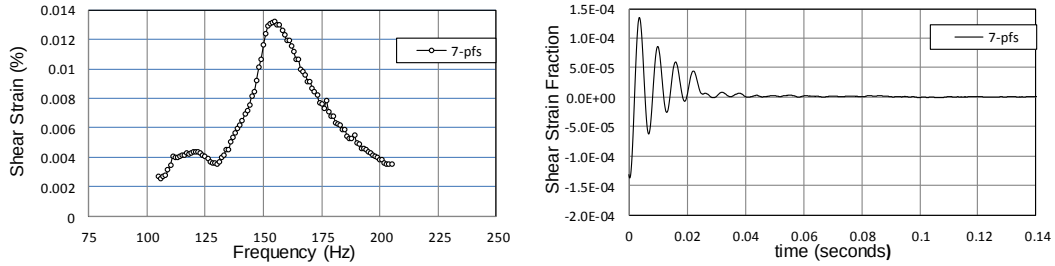

Figure 5.39 SM Soil Response at 7-pfs torque: ($p-u_a$) = 200 kPa, s = 150 kPa

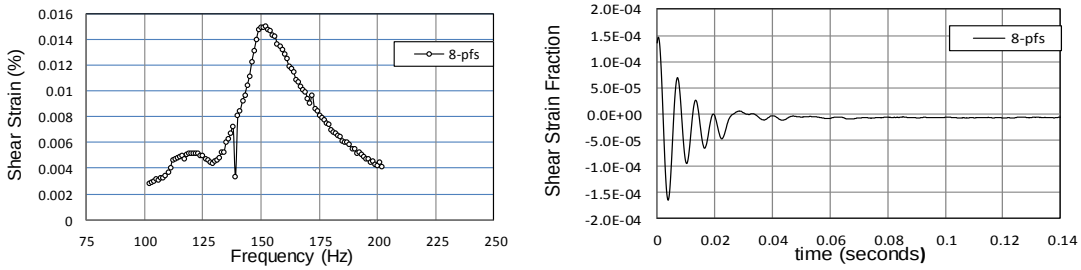

Figure 5.40 SM Soil Response at 8-pfs torque: ($p-u_a$) = 200 kPa, s = 150 kPa

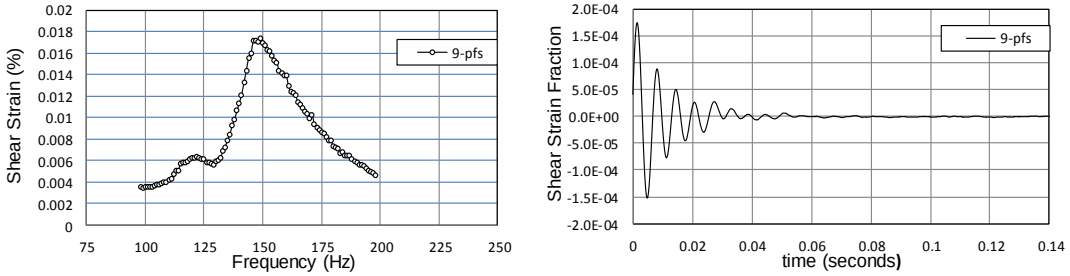

Figure 5.41 SM Soil Response at 9-pfs torque: ($p-u_a$) = 200 kPa, s = 150 kPa

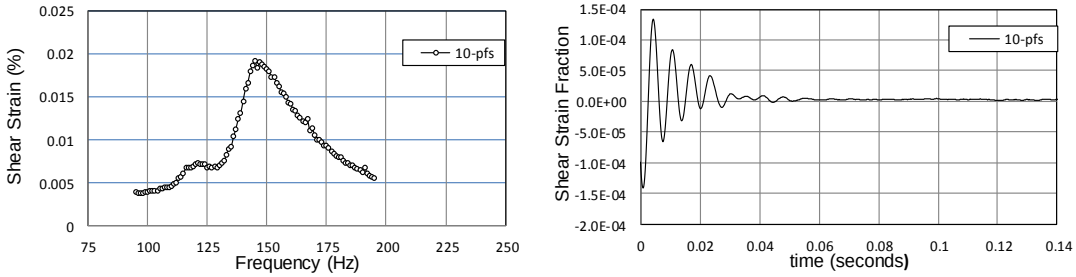

Figure 5.42 SM Soil Response at 10-pfs torque: ($p-u_a$) = 200 kPa, s=150 kPa

It can be observed that the resonant frequency decreases with increasing cyclic torque. There is a well-defined, linearly decreasing resonant frequency, with increasing input torque. This can be attributed to the initial yield loci being exceeded, bringing the soil specimen into the elasto-plastic region.

Fig. 4.43 depicts the resonant response curves for input cyclic torques of 1 through 10-pfs on one single graph for $(p\text{-}u_a)$ =200kPa, and s = 150kPa. The linearly decreasing resonant frequency for increasing input torque (i.e., back-bone curve) can be clearly observed in this graph.

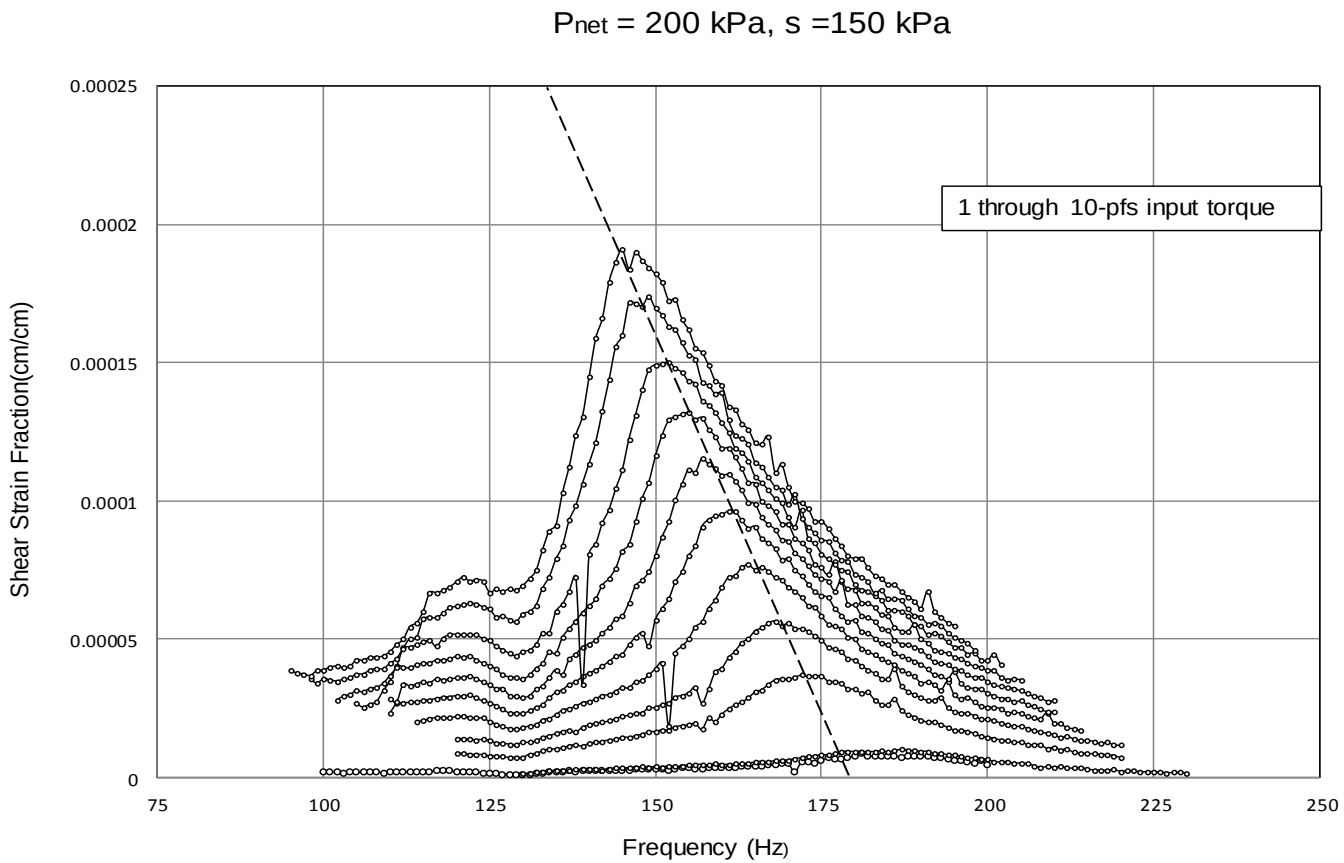

Figure 5.43 SM Soil Backbone Curve at 1 through 10-pfs

Figs. 5.44 through 5.47 show the frequency response curves and free-vibration decay curves for RC tests conducted at net confining pressures, p_{net} = 50, 100, 150, and 200 kPa, respectively, under a constant matric suction, s = (u_a-u_w) = 200kPa. All tests were conducted with a 1-pfs input torque.

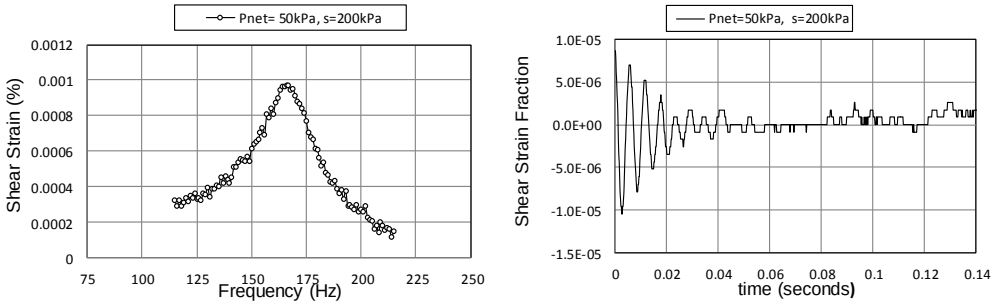

Figure 5.44 SM Soil Response at 1-pfs torque: (p-u_a) = 50 kPa, s = 200 kPa

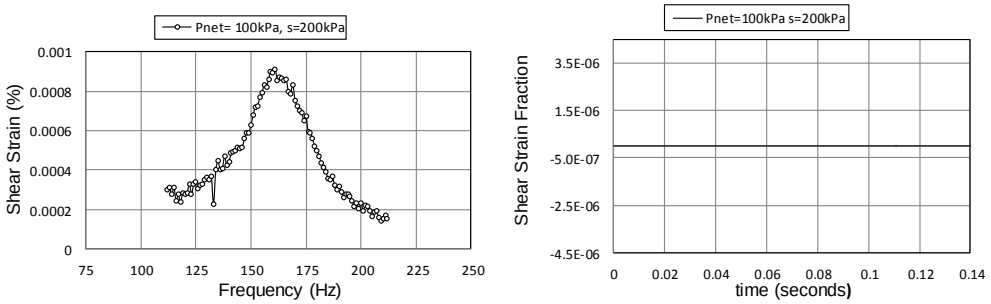

Figure 5.45 SM Soil Response at 1-pfs torque: (p-u_a) = 100kPa, s = 200 kPa

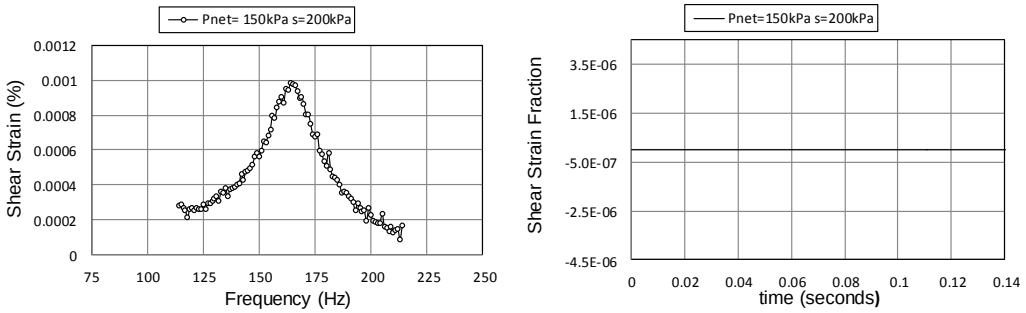

Figure 5.46 SM Soil Response at 1-pfs torque: (p-u_a) = 150kPa, s = 200 kPa

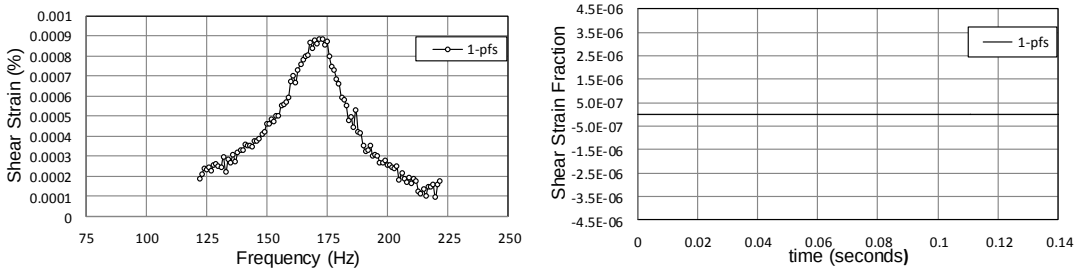

Figure 5.47 SM Soil Response at 1-pfs torque: $(p\text{-}u_a)$ = 200 kPa, s = 200 kPa

It can be observed that the resonant frequency remains approximately constant for the first three (3) tests, then increases for the remaining test.

Figs. 5.48 through 5.56 show the frequency response curves and free-vibration decay curves from RC tests conducted at matric suction, $(p\text{-}u_a)$ = 200kPa and s=200kPa. With 2, 3, 4, 5, 6, 7, 8, 9, and 10-pfs input torque, respectively.

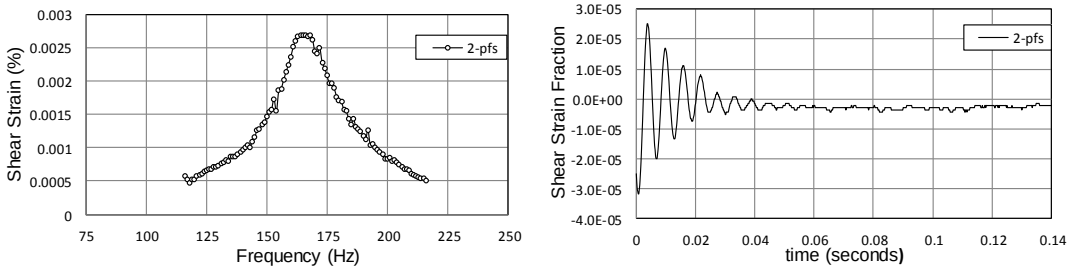

Figure 5.48 SM Soil Response at 2-pfs torque: $(p\text{-}u_a)$ = 200 kPa, s = 200 kPa

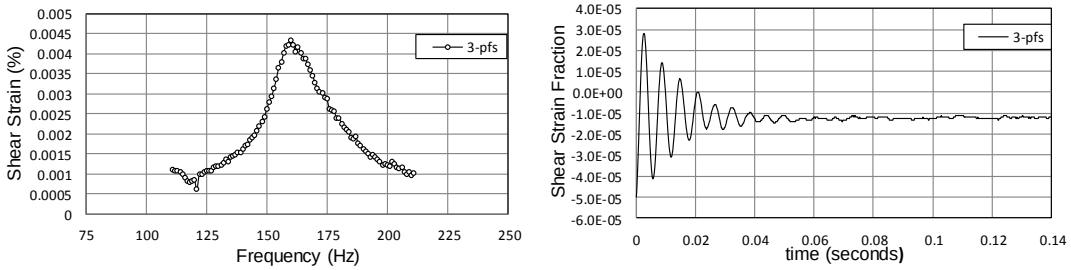

Figure 5.49 SM Soil Response at 3-pfs torque: $(p\text{-}u_a)$ = 200 kPa, s = 200 kPa

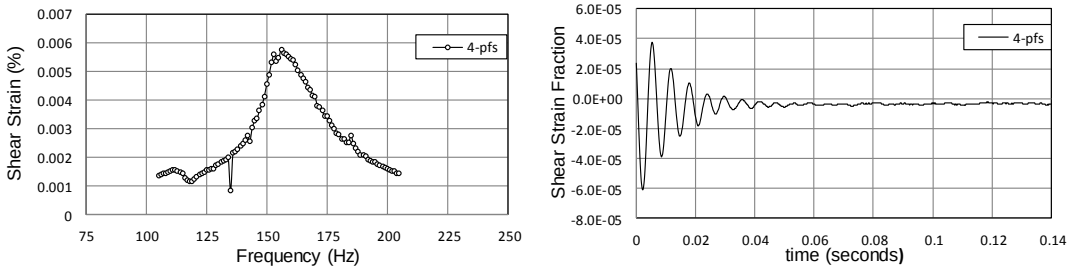

Figure 5.50 SM Soil Response at 4-pfs torque: $(p\text{-}u_a)$ = 200 kPa, s =200 kPa

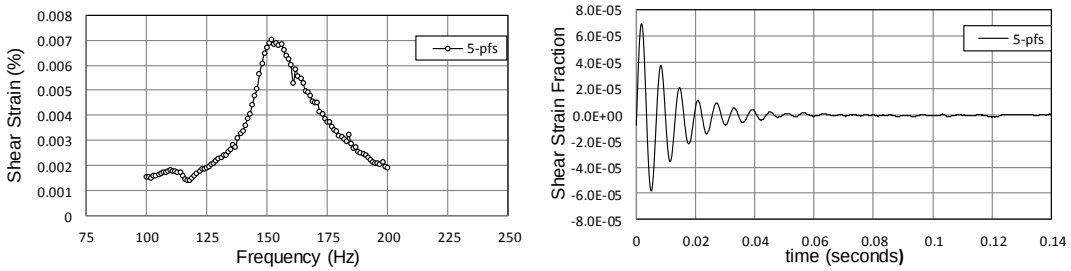

Figure 5.51 SM Soil Response at 5-pfs torque: $(p\text{-}u_a)$ = 200 kPa, s = 200 kPa

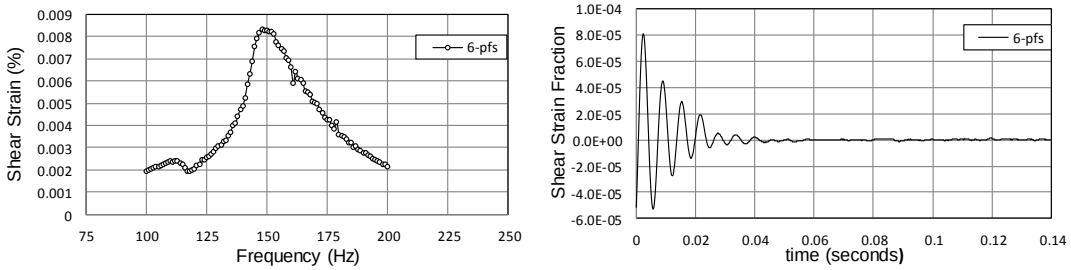

Figure 5.52 SM Soil Response at 6-pfs torque: $(p\text{-}u_a)$ = 200 kPa, s = 200 kPa

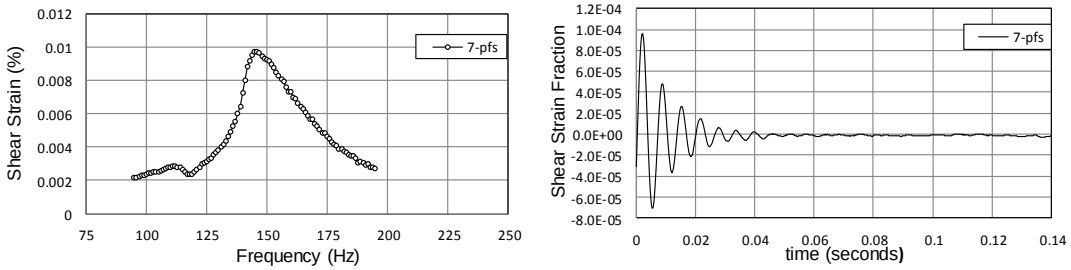

Figure 5.53 SM Soil Response at 7-pfs torque: $(p\text{-}u_a)$ = 200 kPa, s = 200 kPa

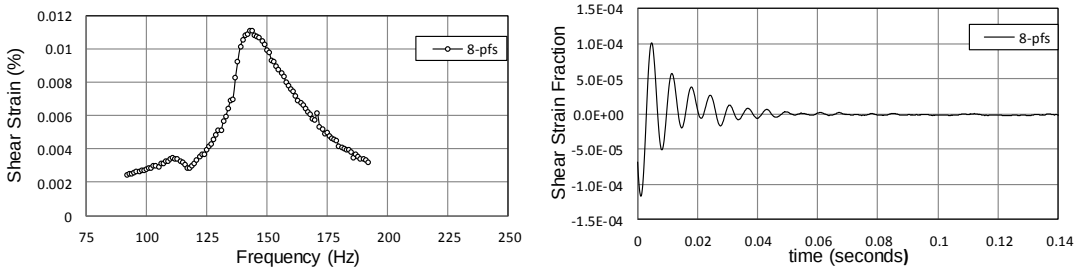

Figure 5.54 SM Soil Response at 8-pfs torque: $(p\text{-}u_a)$ = 200 kPa, s = 200 kPa

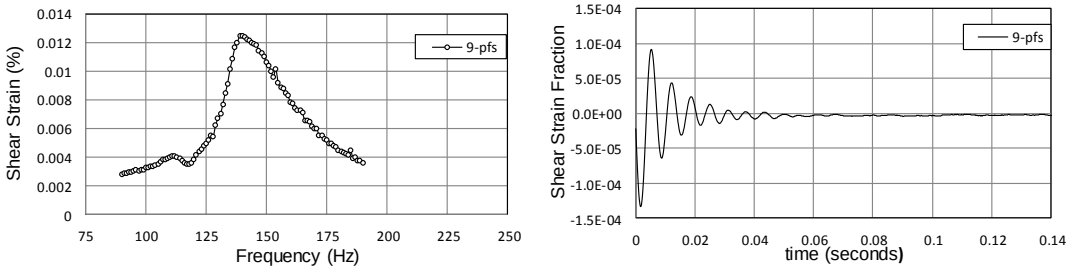

Figure 5.55 SM Soil Response at 9-pfs torque: $(p\text{-}u_a)$ = 200 kPa, s = 200 kPa

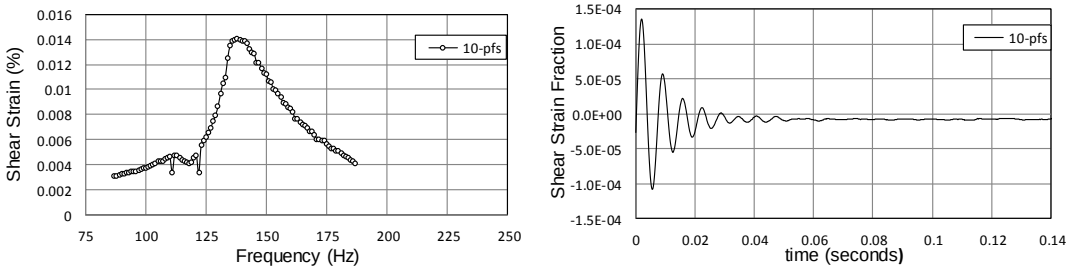

Figure 5.56 SM Soil Response at 10-pfs torque: $(p\text{-}u_a)$ = 200 kPa, s = 200 kPa

It can be observed that the resonant frequency decreases with increasing cyclic torque. There is a well-defined, linearly decreasing resonant frequency, with increasing input torque. This can be attributed to the initial yield loci being exceeded, bringing the soil specimen into the elasto-plastic region.

Fig. 5.57 depicts the resonant response curves for input cyclic torques of 1 through 10-pfs on one graph for $(p-u_a)$ =200kPa, and s = 200kPa. The linearly decreasing resonant frequency for increasing input torque can be clearly observed in this graph.

Figs. 5.58 and 5.59, that follow the backbone curve, depict the normalized shear modulus (G/G_{max}) and normalized damping (D/D_{min}) as a function of shear strain, for varying matric suctions. It can be observed that the normalized shear strain decreased with increasing shear strain. There is no observable correlation for varying matric suction states with respect to normalized shear strain. The normalized damping ratio increases with increasing shear strain. There is no clear relationship for increased matric suction on the normalized damping ratio from this graph.

Fig. 5.60 depicts the threshold strain as a function of matric suction with constant net confining pressure. It can be observed that the threshold strain generally increases with a corresponding increase in matric suction.

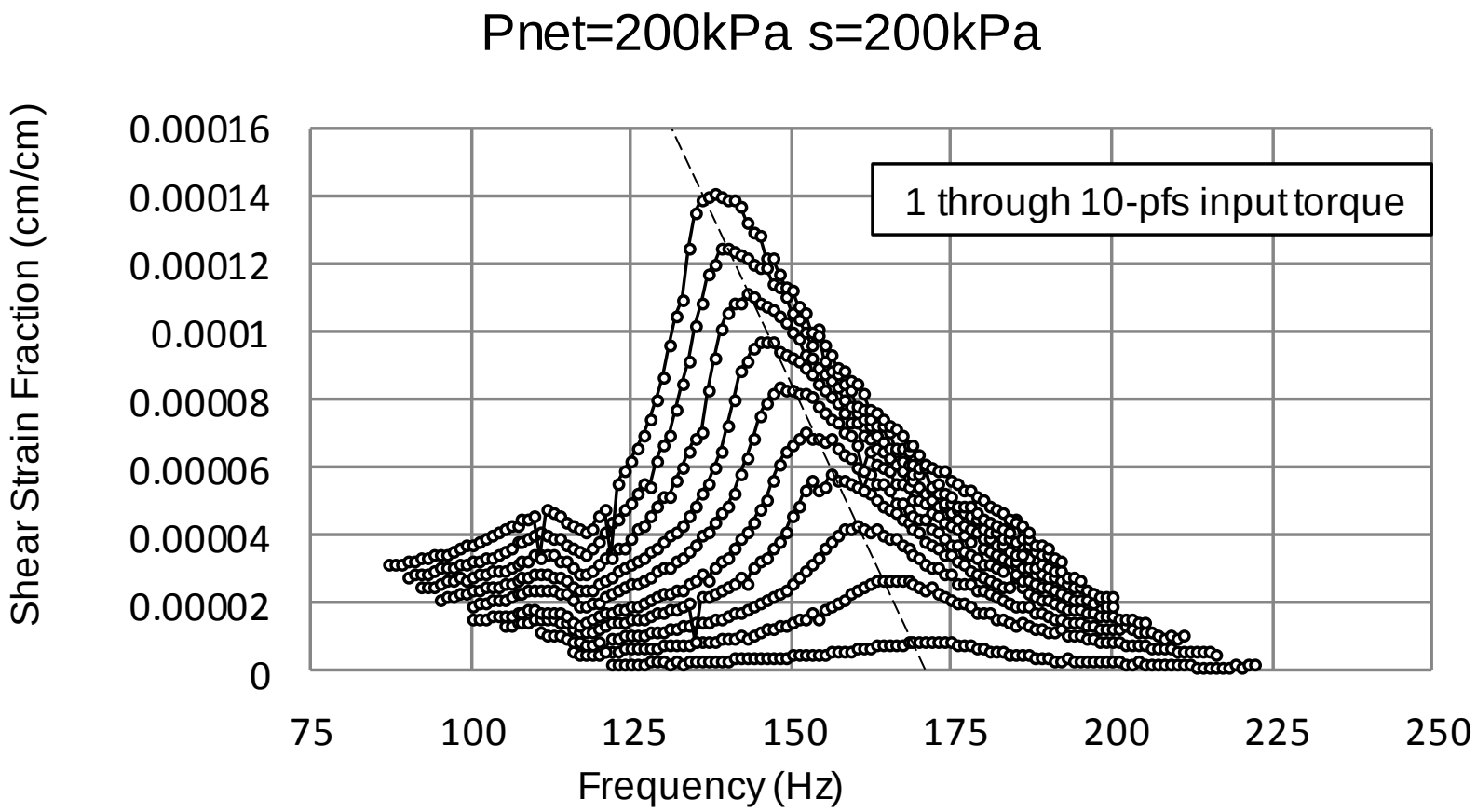

Figure 5.57 SM Soil Backbone Curve at 1 thru 10-pfs

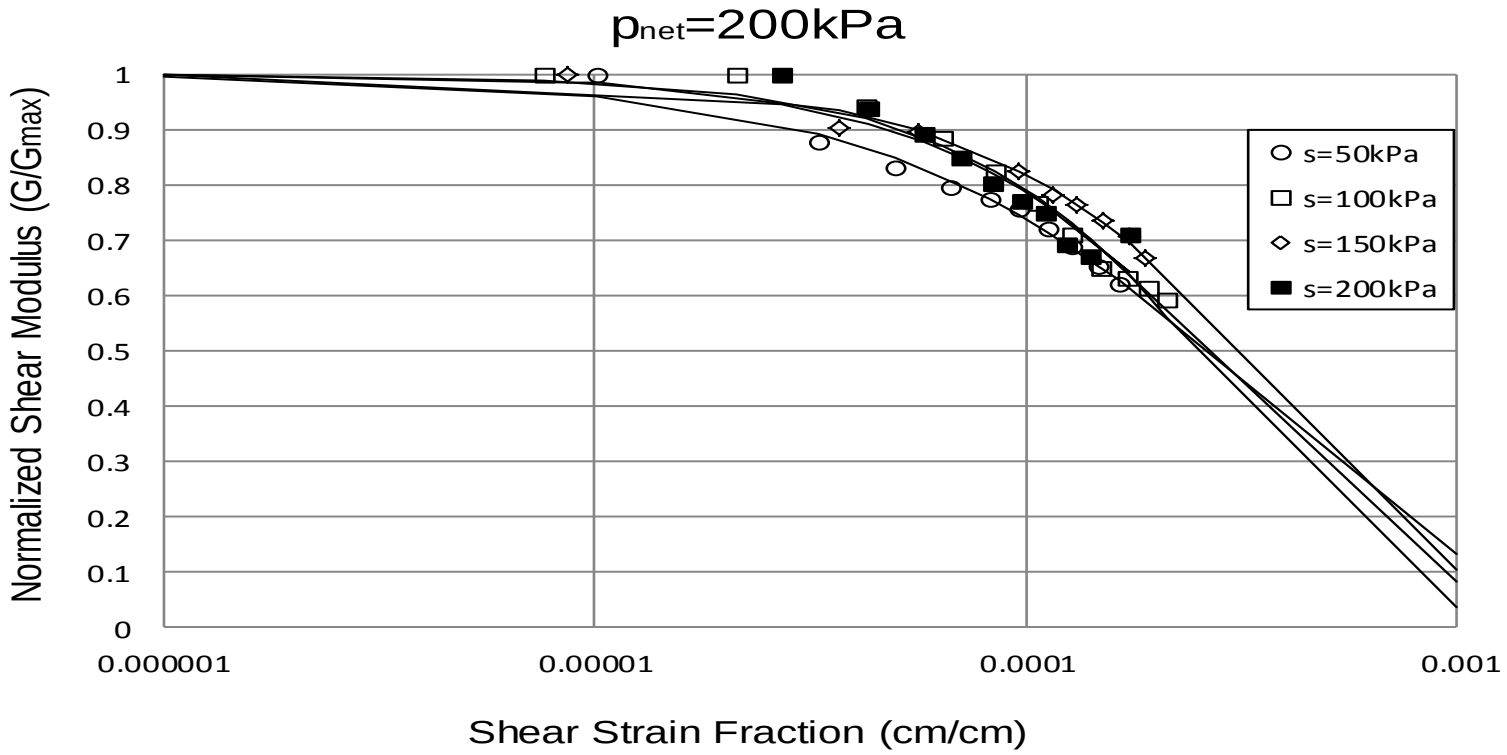

Figure 5.58 Normalized Shear Modulus as a function of Shear Strain

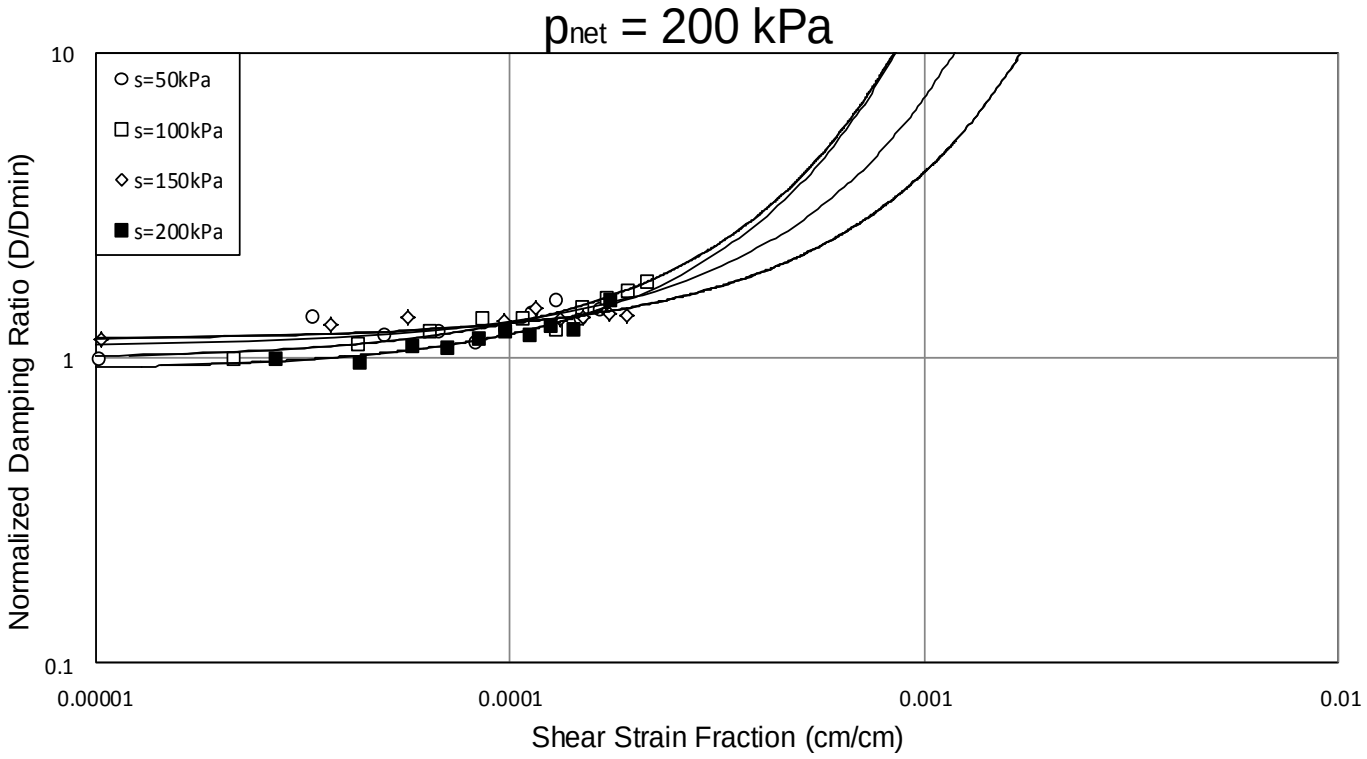

Figure 5.59 Normalized Damping as a function of Shear Strain

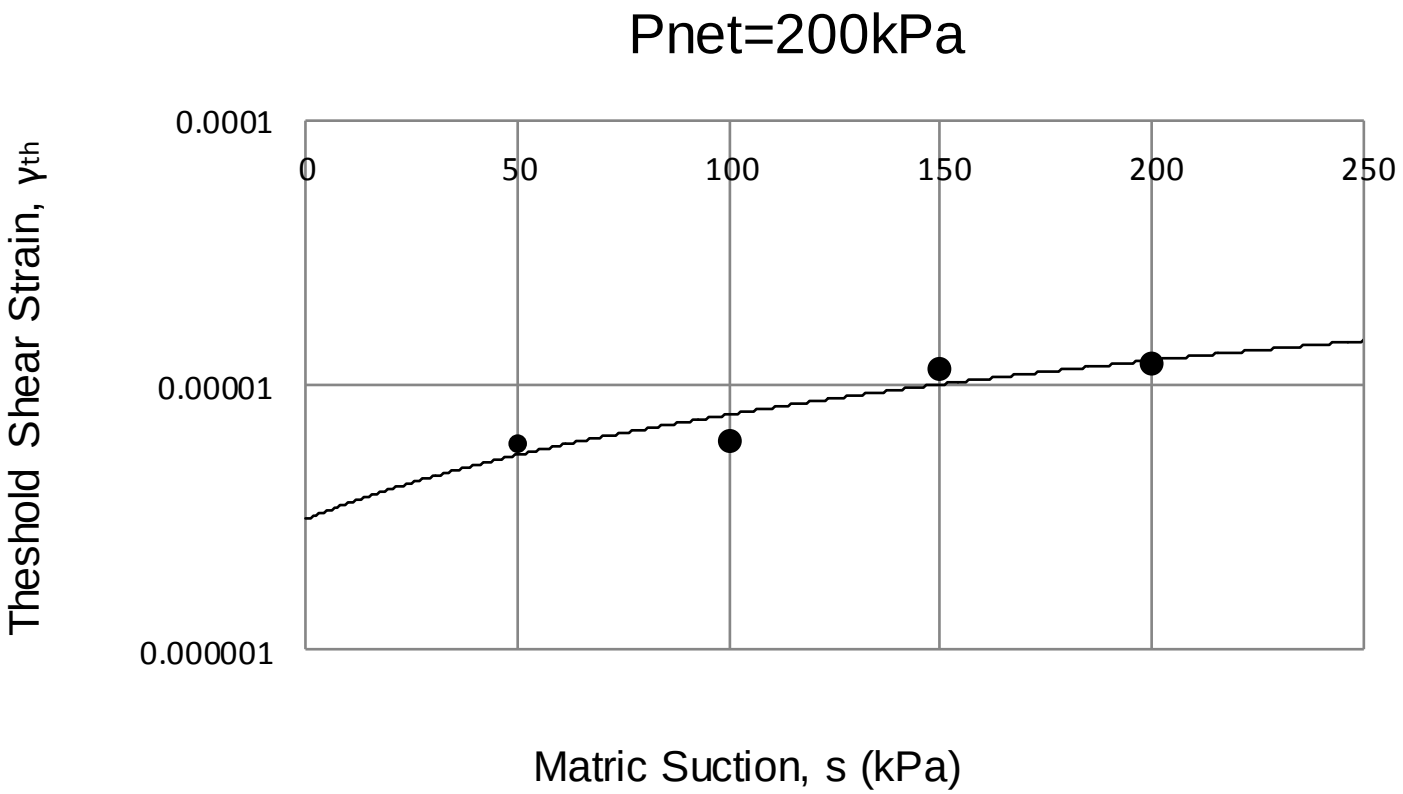

Figure 5.60 Threshold Shear Strain as a function of Matric Suction

Figs. 5.61 through 5.64 show the cyclic hysteresis stress-strain loops for a net confining pressure of $(p\text{-}u_a)$ = 200 kPa , and varying matric suction states of s = 50, 100, 150, and 200 kPa respectively The general pattern indicates a general decrease in the proportional area enclosed by the loops as the input torque increases. This inclination indicates to a decrease in material damping ratio, as this parameter is directly related to the area of the hysteretic loop. The overall observed trend shows that the material damping ratio increases with increased net confining pressure.

p_{net} = 200 kPa, s = 50 kPa

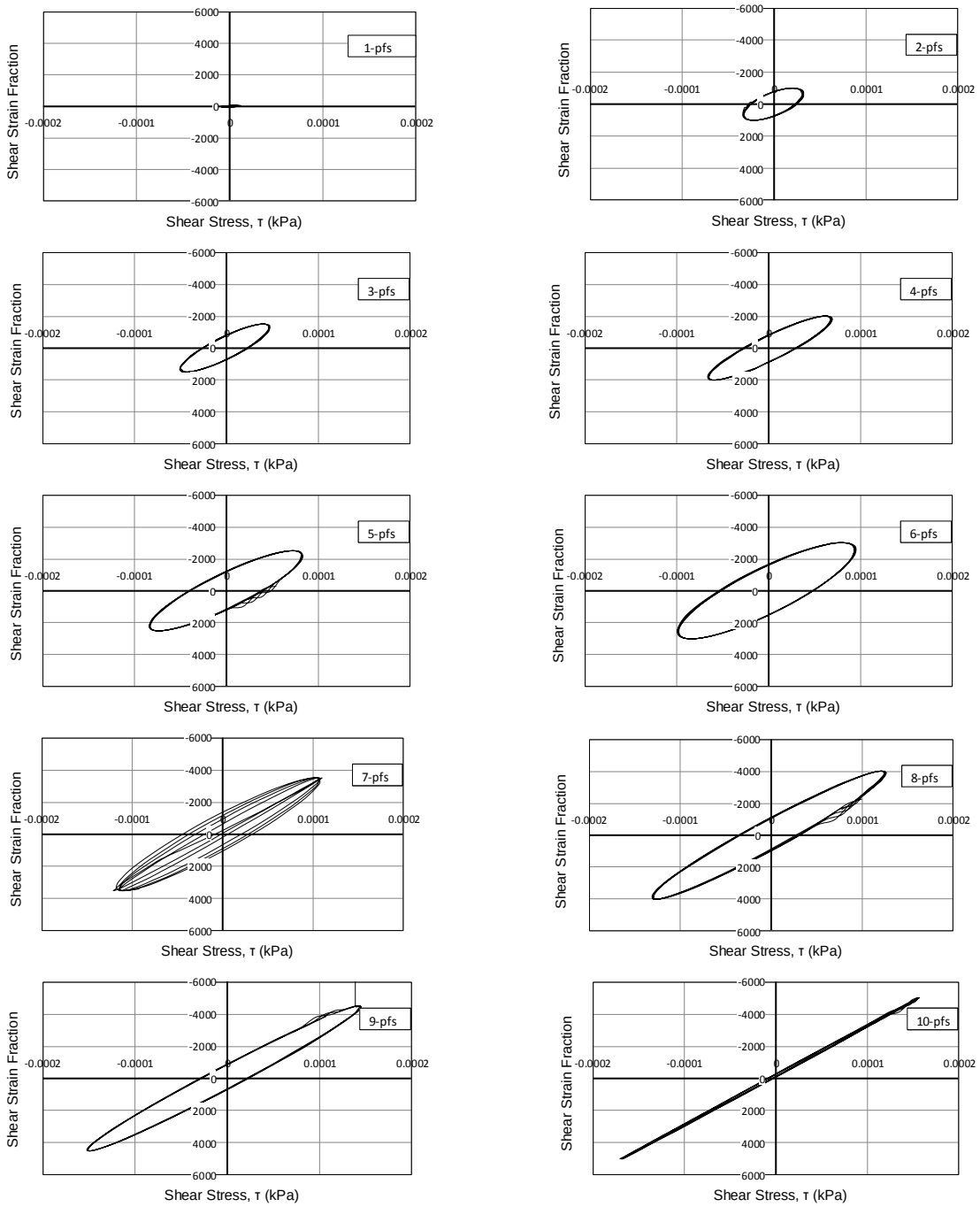

Figure 5-61 Cyclic hysteretic stress-strain loops: $(p\text{-}u_a)$ = 200 kPa, s = 50 kPa

p_{net} = 200 kPa, s =100 kPa

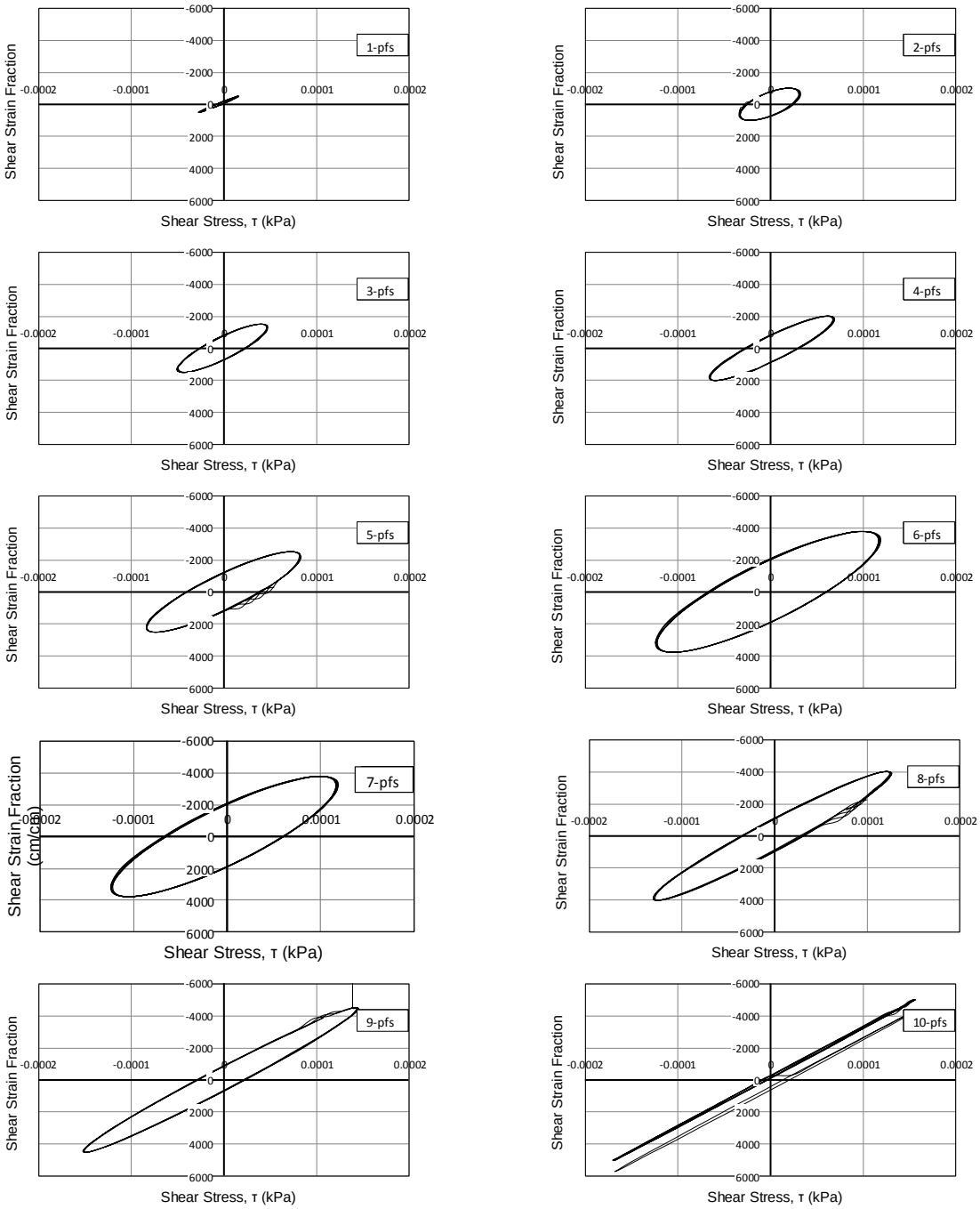

Figure 5-62 Cyclic hysteretic stress-strain loops: $(p\text{-}u_a)$ = 200 kPa, s = 100 kPa

p_{net} = 200 kPa, s =150 kPa

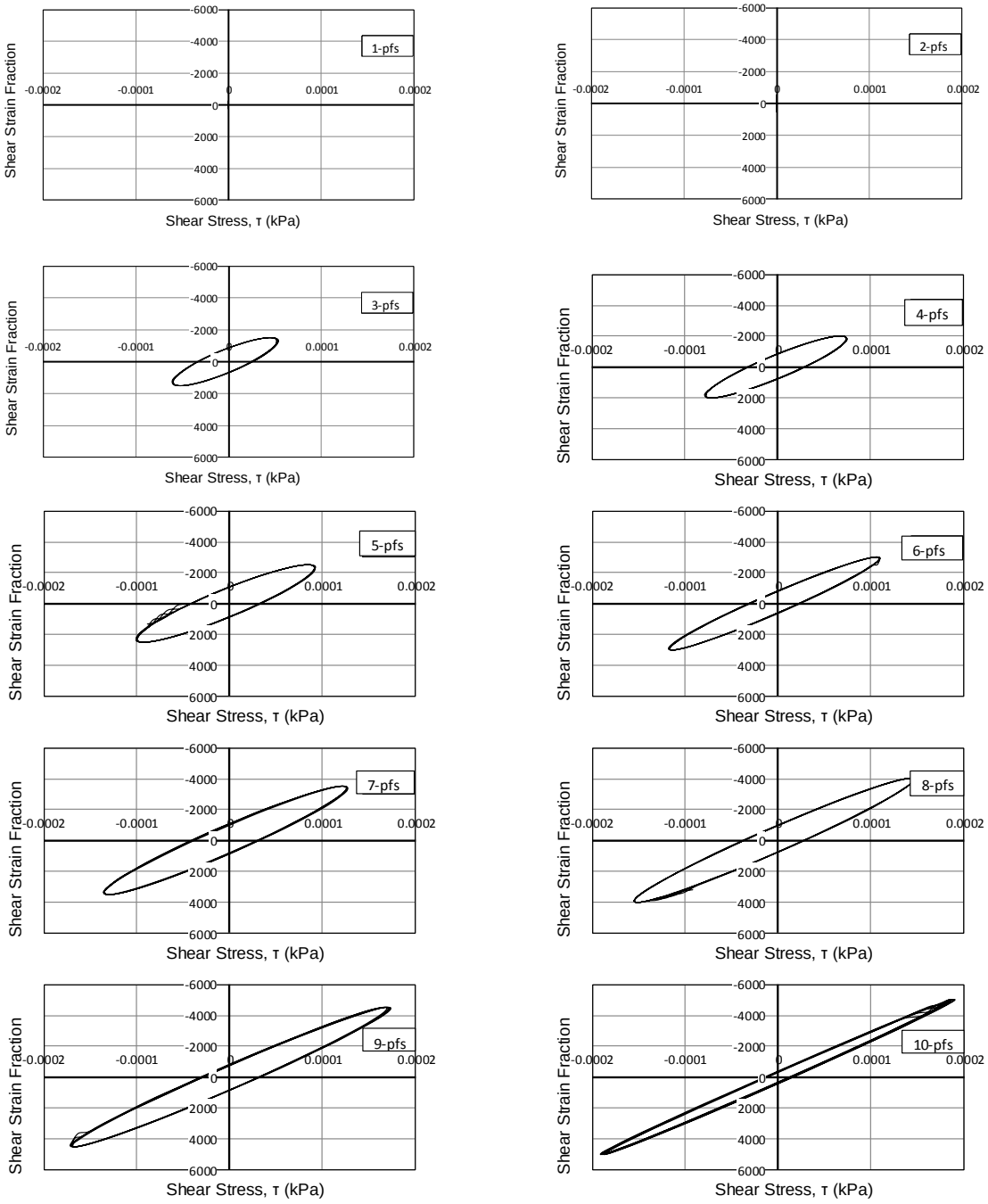

Figure 5-63 Cyclic hysteretic stress-strain loops: (p-ua) = 200 kPa, s = 150 kPa

p_{net} = 200 kPa, s = 200 kPa

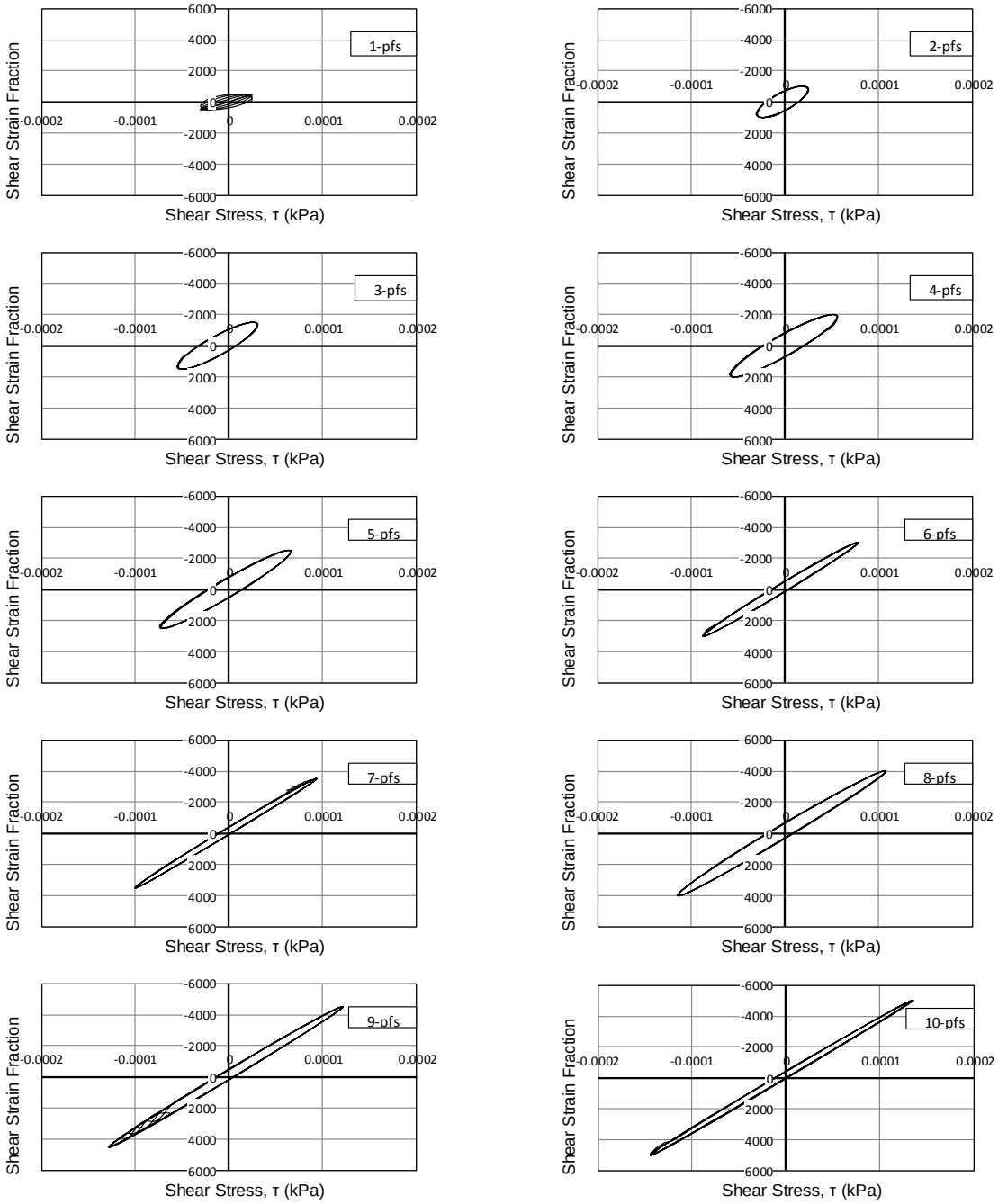

Figure 5-64 Cyclic hysteretic stress-strain loops: (p-ua) = 200 kPa, s = 200 kPa

CHAPTER 6

COMPARATIVE ANALYSIS OF TEST RESULTS TO ASSESS THE EFFECT OF STRESS/SUCTION HISTORY

The overall purpose of this research was to study the effect of dynamic properties of soils at very small shear strain amplitudes under different controlled matric suction states and net confinement loading paths via proximitor-based resonant column device.

One schematic example of a stress/suction loading path is depicted in Fig. 6-1 for each testing series. Experimental Program I was designed to assess the effect of first loading the soil (e.g. a shallow foundation), followed by an increase in suction as a result of a decrease in moisture content in the soil from of a period of dry weather. Experimental Program II was designed to assess the effect of an increase in suction in the soil as a result of a decrease of moisture content, followed by loading of the soil (e.g. a shallow foundation). The dynamic properties of a statically compacted silty sand where then determined when the sample was in the desired stress/suction state. These results are compared and analyzed in the following section.

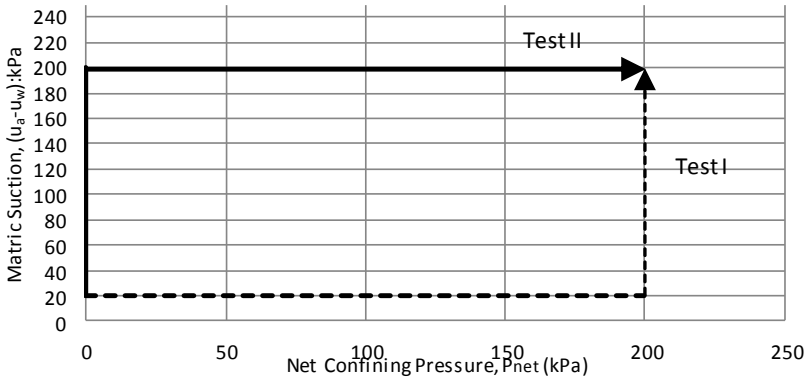

Figure 6.1 Example Stress/Suction Loading Path for Tests I and II

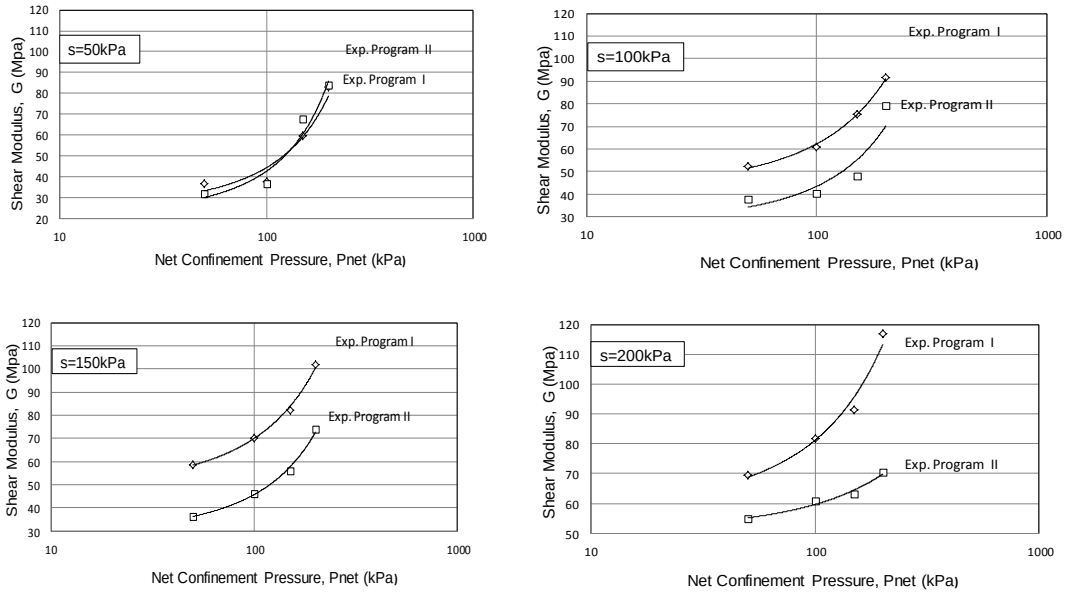

Figure 6.2 Effect of Stress/Suction History on Shear Modulus as a function of net confining pressure

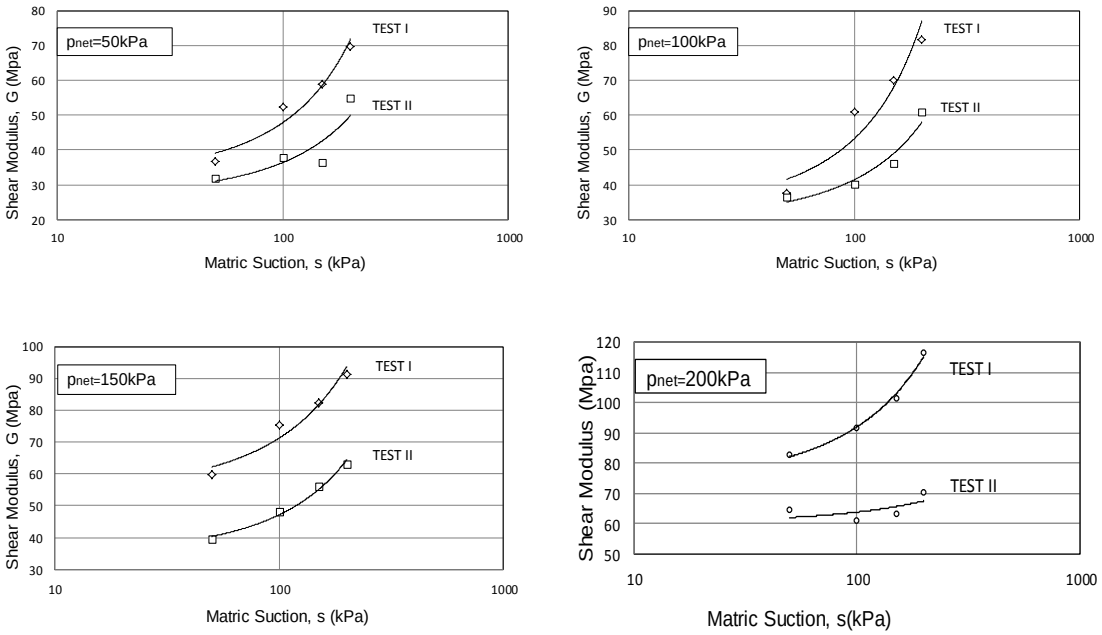

Figure 6.3 Effect of Stress/Suction History on Shear Modulus as a function of matric suction.

It can be readily observed that the stress/suction loading path in Experimental Program II results in a decreasing shear modulus with increased matric suction states. The variation between shear modulus trends representing Tests I and II become more pronounced as the soil undergoes greater matric suction. This is an indication of the significantly greater effects that net confining pressure has on small-strain shear modulus (Test I) compared to that induced by matric suction (Test II). In more general terms, it can be concluded that the stress/suction path does have a significant impact on the small-strain stiffness response of compacted soils, affecting initial structure and fabric in different way depending on the particular stress/suction history induced on the soil.

Figure 6.4 depicts the variation of material damping ratio as a function of net confining pressure with constant matric suction states.

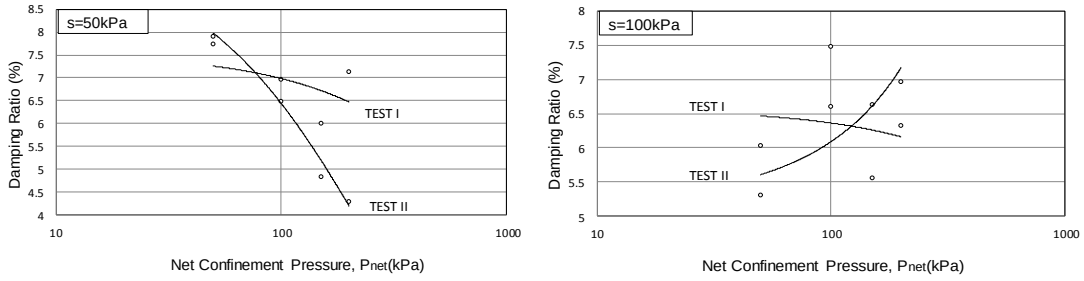

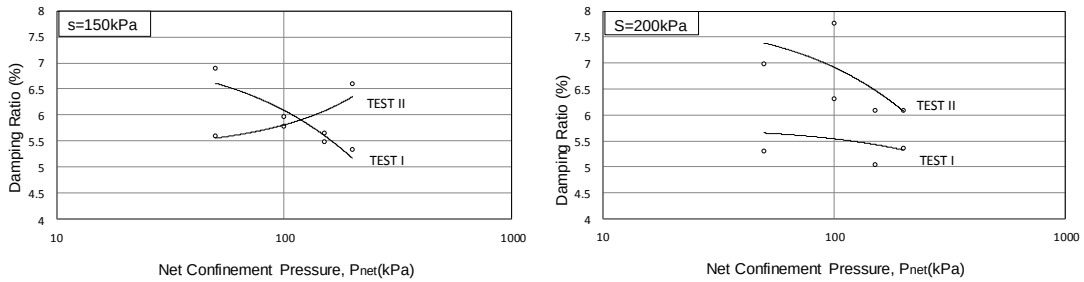

Figure 6.4 Effect of Stress/Suction History on Material Damping as function of net confining pressure

There does not appear to be a clear relationship for material damping as a function of net confining pressure; however, there is also a marked difference in damping values from both experimental programs (i.e., different stress/suction paths). It is also observed that there is a consistent tendency of damping to decrease with increasing confinement from the test performed Experimental Program I, highlighting the marked effect of first increasing confinement pressure.

Figure 6.5depicts the variation of material damping ratio as a function of net confining pressure with constant matric suction states.

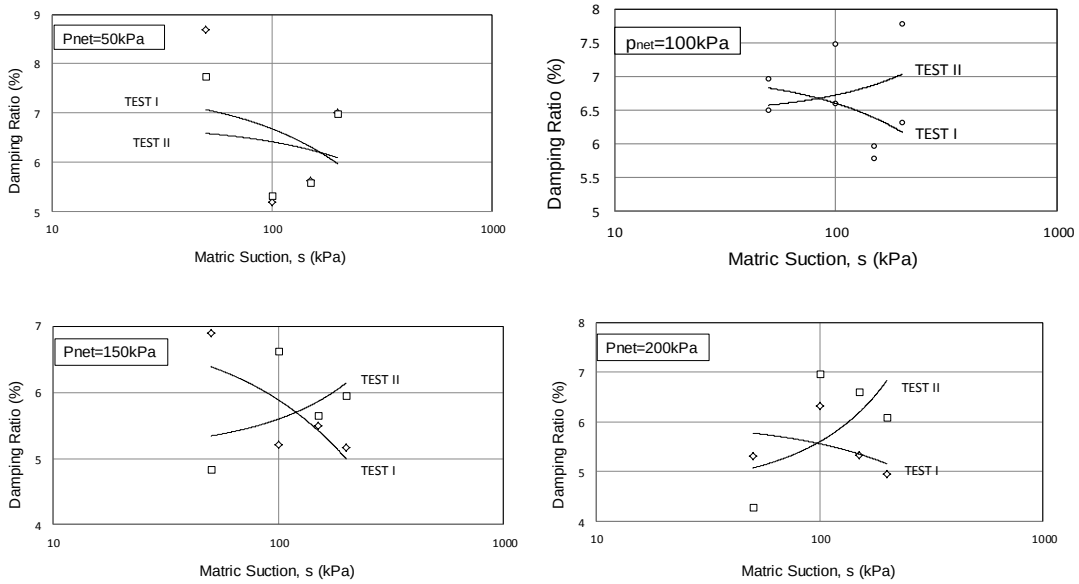

Figure 6.5 Effect of Stress/Suction History on Material Damping as function of matric suction.

There does not appear to be a clear relationship for material damping as a function of net confining pressure; however, there is also a marked difference in damping values from both experimental programs (i.e., different stress/suction paths). It is also observed that there is a consistent tendency of damping to decrease with increasing confinement from the test performed Experimental Program I, highlighting the marked effect of first increasing confinement pressure.

CHAPTER 7

CONCLUSIONS AND RECOMMENDATIONS FOR FUTURE WORK

Small-strain stiffness properties, such as shear wave velocity, shear modulus, and material damping, are important subsoil parameters for a thorough analysis of earth structures subjected static and non-static loading under partially saturated conditions. Traditional geotechnical testing methods do not capture this small- to mid-strain behavior, leading to underestimation of true soil strength, which leads to inadequate design. Recently, more effort has been made in an attempt to gain a better understanding of unsaturated soil behavior using field and laboratory based measurements of soil suction, the analysis of swell-collapse behavior, and the assessments of soil-water retention properties; however, these efforts have not contributed to a clearer understanding of small- to mid-strain response of unsaturated soils .

The overall purpose of this research was to study the dynamic properties of soils and the effect of stress/suction history on these characteristics. The first series of testing involved a broad ranging sequence of suction-controlled resonant column tests conducted on statically compacted samples of silty sand with constant net confining pressure states, ranging between 50 kPa and 200 kPa, and at varying matric suction states. The second series of testing involved a broad ranging sequence of suction-controlled resonant column tests conducted on statically compacted samples of silty sand with a constant matric suction states ranging between 50 kPa and 200 kPa, at varying net confining pressures. The results have shown the vital role of matric suction on the small- to mid-strain response of the tested soil.

7.2 Conclusions

The following conclusions have been drawn based on the experimental findings of the current research project:

Modifications to the Proximitor-based RC device

1. The tubing connection which transmits pore-air pressure should be replaced with a connection which does not allow air infiltration once the tubing experiences restriction.. This would also eliminate potential problems with the confinement pressure squeezing this tubing to a point in which pore air pressure was not allowed entry into the sample.

Small- to mid-strain dynamic response of compacted SM soil

1. A complete series of RC tests was conducted on compacted SM soil specimens using the new suction-controlled proximitor-based resonant column device. Results have shown that the apparatus was able to give reproducible results.
2. As anticipated, the small- to mid-strain shear modulus, G_{max}, had a tendency to increase with a corresponding increase in the matric suction state. This can be readily ascribed to an increase in suction causes an increase in the effective stress, thereby improving the soil stiffness properties.
3. Experimental Program II results in a decreasing shear modulus with increased matric suction states.
4. The variation between shear modulus trends representing Tests I and II become more pronounced as the soil undergoes greater matric suction.

5. Iit can be concluded that the stress/suction path does have a significant impact on the small-strain stiffness response of compacted soils, affecting initial structure and fabric in different way depending on the particular stress/suction history induced on the soil.
6. The small- to mid-strain shear modulus, G_{max}, demonstrated an increase with a corresponding increase in the net mean stress.
7. As expected, the normalized shear modulus decreased with increasing shear strain.
8. As expected, the normalized material damping ratio, D/D_{min}, increased as the shear strain increased.
9. The results of the main objective of this research concluded that the shear modulus decreased significantly for a stress/suction loading path that mimicked first inducing stress (e.g. a shallow foundation), followed by an increase in matric suction.
10.

7.3 Recommendations for Future Work

The following recommendations can be made to further study the dynamic properties of soils at small- to mid-strain levels using the suction controlled proximitor-based resonant column device used in this work:

1. A detailed analysis of the dynamic response of unsaturated soils at higher suction states is needed to gain a clearer understanding of the role matric suction states in excess of 100,000kPa.
2. A clear understanding of the thermal effects on small- to mid-strain stiffness of unsaturated soils as part of energy foundation systems.

REFERENCES

[1] Alonso, E.E., A. Gens & Josa (1990). “A constitutive model for partially saturated soils.” Geotechnique 40(3), 405-430.

[2] ASTM (1993) “Test methods for modulus and damping of soils by the resonant column method,” Standard D 4015-92, ASTM, Philadelphia, PA, pp. 581-593.

[3] Borden, R.H., Shao, L. and Gupta, A. (1996).”Dynamic properties of piedemont residual soils”. J. of Geotechnical Engineering, ASCE, 122(10): 813-821.

[4] Brull, A. (1980). Caracteristiques mécaniques des sols de fondation de chaussées en fonction de leur état d’humidité et de compacité. Proc., International Conf. on Soil Compaction, Paris, vol. 1: 113-118.

[5] Cabarkapa, Z., T. Cuccovillo & M Gunn (1999). “Some aspects of the pre-failure behaviour of unsaturated soil.” II International Conference on pre-failure behaviour of geomaterials, Turin 1, 159-165.

[6] Cho, G., and Santamarina, J.C. (2001). Unsaturated particulate materials: Particle-level studies. J. of Geotechnical and Geoenvironmental Engineering, ASCE, 127(1): 84-96.

[7] Fredlund, D. G. and Rahardjo, H. (1993). "Soil mechanics for unsaturated soils," John Wiley and Sons, Inc., New York.

[8] Fredlund, D. G., Xing, A., Huang, S., (1994). “Predicting the permeability functions for unsaturated soils using the soil-water characteristic curve.” Can. Geotech. J. 31, 533-546.

[9] Fredlund, M. D., Wilson, G. W., and Fredlund, D. G., (1997). “Prediction of the soil-water characteristic curve from the grain-size distribution curve.” Proceedings of the 3rd Symposium on Unsaturated Soil, Rio de Janeiro, Brazil, 13-23.

[10] Fredlund D. G. (1998). “Bringing unsaturated soil mechanics into engineering practice.” II International Conference on Unsaturated Soils, UNSAT ’98, Beijing 2, 1-36.

[11] Fredlund, M. D., Fredlund, D. G., and Wilson, G. W. (2000). “An equation to represent grain-size distribution.” Can. Geotech. J., 37(4), 817-827.

[12] Geotechnical Consulting and Testing System (2009). CATS Resonant column and torsional shear test mode 1.8: User guide and reference. GCTS, Tempe, AZ.

[13] Greening, P.D. and Nash, D.F. (2004). “Frequency domain determination of Go using bender elements.” Geotechnical Testing Journal, 27(3), 1-7.

[14] Hoyos, L. R., Suescun, E.A., Pineda, J. and Puppala A. (2010). “Small-strain stiffness of compacted silty sand using a proximitor-based suction-controlled resonant column device.” Fifth International Conference Unsaturated Soils, Barcelona, Spain.

[15] Huoo-Ni, S. (1987). Dynamic properties of sand under true triaxial stress states from resonant column/torsional shear tests. Ph.D. Dissertation, Univ. of Texas, Austin, TX.

[16] Kramer, Steven L. (1996), “Geotechnical earthquake engineering,” Prentice Hall, First Edition..

[17] Leong, E.C., Cahyadi, J. and Rahardjo, H. (2006). “Stiffness of a compacted residual soil”. *Unsaturated Soils 2006*, 1169-1180..

[18] Mancuso, C., Vassallo R., and d’Onofrio A. (2002). Small strain behavior of a silty sand in controlled-suction resonant column–torsional shear tests. Canadian Geotechnical Journal, 39: 22-31.

[19] Mitchell, J. K. (1993). “Fundamental of soil behavior,” John Wiley & Sons, New York.

[20] Picornell, M., and Nazarian, S. (1998). Effects of soil suction on low-strain shear modulus of soils. Proc., 2nd International Conf. on Unsaturated Soils, Beijing, vol. 2: 102-107.

[21] Qian, X., Gray, D.H., and Woods, R.D. (1991). Resonant column tests on partially saturated sands. Geotechnical Testing Journal, ASTM, 14(3): 266-275.

[22] Stokoe, K. H. II, Anderson, A. M., Hoar, R. J., and Isenhower, W. M. (1978). "Insitu and laboratory shear velocity and modulus," Proceedings from Earthquake Engineering and Soil Dynamics Conference, ASCE, III, The University of Texas, Austin, TX, pp. 1498-1502.

[23] Stoke, K. H. and Huoo-Ni, S. (1985). "Effects of stress state and strain amplitude on shear modulus of dry sand," Proceedings of the Second Symposium on the Interaction of Non-Nuclear Munitions with Structures, Panama City, FL, pp. 407- 412.

[24] Suescun, Eduardo Alfonso, (2010). "Development of a suction controlled resonant column apparatus with self-contained bender elements". M.S. Thesis, The University of Texas at Arlington, Arlington, Texas

[25] Vassallo, R., Mancuso, C., and Vinale, F. (2006). Effects of net stress and suction history on small strain stiffness of a compacted clayey silt. Canadian Geotechnical Journal, 44(4): 447-462.

[26] Vinale, F., A. d'Onofrio, C. Mancuso, F. Santucci De Magistris & F. Tatsuoka (1999). "The prefailure behaviour of soils as construction materials." II International Conference on pre-failure behaviour of geomaterials, Turin.

[27] Takkabutr, P. (2006). "Experimental investigations on small-strain stiffness properties of partially saturated soils via resonant column and bender element testing". Ph. D. Dissertation, The University of Texas at Arlington, Arlington, Texas.

[28] Wu, S., Gray, D.H., and Richart, Jr., F.E. (1984). Capillary effects on dynamic modulus of sands and silts. Journal of Geotechnical Engineering, ASCE, 110(9): 1188-1203.

[29] Zhang, J., Andrus, R. and Juang H. (2005). “Normalized shear modulus and material damping ratio relationships”. Journal of Geotechnical and Environmental Engineering, ASCE, 131(4): 453-464

BIOGRAPHICAL INFORMATION

William Allan Douglas was born on July 24, 1971 in El Paso, Texas. He received his bachelor degree in Civil Engineering from The University of Texas at Arlington in December 2010, and obtained his Engineer-in-training certificate in January of 2011. After graduating, he worked on a part-time basis for CH2MHILL while he attended graduate school on a full-time basis. Mr. William Douglas received his Master of Science degree Geotechnical Engineering from The University of Texas at Arlington in May 2012.